2007

NAD(P)H:QUINONE OXIDOREDUCTASE (NQO1)-DIRECTED LAVENDAMYCIN ANTITUMOR AGENTS: STRUCTURE-BASED DESIGN, MOLECULAR MODELING AND STRUCTURE-ACTIVITY STUDIES

Mary Hassani
The University of Montana

NAD(P)H:QUINONE OXIDOREDUCTASE (NQO1)-DIRECTED LAVENDAMYCIN ANTITUMOR AGENTS: STRUCTURE-BASED DESIGN, MOLECULAR MODELING AND STRUCTURE-ACTIVITY STUDIES

By

Mary Hassani

PharmD Pharmacy, Pharmacy School of Azad University of Tehran, Iran 1997

Dissertation

presented in partial fulfillment of the requirements
for the degree of

Doctor of Philosophy
in Toxicology

The University of Montana
Missoula, MT

Spring 2007

Approved by:

Dr. David A. Strobel, Dean
Graduate School

Howard D. Beall, Chair
Department of Biomedical and Pharmaceutical Sciences

Mark Pershouse
Department of Biomedical and Pharmaceutical Sciences

Fernando Cardozo-Pelaez
Department of Biomedical and Pharmaceutical Sciences

Christopher Esslinger
Department of Biomedical and Pharmaceutical Sciences

Kent D. Sugden
Department of Chemistry

Hassani, Mary, Ph.D., Spring 2007 Toxicology

NAD(P)H:quinone oxidoreductase (NQO1)-directed lavendamycin antitumor agents: Structure-based design, molecular modeling and structure-activity studies

Chairperson: Howard D. Beall

NAD(P)H:quinone oxidoreductase 1 (NQO1) is a two-electron reductase that catalyzes an NAD(P)H-dependent activation of many quinone-based antitumor agents. NQO1, expressed at high levels in many human solid tumors, can be used as a target for enzyme-directed bioreductive antitumor drug development. We hypothesized that lavendamycins, quinolinedione antitumor antibiotics, can be activated by NQO1 in cancer cells that overexpress NQO1 to exhibit selective toxicity toward those cells. The effects of functional group changes on the metabolism of lavendamycins by recombinant human NQO1 were studied using a spectrophotometric assay. These structure-activity relationship (SAR) studies determined key structural features that were required for lavendamycin substrate specificity. Cytotoxicity toward human colon adenocarcinoma NQO1-deficient (BE) and NQO1-rich (BE-NQ) cells was also determined using colorimetric and clonogenic assays. The best lavendamycin substrates for NQO1 were also the most selectively toxic to the BE-NQ cells compared to BE cells. To facilitate structure-based design of more optimal lavendamycin substrates and NQO1-directed lavendamycin antitumor agent development, we developed a 1H69 crystal structure-based *in silico* model of the NQO1 active site and performed lavendamycin-docking studies. The docking was performed using the FlexX module of SYBYL software. Lavendamycin analogues were designed as NQO1 substrates utilizing our SAR and docking data as structure-based design criteria. Docking and biological studies on the analogues were performed and were consistent suggesting the *in silico* model of the enzyme possessed practical predictive power. Our results also suggested practicality of the design criteria resulting in the discovery of good NQO1 substrates with selective toxicity toward BE-NQ cells. The mechanisms of NQO1-mediated selective cytotoxicity of good lavendamycin substrates in BE and BE-NQ cells were also investigated including induction of oxidative stress and apoptosis. Biomarkers of oxidative stress including formation of 8-hydroxy-2'-deoxyguanosine (8-oxo-2dG), an indicator of oxidative DNA damage, and depletion of reduced glutathione (GSH) were examined using an HPLC-based method and a colorimetric assay, respectively. Induction of apoptosis was examined using a colorimetric assay. Our results revealed that oxidative stress and subsequent apoptosis induction by a good lavendamycin substrate was NQO1 dependent and that the poor substrate for NQO1 caused neither oxidative stress nor apoptosis.

Acknowledgements

I would first like to thank the Center for Environmental and Health Sciences and the Department of Biomedical and Pharmaceutical Sciences for providing me with the outstanding educational opportunity and resources to complete my dissertation.

I extend my heartfelt appreciation to the members of my dissertation committee: Drs. Beall, Pershouse, Sugden, Cardozo-Pelaez and Esslinger.

I would especially like to express my gratitude to my mentor, Dr. Howard D. Beall for his patience and guidance in helping me to complete this project throughout the past years.

I also extend my appreciation to Drs. Gerdes and Behforouz for providing me with modeling facilities and lavendamycin compounds.

I would also like to thank the Molecular Computational Core Facility and Departments of Chemistry of the University of Montana and Ball State University.

Finally, to my family, I am grateful for all that you have done to support me.

Table of Contents

List of Charts

List of Tables

List of Figures

Chapter 1

Introduction: NAD(P)H:Quinone Oxidoreductase 1 (NQO1)-directed Lavendamycin Antitumor Agents

1.1 Enzyme-directed Bioreductive Drug Development

The goal of current cancer therapy and antitumor drug development is to design cytotoxic drugs that selectively interact with molecular targets ideally unique to tumor cells with minimal toxicity to normal cells.[1-5] This approach, selective anticancer therapy, aims to design drugs that employ the feasible biochemical and physiological differences between tumor and uninvolved tissues.[4] One approach to achieve selective toxicity is through bioreductive activation and identifying reductase enzymes that are overexpressed in tumor cells in comparison to normal counterparts.[1,3-5] Workman and Walton presented the concept of enzyme-directed bioreductive drug development for the first time at an international symposium in Italy in 1989.[5,6] They published their report on the proposed concept in the conference proceedings in the following year.[5,6] In the enzyme-directed approach, tumor selectivity utilizes the presence of specific reductase enzymes in high enough levels in tumors to reductively bioactivate chemical agents that are substrates for the reductases.[1,3-7] Potential substrates known as bioreductive anticancer agents can then undergo reductive activation to selectively produce highly cytotoxic species in the corresponding tumors.[1,3,6-8]

In the conference proceedings and 1994 review paper, Workman et al. defined the major elements of this approach in detail.[5,6] Enzyme-directed bioreductive drug therapy can take advantage of medicinal chemistry as a proper tool to design improved substrates

for the related enzymes to maximize metabolic reduction of the substrates and subsequent antitumor response.[1,4-6] Another cornerstone of this approach is to determine appropriate enzymological features of patient tumors (enzyme profiling of tumors).[1,4-6] This will determine presence of elevated levels of reductases in the corresponding tumors and select patients with the desired enzymatic profile who will most likely respond to bioreductive anticancer agents.[1,4,5] Appropriate design and conduct of clinical trials in the enzyme-directed approach will be required to correctly assess the efficacy of bioreductive agents and achieve clinical efficacy.[4,5]

It has been suggested that NAD(P)H:quinone oxidoreductase 1 (NQO1) is one important candidate for the enzyme-directed bioreductive drug discovery approach due to its unique features.[1,4,6,8] Elevated NQO1 activity and expression in many solid tumors as well as the ability of this enzyme to reductively bioactivate many quinone-based antitumor agents have centered the focus on NQO1 as a proper target for bioreductive therapy.[1,4,6,8]

1.2 NAD(P)H:Quinone Oxidoreductase 1 (NQO1)

NAD(P)H:quinone oxidoreductase 1 (NQO1, DT-diaphorase, DTD, QR1 or EC 1.6.99.2) is a widely distributed homodimeric flavoenzyme composed of two closely associated monomers of 273 residues, each containing one molecule of the noncovalently attached FAD cofactor molecule that is required for NQO1 catalytic activity.[9-13] This enzyme was first detected by Ernster and Navazio in 1956 and they presented their findings on the enzyme at both the Swedish Biochemical Society meeting and Federation

Meetings in the United States in 1958.[14] The purification procedure for NQO1 from rat liver and assay conditions, stability, inhibitors, activators and electron acceptors of the enzyme were detailed by Ernster et al. in 1962.[15] This obligate two-electron reductase is present in cytosol (> 90%)[16] and nucleus,[17] and catalyzes a nicotinamide nucleotide [NAD(P)H]-dependent two-electron reduction[14,18] and the bioactivation of many quinone-based anticancer compounds. Antitumor quinones including streptonigrin (SN),[19-21] mitomycin C (MMC),[22,23] β-lapachone (a 1,2-naphthoquinone analogue),[24,25] various indolequinones such as EO9 ,[26-28] and a number of aziridinylbenzoquinones such as RH1[29-32] and diaziquone (AZQ)[33-35] are bioactivated by NQO1 (Chart 1.1).

1.2.1 NQO1 Structure. The crystal structures of the apo human NQO1[12,13] and human NQO1 in complex with several agents have been reported.[13,36-38] Each monomer of the physiological dimer of NQO1 is composed of two distinct domains, a major catalytic (1-220 residues) and a small C-terminal domain (221-273 residues).[10,13,37,38] Two equivalent active sites are located at the dimer interface and are formed by portions of both subunits.[12,13] The active site of the enzyme is a hydrophobic and plastic pocket that is capable of forming van der Waals and hydrogen bond interactions with quinone compounds.[13,37,39]

Chart 1.1. Chemical structures of qninone-based bioreductive antitumor agents.

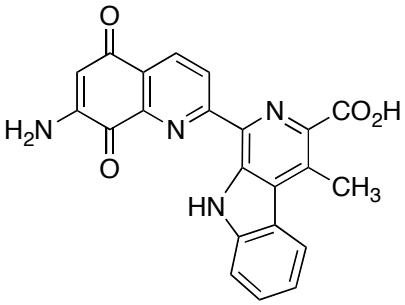

Lavendamycin

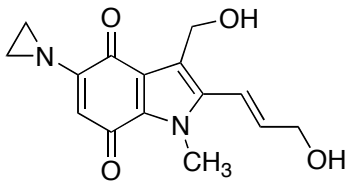

EO9

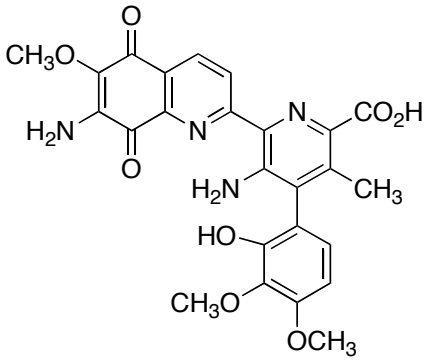

Streptonigrin

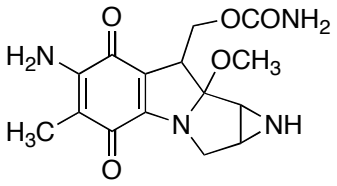

Mitomycin C

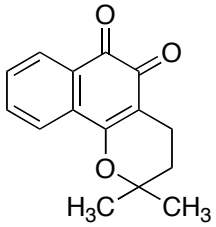

β-lapachone

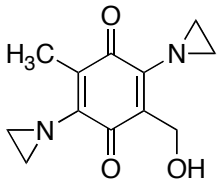

RH1

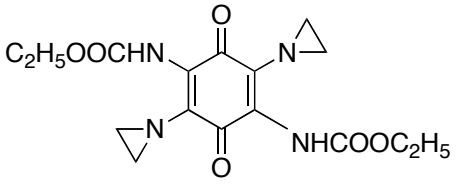

Diaziquone

In the NQO1 active site, Tyr-126, -128 and Phe-178 amino acid residues form the roof of the active site.[13,37] The floor is made up of the isoalloxazine ring of FAD, while Trp-105, Phe-106 and -178 residues form the internal wall and His-161, Gly-149 and -150 residues flank the cavity.[13,37] Gly-149, -150 and His-194 residues also restrict the entrance to the active site.[13]

1.2.2 NQO1 Enzymatic Mechanism. The substrate binding pocket of the enzyme sequentially binds NAD(P)H (electron donating cofactor) and the quinone substrate during an obligatory two-electron reduction process known as a ping-pong mechanism (Figure 1.1).[10,13,37] In the first half of the reaction a hydride ion from NAD(P)H is transferred to the N5 of FAD followed by the release of $NAD(P)^+$.[10,40,41] The hydride donation from the $FADH_2$ N5 to the quinone hydride-acceptor substrate (across a 4 Å distance[41]) can then be done at either a carbonyl oxygen or ring carbon followed by hydroquinone release. The remaining proton can be provided by Tyr-126, -128 or His-161.[10,40,41] Quinone substrates can bind to the NQO1 active site in more than one orientation, and homologous compounds with different substituents may bind to the NQO1 active site in different orientations.[37,40]

Figure 1.1. Ping-pong enzymatic mechanism of NQO1.[42]

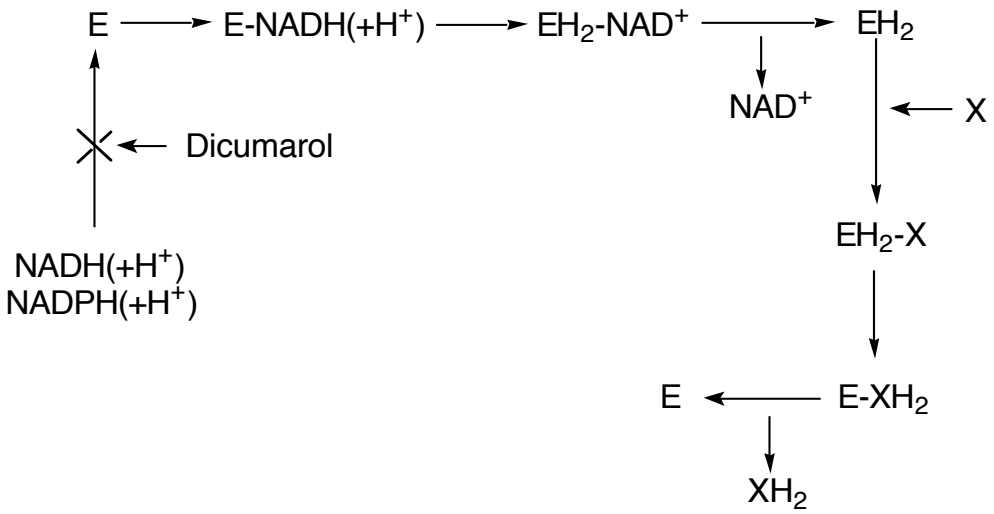

1.2.3 NQO1 Overexpression in Tumors. One crucial element of enzyme-directed bioreductive drug development in cancer therapy is the presence of high levels of reductase enzymes in tumors.[1,3-7] Increased NQO1 enzymatic activity has been reported in human lung, breast, colon and liver primary solid tumors compared to corresponding normal tissues from the same patients.[43] The NQO1 enzymatic activity in the lung adenocarcinoma sample of a patient was found to be 123-fold higher than the adjacent uninvolved tissue.[43] Lung tumors from cancer patients also displayed up to 80-fold higher NQO1 activity than the paired surrounding normal tissue.[44] Comparison of the NQO1 gene expression in liver biopsy samples of normal individuals and cancer patients determined a 50-fold increase in NQO1 mRNA level in liver tumors compared to normal human liver tissue.[45] It has also been suggested that the NQO1 gene is expressed at high levels in mouse hepatoma cells versus normal mouse liver.[45] A good correlation between NQO1 mRNA levels and enzymatic activity has been observed in many lung tumor cell lines.[44] These studies have clearly demonstrated increased NQO1 enzymatic activity and mRNA levels in various tumor tissues versus normal counterparts.

Increased levels of NQO1 protein in tumor tissues have also been reported. One group utilized Western blot analysis for immunological detection of NQO1 protein using a mouse anti-human monoclonal NQO1 antibody in paired colorectal tumors and normal peripheral tissues.[46] They detected higher amounts of NQO1 protein in colorectal tumors in comparison to related normal tissues.[46] They also determined that there was an excellent correlation between the levels of the enzyme and its activity in colon and gastric carcinoma cell lines, and surgically removed colorectal adenocarcinoma tumors.[46] In addition, elevated levels of NQO1 protein in pancreatic cancer cell lines as well as a

significant increase in the amount of the protein in human pancreatic adenocarcinoma tumors compared to normal pancreas specimens have been observed .[21] High levels of NQO1 enzymatic activity, mRNA and protein in tumor versus normal tissues demonstrated in these studies suggest that NQO1 is an important target for bioreductive therapy.

1.2.4 NQO1 Polymorphism. One important element of enzyme-directed bioreductive drug development is the individualization of patient treatment that can be accomplished through identification of patients with appropriate enzymatic profiles.[5,8] One means of individualizing patient therapy in the enzyme-directed approach is pharmacogenetic analysis of polymorphisms in the reductase of interest.[47] Since NQO1 is considered a good target in enzyme-directed bioreductive drug development, its potential polymorphisms that affect NQO1 enzymatic activity would be anticipated to impact quinone-based cancer therapy.[47,48]

The human NQO1 gene is approximately 20 kb long, possesses six exons with five interrupting introns and is located on human chromosome 16q22.1.[49-51] Traver et al. have characterized an important polymorphism in the NQO1 gene (NQO1*2) in human colon adenocarcinoma cells (BE) and human non-small-cell lung cancer (NSCLC) H596 cells that results in the loss of NQO1 activity in these cell lines.[52,53] They did not detect the mutant NQO1 protein in the cytosol of BE and H596 cells utilizing immunoblot analysis suggesting the possible cause for the lack of NQO1 activity was the lack of the NQO1 protein.[48,52,53] Both cell lines exhibited high levels of mRNA, but no NQO1 enzymatic activity.[48,52,53] This polymorphism, NQO1*2/*2, is a homozygous C to T point mutation at position 609 of the coding region of the human NQO1 gene, exon 6.[52,53]

This mutation results in a protein with a proline to serine substitution at position 187 that possesses only 2-4% of the enzymatic activity of the wild-type NQO1.[52,53] The NQO1*2/*2 genotype possesses an incidence of 4-22% varying across different ethnic groups.

The NQO1*2 polymorphism can highly impact bioreductive cancer therapy.[48] One clinical study determined that among patients with peritoneal cancer that were administered MMC, individuals with heterozygous or homozygous NQO1*2 polymorphisms exhibited reduced survival compared to those with the wild-type NQO1 genotype (NQO1*1/*1).[54] The authors also confirmed genotype-phenotype relationships such that individuals with the heterozygous genotype displayed less tumor NQO1 activity in comparison to patients with the wild-type genotype.[54] This study highlights the significant impact that NQO1*2 polymorphism could have on the outcome of NQO1-directed quinone anticancer therapy. Genotyping of patients to identify the NQO1*2 polymorphism could greatly contribute to individualization of patient treatment in bioreductive cancer therapy.[47]

1.2.5 Reductive Activation of Antitumor Quinones by NQO1. The role of NQO1 in the reductive activation of many quinone-containing bioreductive agents has been reported. SN, MMC, EO9, RH1 and AZQ are examples of quinone-based bioreductive agents that are activated by NQO1. Siegel et al. determined MMC-induced DNA interstrand cross-link formation in human colon adenocarcinoma HT-29 cells (NQO1-rich) when compared to BE cells (NQO1-deficient).[22] They observed higher levels of sensitivity to MMC-induced cytotoxicity in HT-29 cells versus BE cells.[22] NQO1-mediated metabolism of MMC in a cell-free system has also been shown to result

in the bioactivation of MMC, and induction of DNA adduct formation and DNA cross-linking.[23] In addition, Beall et al. reported selective toxicity of a number of indolequinones and mitosenes toward the NSCLC H460 cell line with high NQO1 activity compared to H596 cells with no measurable NQO1 activity,[28] and the indolequinone EO9 was found to be 92 times more toxic to the H460 cells compared to the H596 cells.[55] Another bioreductive quinone anticancer agent, SN, exhibited similar preferential cytotoxicity toward H460 cells versus H596 cells (86-fold).[56] Furthermore, SN displayed higher levels of toxicity (similar to MMC) and DNA strand breaks in HT-29 cells compared to BE cells.[19] These studies determine that NQO1-mediated activation of bioreductive agents MMC, SN and EO9 in NQO1-rich versus NQO1-deficient cancer cells results in the selective toxicity of these agents toward NQO1-rich cells.

Bioreductive activation of aziridinylbezoquinones by NQO1 has also been reported. BE and HT-29 cells have been used as a model system to investigate bioreductive activation of AZQ by NQO1.[34] In this study, DNA interstrand cross-linking by AZQ was examined in both BE and HT-29 cell lines.[34] A high degree of dose-dependent cross-linked DNA was detected in HT-29 cells whereas low levels of DNA cross-links were observed in BE cells after exposure to AZQ at the same concentrations.[34] Significant generation of cross-linked DNA in the human breast adenocarcinoma cell line MDA468 transfected by wild-type NQO1 (NQ16) was observed after treatment by another bezoquinone, RH1, at a concentration as low as 50 nM.[30] However, very low induction of DNA cross-linking was observed in the parental cell line (MDA468) that had no measurable NQO1 activity after exposure to RH1 at a concentration 10-times higher than the concentration used in NQ16 cells.[30] One group

also determined activation of RH1 both *in vitro* and *in vivo* in NQ16 cell line and NQ16 xenografts, respectively.[31] The authors observed a significant dose-dependent reduction in tumor size in mice bearing NQ16 human tumor xenografts after treatment with low-, medium- and high-dose RH1.[31] In contrast, tumor growth inhibition in mice with NQO1-deficient MDA468 xenografts was demonstrated only at high doses of RH1.[31]

Selective formation of DNA interstrand cross-links, adducts and strand breaks by the quinone-based anticancer agents, and their preferential cytotoxicity in different NQO1-rich versus NQO1-deficient cells in these studies demonstrate the important role that NQO1 plays in the bioreductive activation of these agents. This is of primary interest since agents that are bioactivated by NQO1 can result in selective tumor toxicity without high levels of toxicity to normal tissues.[9] This characteristic of NQO1 is considered as one major element of enzyme-directed bioreductive drug development.[5]

1.3 Antitumor Quinones

Quinones are among the most important and largest groups of natural and synthetic anticancer drugs.[57] Two general mechanisms of quinone-based toxicity have been identified; redox cycling and macromolecule alkylation reactions.[57]

1.3.1 Quinone-based Bioreductive Agents in Use or in Clinical Trials. SN, MMC, EO9, AZQ and RH1 are examples of quinone-based bioreductive agents that are currently in use, clinically evaluated or in clinical trials.[1]

SN is a natural aminoquinone antitumor antibiotic that has demonstrated antitumor activity toward a broad range of tumors such as lung, head and neck, breast,

lymphoma and melanoma.[58] This drug was in clinical use until the 1970s when its use in chemotherapy was discontinued due to high toxicity and severe bone marrow depression.[58] MMC, a naturally occurring antitumor bioreductive drug, is the only quinone-containing alkylating agent that is currently in use in the clinic.[1] MMC possesses activity against stomach, lung, prostate, head and neck, bladder and breast tumors.[1,9] However, its dose-limiting toxicity, delayed bone marrow suppression, has greatly restricted the clinical use of this drug.[1,9,59]

The aziridinylbenzoquinone AZQ with good solubility, underwent clinical trials for the treatment of central nervous system (CNS) tumors.[1,9,59] Although it displayed some antitumor activity against brain tumors, it was not significantly more effective than other agents already in use.[9,59] AZQ also exhibited dose-limiting toxicities such as leukopenia and thrombocytopenia.[1,59] EO9, a synthetic analogue of MMC, is an improved substrate for NQO1 compared to MMC.[9] It was selected for clinical trials in the early 1990s due to its excellent antitumor activity in preclinical studies and lack of bone marrow suppression.[1,9] Despite the promising preclinical results, EO9 failed to exhibit any antitumor activity against breast, colon, gastric, pancreatic and non-small-cell lung cancer in phase II clinical trials.[1,9] EO9's failure in the clinical trials has been attributed to its short half-life and poor tissue penetration.[1,9,59] RH1, a water-soluble aziridinylbenzoquinone, is an excellent substrate for NQO1 and is currently in clinical trials.[9] Bone marrow suppression and inflammation in the injection site have been reported as the RH1 toxicities.[9] Due to the high levels of toxicity of these compounds there is an ongoing need for discovery of improved bioreductive quinone-based antitumor agents with higher safety profiles.

1.3.2 Lavendamycin. Lavendamycin, a naturally occurring 7-aminoquinoline-5,8-dione antitumor antibiotic, was first isolated from the fermentation broth of *Streptomyces lavendulae* (strain C-22030) by Balitz et al. in 1981 and was reported in 1982.[60] They characterized the producing culture, fermentation and isolation conditions of lavendamycin, and tested its biological activity.[60] Prior to this report, the structure of lavendamycin was determined and reported by Doyle et al. in 1981.[61] This study determined that lavendamycin is a 7-aminoquinoline-5,8-dione pentacyclic structure with two moieties including quinoline-5,8-dione and indolopyridine (β-carboline) (Chart 1.1).[61]

Lavendamycin has been shown to possess both *in vitro* and *in vivo* antitumor activity.[60,62] In an *in vivo* study, this compound exhibited antitumor effects against P-388-J leukemia ascites cells implanted into BDF1 mice (i.p.) when administered on a daily basis for 9 days.[60] Lavendamycin increased the median survival time (MST) of the treated animals compared to control animals that received saline.[60] Lavendamycin-treated animals also displayed higher MST values and MST treated/MST control x 100 ratios when results were expressed in days and as percentage of control MST, respectively.[60] In addition, lavendamycin has displayed *in vitro* antiproliferative activities against cancer cell lines such as P388 murine leukemia, MKN45 human gastric carcinoma and WiDr colon adenocarcinoma cells.[62] The maximum tolerated dose of lavendamycin in mice is 12.8 mg/kg which is 32 folds higher than that for SN and is therefore less toxic than SN.[60] Despite the interest in lavendamycin as an antitumor agent, this agent was precluded from preclinical development due to its poor aqueous solubility and its toxicity toward normal human cells.[63-65]

1.3.3 Lavendamycin Analogues and Significance. Lavendamycin has been the focus of several synthetic studies to elucidate the structural features that are required for its cytotoxic activity and to develop improved analogues with potent antitumor properties and lower animal toxicity. Initial structure-activity relationship (SAR) studies have demonstrated that the essential moiety for the cytotoxic activity of lavendamycin is the 7-aminoquinoline-5,8-dione moiety.[63] In a recent study *in vitro* and *in vivo* antitumor effects of several lavendamycin analogues were tested.[65] Four analogues, MB-21, -47, -121 and -311, suppressed the clonogenic survival of A549 human lung carcinoma cells at concentrations less than 100 nM with MB-121 being the most potent analogue that inhibited A549 colony growth by 70% at a concentration of 100 nM.[65] Also, the colony outgrowth of the cells was reduced by 70% at 10 nM and by 100% at 100 nM concentration of the lavendamycin analogue MB-97.[65] Although PC-3 human prostate cancer cell line is rather resistant to antitumor effects of many antitcancer agents, these cells displayed sensitivity toward the cytotoxic properties of MB-97 at a concentration as low as 10 nM.[65] MB-97 also exhibited promising antiproliferative activities against cancer cell lines of the National Cancer Institute (NCI) 60-cell line panel including colon, ovarian and renal cells, and cancer cells in a hollow fiber tumorigenesis assay.[65]

It has been reported that lavendamycin analogues possess low animal toxicity especially compared to SN and the parent lavendamycin compound.[64,66] The NCI *in vivo* studies have reported that the maximum tolerated dose of three lavendamycin analogues MB-22, -76 and -97 in mice is 400 mg/kg which is 31 and 1000 times higher than that for lavendamycin and SN, respectively.[64,66] The lavendamycin analogue MB-51 greatly reduced tumor volume (up to 80%) in mice bearing tumor xenografts at a daily dose of

300 mg/kg for 10 days without exhibiting drug-related weight loss or lethality.[67] A recent study also demonstrated that the normal rat kidney epithelial cell line (NRK-52E) exhibited much less sensitivity to several lavendamycin analogues compared to the tumor cells with the same origin.[64] When lavendamycin analogues MB-50 and -51 at a daily dose of 300 mg/kg and MB-21 at a daily dose of 100 mg/kg were administered to nude mice for eight and seven days, respectively, no drug-related deaths or toxicity were observed.[64] Analogues MB-21, -50 and -51 inhibited tumor growth in nude mice by 69, 88 and 78%, respectively, when administered at 100, 150 and 300 mg/kg for 7, 8 and 8 days, respectively.[64] These studies demonstrate remarkable low *in vivo* toxicity of lavendamycin analogues and highlight them as appropriate candidates for anticancer drug development.

1.4 NQO1 X-ray Crystal Structures and Molecular Docking Studies

1.4.1 NQO1 Crystal Structures. X-ray crystallography is the principal source to acquire structural information for protein-ligand complexes.[68] X-ray crystal structures of protein-ligand complexes have played a key role in drug discovery and development for therapeutically relevant target proteins in recent years.[69-71] Complex crystal structures of protein-ligand have provided researchers with useful information on the ligand orientation in the active site and corresponding protein-ligand interactions.[69] These data can in turn contribute to SAR studies and subsequent structure-based ligand design and optimization.[69] NQO1 crystals for the purpose of x-ray crystallographic studies were first prepared from mouse and rat liver in the late 1980s by Amzel et al. and Ysern et al.[72,73] They reported preliminary x-ray diffraction data on NQO1 crystals.[72,73]

Detailed structural information of NQO1 has been a crucial factor in proper understanding of the catalytic mechanism (ping-pong mechanism) of the obligatory two-electron reduction by NQO1.[10] Li et al. employed three-dimensional (3D) crystal structures of NQO1 to elucidate the enzymatic ping-pong mechanism of NQO1.[10] In 1995, They determined the crystal structure of rat liver NQO1 by x-ray diffraction to a resolution of 2.1 Å (Protein Data Bank = PDB ID: 1QRD).[10] They prepared two complex NQO1 crystal structures, complex I containing both Cibacron blue (a potent inhibitor of NQO1) and duroquinone, tetramethyl-1,4-benzoquinone, and complex II containing $NADP^+$.[10] Comparison of the two complexes indicated that duroquinone overlaps the position occupied by the nicotinamide ring of $NADP^+$.[10] This clearly explains the ping-pong catalytic mechanism of NQO1 where substrate binding and reduction cannot occur until $NADP^+$ is released.[10] They also determined that Cibacron blue occupied the same position as the rest of the $NADP^+$, but did not overlap the duroquinone position.[10] This observation shed light on the inhibition pattern of NQO1 by Cibacron blue that is competitive with respect to NADH and noncompetitive in regard to quinone substrates.[10]

The information obtained in another study from the 3D crystal structures of human NQO1 in complex with RH1, EO9 and ARH019 (PDB ID: 1H66, 1GG5 and 1H69, respectively) determined that antitumor quinones can bind to NQO1 in different orientations.[37] The study of these complex crystal structures further determined that NQO1 possesses a highly plastic active site that can accommodate quinone compounds of different sizes.[37] The authors suggested that these complex crystal structures could provide crucial insights for the optimization of bioreductive anticancer quinones.[37] They demonstrated that amino acid residues Tyr-126, -128 and His-161 can interact with the

quinone substrates inside the active site and stabilize the binding.[37] This group also determined the crystal structure of NQO1 in complex with duroquinone to 2.5-Å resolution.[13] They subsequently defined the NQO1 active site structure and demonstrated the importance of Trp-105, -106, Tyr-126, -128 and Phe-178 residues in formation of interactions with the ligand.[13] The crystal structure of NQO1 in complex with indolequinone ARH019 was recommended by this group as a potential model for docking studies of other anticancer quinones including SN.[37]

The binding characteristics of lavendamycin analogues in the NQO1 active site are not yet known. Due to the fact that there are no available complex crystal structures of NQO1 with lavendamycin analogues, one can utilize crystal structure-based molecular docking studies to obtain detailed understanding of the molecular basis of interactions of these compounds with NQO1.

1.4.2 Molecular Docking Studies of Bioreductive Quinones with NQO1.

Molecular modeling studies of quinone-based antitumor compounds with NQO1 could indicate structural limitations on the potential substrates for the enzyme.[74] Docking studies could greatly assist with SAR studies and structure-based design of novel NQO1 quinone substrates.[1,74] These studies could also predict the preferred orientation of quinone antitumor compounds within the active site.[40] Molecular docking studies also assist researchers to obtain insights into the role that amino acid residues play in substrate binding affinity.[75]

The indolequinone SAR study by one group demonstrated that when the aziridinyl group of EO9 or the methoxy group of another indolequinone at the C5 position was replaced with methylaziridine, substrate specificity of the compounds was

reduced.[74] They were able to explain this observation by performing molecular modeling studies of the indolequinone EO9 with NQO1.[74] They determined that the Trp-106 played a major role in forming favorable van der Waals interactions with an aziridinyl or a methoxy group at the C5 position.[74] However, methylaziridinyl substituent at C5 created steric interactions with the Trp-106 residue resulting in unfavorable positioning of the quinone moiety for reduction.[74] In addition, Zhou et al. observed that when the number of fused rings in the quinone nucleus of quinone compounds increased from one ring in benzoquinones to two or three rings in naphthoquinones or anthraquinones, respectively, the substrate specificity of the compounds was improved.[40] They took advantage of docking studies to demonstrate the importance of π-ring stacking in determination of ligand binding affinity.[40] Another group designed a series of quinone substrates including dipyrroloimidazobenzimidazole and dipyridoimidazobenzimidazole systems as potential good substrates for NQO1 compounds.[75] They then modeled these substrates into the NQO1 active site to investigate the correlation of docking data with the substrate specificity of the compounds.[75] The correlation of the docking models with biological data provided the researchers with information regarding structural requirements of the substrates.[75] They observed that derivatives with unsubstituted pyrido or pyrrolo rings, or with one acetate group on the rings were excellent substrates for NQO1.[75] Docking models displayed that the pyrido or pyrrolo ring of derivatives bearing no or only one substituent could intercalate between and form favorable van der Waals interactions with the Trp-105 and Phe-106 residues. However, derivatives with substituents on both rings created steric interactions with the residues leading to poor

substrate specificity of these compounds.[75] All these studies took advantage of docking studies to explain observed substrate specificity of ligands and the related SAR data.

Molecular docking methods have become very useful tools in structure-based ligand design because they provide information on the binding events and key interactions between a known or newly designed ligand and its target protein. Understanding these interactions is crucial to the success of drug design for bioreductive antitumor quinone development.

1.5 Structure-based Ligand Design

Structure-based ligand design - also known as structure-based design or rational ligand design - is a process that involves the optimization of ligand affinity and logic-based transformation of hit compounds to candidate drugs.[68,76] The theory behind the structure-based design process is that development of improved ligands will result in higher binding affinities and higher activities against the biological targets.[77,78] The 3D structure of therapeutic targets is the starting point in this process and due to increasing availability of these structures, structure-based design has gained momentum in recent years.[77,78] This process utilizes information obtained from an available 3D structure of a biological target-ligand complex to design new drugs for human diseases.[77] In a practical structure-based design process computational docking tools are very useful in extracting the information about binding events.[77,78] They are utilized to characterize the type of interactions between a known or designed ligand and the target protein.[77,78] Use of *in silico* (computer-based) methods in structure-based design entails a sequence of steps

such as coordinate preparation of target molecule, docking and post-docking analysis to extract the required structural information.[76] This contributes to the design of improved ligands from which a small, most promising group can be selected to be synthesized and tested.[68,77] It has been reported that on average it takes 14-15 years and hundreds of millions of dollars for a hit compound to evolve to an approved drug.[76,77] Computational methods including docking programs and ligand scoring functions used in drug design can accelerate this process and decrease high expenses of drug discovery and development.[77] The discovery of important classes of drugs such as HIV-protease inhibitors, carbonic anhydrase II inhibitors, and late-clinical-stage candidates including inhibitors of human non-pancreatic secretory phospholipase A2 has been greatly facilitated by the structure-based design process.[68]

1.6 Redox-cycling Bioreductive Antitumor Quinones

NQO1 plays a major role in the bioactivation of several quinone-based anticancer agents including SN,[19,20] MMC,[22] β-lapachone,[24] AZQ[33-35] and RH1.[30,31] The hydroquinone produced after the two-electron reduction of these agents is the biologically active form that can cause DNA alkylation and/or oxidative stress.[1,24,79] Quinones are powerful redox active agents that can undergo redox cycling, which is the enzymatic reduction of quinones and subsequent auto-oxidation of the reduced forms to parent compounds with concomitant generation of superoxide anion radical ($O_2^{\cdot-}$) .[79,80] When quinones undergo redox cycling following a two-electron reduction by NQO1, the corresponding redox active hydroquinones can react with molecular oxygen through a

one-electron oxidation process to yield semiquinones and $O_2^{-\cdot}$.[79,80] Semiquinones can then react with molecular oxygen to generate $O_2^{-\cdot}$ and auto-oxidize back to parent quinones.[79,80]

Produced $O_2^{-\cdot}$ in this process is a propagating species that can dismutate into hydrogen peroxide (H_2O_2) with ultimate production of extremely toxic hydroxyl radicals ($OH^{\cdot}$).[9,42,58,81-83] This NQO1-mediated redox-cycling process of quinones can produce large quantities of reactive oxygen species (ROS).[83] Excessive levels of produced ROS in cells can overpower the antioxidant defense systems and modulate the intracellular redox balance leading to a situation known as oxidative stress.[84,85]

Many studies have demonstrated the NQO1-mediated redox-cycling ability of anticancer quinone-based agents. Hydroxyethylaminoalkylamino-substituted anthraquinones (AQs) such as 1-AQ and 1,8-AQ have displayed redox-cycling characteristics in NQO1-rich human breast cancer MCF-7 cells.[86] Also, NQO1-mediated ROS and semiquinone formation by AZQ, hydroxyl radical formation by a variety of quinone antitumour compounds and ROS formation by anthraquinone-based antitumour agents in the presence of purified rat liver NQO1 and NQO1-rich MCF-7 cells have been determined.[35,87-89] These studies have demonstrated that the hydroquinone form of these quinone agents, following reduction by NQO1, undergoes a two-step one-electron oxidation process with concomitant production of the damaging species such as semiquinones and ROS.

Indolequinones, naphthoquinones and quinolinediones are also among the antitumor compounds that generate biologically active species after reduction by NQO1 via redox cycling. The ability of the indolequinone EO9 to redox cycle in the presence of

purified rat Walker tumor cell NQO1 and NAD(P)H following a two-electron reduction has been reported.[90] Furthermore, Pink et al. determined that NQO1 reduces β-lapachone to an unstable hydroquinone that can auto-oxidize back to the parent form, possibly through a semiquinone intermediate.[24] They proposed this redox cycling can cause oxidative stress and cytotoxicity.[24] SN, a prototypical and efficient redox-cycling antitumor agent, can also produce large quantities of ROS after bioactivation by NQO1.[19,56,83] The ability of SN to undergo redox cycling after bioactivation by NQO1 in NQO1-rich HT-29 cells and to produce hydroxyl radical-mediated DNA strand breaks has been reported.[19] These studies suggest that NQO1-mediated metabolism of redox-cycling antitumor quinones can alter the intracellular redox balance, cause DNA damage and the corresponding cytotoxicity.

1.6.1 Redox-cycling Antitumor Quinones and Intracellular Redox State. The intracellular redox responses and antioxidant defense systems in neoplastic cells play a major role in their protection against antitumor agents.[79,85] Chemotherapeautic agents that possess the ability to alter the intracellular redox environment in favor of oxidative stress can induce apoptosis and be utilized in cancer treatment.[79,85] It has been determined that the production of ROS is an important mechanism of cytotoxicity of many antitumor agents.[85] Tumor cells employ antioxidant defense systems such as reducing species to neutralize ROS and avoid potential ROS-mediated cellular damage and subsequent induction of apoptosis.[85] Glutathione (GSH), a non-protein cellular thiol, is a key component of the intracellular defense system against oxidative stress and is involved in detoxification of ROS.[85] The ability of cells to maintain GSH levels during

an oxidative challenge is of vital importance in the maintenance of cellular function, integrity and viability.[91]

Thiol oxidation by the ROS produced during metabolism and redox cycling of quinones is a key feature of quinone toxicity.[81] GSH oxidation and depletion in a cell-free system due to NQO1-mediated redox cycling of AZQ have been demonstrated.[92] Menadione, a redox cycling 1,4-naphthoquinone, caused oxidative stress in cultured human-derived endothelial cells (EA.hy926) that was assessed by oxidation of intracellular dihydrofluorescein.[93] This compound at a concentration of 100 μM significantly reduced the intracellular GSH levels in EA.hy926 cells after a 30-minute exposure period.[93] GSH oxidation and consumption by $O_2^{\cdot-}$ during NQO1 catalysis of 2-methylmethoxy-1,4-naphthoquinone have also been observed.[94] The reduction of 2-methylmethoxy-1,4-naphthoquinone by NQO1 in this study was associated with formation of calf thymus DNA strand breaks that were suppressed by the presence of superoxide dismutase and catalase by 85-90%.[94] These findings suggest that intracellular redox state alteration can occur as the result of metabolism of redox-cycling quinones. The ability of a cell to maintain a proper oxidant-antioxidant balance can determine the outcome of an apoptosis-triggering signal.[79] Production of ROS and depletion of GSH can lead to oxidative stress with subsequent induction of apoptosis in cancer cells.[85]

1.6.2 Redox-cycling Antitumor Quinones and Oxidative DNA Damage.

DNA has been recognized as the principal target of quinone-based antineoplastic compounds.[57] Quinone redox cycling can generate excessive amounts of ROS and when the generated ROS are not adequately neutralized, they become involved in many oxidative stress-related events such as DNA strand breaks or oxidative DNA damage.[57,95]

Hydroxyl radical, the most destructive species among oxygen radicals, is highly toxic, capable of attacking DNA, and oxidizing guanine bases resulting in the formation of mutagenic 8-hydroxy-2'-deoxyguanosine (8-oxo-2dG) lesions.[57] Among the purine and pyrimidine bases of DNA, guanine is the most sensitive base to oxidation.[96,97] During an oxidative attack, a hydroxyl group is added to the eighth position of the guanine base generating an 8-oxo-2dG oxidative adduct.[96] 8-Oxo-2dG is one of the most frequently studied and predominant forms of oxidative DNA damage.[98] During DNA replication, the modified base, 8-oxo-2dG, pairs with adenine instead of cytosine, resulting in G:C → T:A transversion mutations.[97]

The most important reactions involving quinones are generation of ROS and DNA damage.[79] It has been reported that redox cycling of AZQ produces 8-oxo-2dG lesions (unpublished data).[95] Pagano et al. also demonstrated significant production of 8-oxo-2dG in sea urchin embryos after exposure to the antitumor quinone MMC at a concentration as low as 1 μM.[99] Their results further associated MMC-induced toxicity with the induction of oxidative stress and oxidative DNA damage.[99] Investigation of DNA damage production by antitumor agents is important since it has been known for more than 25 years that DNA damage can induce apoptosis.[100]

1.6.3 Redox-cycling Antitumor Quinones and Apoptosis. Apoptosis, or programmed cell death, can be induced by DNA damage,[100] and plays a key role in tumor suppression and in regulation of cell populations.[101] Many cancer cells develop strategies to deregulate or circumvent apoptosis and these are important contributing factors in tumor development.[101] Therefore, the ability of anticancer agents to efficiently induce apoptosis in tumor cells is of great importance. Although, apoptosis can be induced in

various ways, it can be distinguished by highly conserved morphological characteristics including nuclear condensation, cell shrinkage and DNA fragmentation into oligonucleosomes.[101]

Quinones are an important group of anticancer agents that induce apoptosis via redox cycling.[102] Since the mechanism of cytotoxicity of redox-cycling quinones is due to free radical production, induction of oxidative stress and DNA damage, quinones are considered as powerful inducers of apoptosis.[79] Induction of apoptosis is the principal mechanism of cytotoxicity of β-lapachone in human prostate[103] and breast[104] cancer cells. NQO1 activity is a key determinant of β-lapachone-mediated cytotoxicity and apoptosis induction in NQO1-expressing prostate cancer cells.[25] In addition, MMC, MeDZQ (an aziridinylbenzoquinone) and SN can preferentially induce NQO1-mediated apoptosis in NQO1-rich HT-29 cells compared to NQO1-deficient BE cells.[20] Therefore, an association between the NQO1 activity in these cells and the corresponding cytotoxicity and apoptosis induction by these quinone anticancer compounds is observed.

1.7 *In Vitro* Models for NQO1-directed Bioreductive Anticancer Quinone Development

To examine the importance of the role of NQO1 in the bioactivation of quinone-based antitumor agents, a common approach has been to use tumor cell lines that differ in NQO1 expression levels.[22,28,34,56] When non-isogenic paired cell line models are utilized, the results of bioreductive activation of compounds by NQO1 are prone to the effects of confounding factors including genotypic differences in the cell lines.[31,105,106] Differences

in activities of other reductases and in the expression of genes that impact drug metabolism are examples of different genotypic profiles of non-isogenic cell lines.[31,105] To better control and study the role of NQO1 in the bioreductive activation of antitumor quinones, isogenic cell line pairs that only differ in NQO1 expression have been developed.[31,105,106]

An isogenic cell model for NQO1 expression employing BE cells was established by Sharp et al in 2000.[105] They stably transfected BE cells, which possess no NQO1 activity due to a disabling genetic polymorphism (NQO1*2/*2), with an expression vector containing human NQO1 cDNA.[105] They demonstrated stable high-expression levels of NQO1 in the transfected cells (BE2) using Western blot analysis and enzyme activity assay.[105] They did not observe any differences in the cell lines in regards to the activity of other reductases that may be involved in drug metabolism.[105] This group observed selective toxicity of EO9 and SN towards NQO1-rich clones compared to NQO1-deficient BE cells.[105] Similar to this model, stably transfected BE-NQ cells that express wild type NQO1 were also developed using BE cells by a second group in 2001.[106] They demonstrated using MTT and clonogenic assays that BE-NQ cells were more susceptible to the cytotoxic effects of SN and RH1 in comparison with BE cells.[106] These pairs of isogenic cell lines have been suggested as proper models for NQO1-mediated mechanistic studies and antitumor quinone development.[105,106]

Dehn et al. have also developed and validated an isogenic cell line pair using human breast adenocarcinoma cells, MDA468, which lacks NQO1 activity due to the same homozygous point mutation in the NQO1 gene.[31] They stably transfected MDA468 cells with human wild-type NQO1 cDNA to generate the NQ16 cells that express very

high levels of NQO1.[31] Levels of reductases, soluble thiols and superoxide dismutase were compared in both cell lines and no significant differences in the corresponding levels were determined.[31] The selective toxicity of RH1 and SN towards NQ16 cells compared to NQO1-deficient MDA468 cells demonstrated functional validation of this isogenic model.[31]

1.8 Hypothesis

Using SAR, metabolism, *in vitro* cytotoxicity studies, and computer-aided and structure-based ligand design methods, this project studied NAD(P)H:quinone oxidoreductase (NQO1)-directed lavendamycin antitumor agents. We hypothesized that NQO1 could bioactivate good lavendamycin substrates resulting in their redox cycling with concomitant induction of oxidative stress. The activated lavendamycin substrates would be expected to display selective toxicity towards NQO1-rich cancer cells via thiol depletion, oxidative DNA damage and apoptosis induction. In addition, development of an *in silico* model of the NQO1 active site in conjunction with SAR studies would highly contribute to the structure-based design of more optimal lavendamycin substrates and NQO1-directed lavendamycin antitumor agent development.

1.9 Specific Aims

1.9.1 Specific Aim I. Determine the role of NQO1 in the bioreductive activation and cytotoxicity of lavendamycin analogues in NQO1-deficient (BE) and

NQO1-rich (BE-NQ) cancer cells and indicate the structural requirements for substrate specificity of these compounds - SAR studies (Chapter 2).

1.9.2 Specific Aim II. Develop an *in silico* NQO1 active site model and perform docking studies to facilitate NQO1-directed lavendamycin antitumor agent development and structure-based design of novel lavendamycin analogues (Chapters 3 and 4).

1.9.3 Specific Aim III. Investigate mechanisms of NQO1-mediated selective cytotoxicity of good lavendamycin substrates towards NQO1-rich BE-NQ cell line compared to BE cells (Chapter 5).

1.10 References

(1) Beall, H. D.; Winski, S. I. Mechanisms of action of quinone-containing alkylating agents. I: NQO1-directed drug development. *Front. Biosci.* **2000**, *5*, 639-648.

(2) Rooseboom, M.; Commandeur, J. N.; Vermeulen, N. P. Enzyme-catalyzed activation of anticancer prodrugs. *Pharmacol. Rev.* **2004**, *56*, 53-102.

(3) Workman, P. Keynote address: Bioreductive mechanisms. *Int. J. Radiat. Oncol. Biol. Phys.* **1992**, *22*, 631-637.

(4) Phillips, R. M. Prospects for bioreductive drug development. *Exp. Opin. Invest. Drugs* **1998**, *7*, 905-928.

(5) Workman, P. Enzyme-directed bioreductive drug development revisited: A commentary on recent progress and future prospects with emphasis on quinone anticancer agents and quinone metabolizing enzymes, particularly DT-diaphorase. *Oncol. Res.* **1994**, *6*, 461-475.

(6) Workman, P.; Walton, M. I. Enzyme-directed bioreductive drug development. *Selective activation of drugs by redox processes* **1990**, 173-191.

(7) Adams, G. E.; Stratford, I. J. Bioreductive drugs for cancer therapy: the search for tumor specificity. *Int. J. Radiat. Oncol. Biol. Phys.* **1994**, *29*, 231-238.

(8) Workman, P.; Stratford, I. J. The experimental development of bioreductive drugs and their role in cancer therapy. *Cancer Metastasis Rev.* **1993**, *12*, 73-82.

(9) Danson, S.; Ward, T. H.; Butler, J.; Ranson, M. DT-diaphorase: A target for new anticancer drugs. *Cancer Treat. Rev.* **2004**, *30*, 437-449.

(10) Li, R.; Bianchet, M. A.; Talalay, P.; Amzel, L. M. The three-dimensional structure of NAD(P)H:quinone reductase, a flavoprotein involved in cancer chemoprotection and chemotherapy: Mechanism of the two-electron reduction. *Proc. Natl. Acad. Sci. U. S. A.* **1995**, *92*, 8846-8850.

(11) Lind, C.; Cadenas, E.; Hochstein, P.; Ernster, L. DT-diaphorase: Purification, properties, and function. *Methods Enzymol.* **1990**, *186*, 287-301.

(12) Skelly, J. V.; Sanderson, M. R.; Suter, D. A.; Baumann, U.; Read, M. A.; Gregory, D. S.; Bennett, M.; Hobbs, S. M.; Neidle, S. Crystal structure of human DT-diaphorase: A model for interaction with the cytotoxic prodrug 5-(aziridin-1-yl)-2,4-dinitrobenzamide (CB1954). *J. Med. Chem.* **1999**, *42*, 4325-4330.

(13) Faig, M.; Bianchet, M. A.; Talalay, P.; Chen, S.; Winski, S.; Ross, D.; Amzel, L. M. Structures of recombinant human and mouse NAD(P)H:quinone oxidoreductases: Species comparison and structural changes with substrate binding and release. *Proc. Natl. Acad. Sci. U. S. A.* **2000**, *97*, 3177-3182.

(14) Ernster, L. DT Diaphorase: A historical review. *Chem. Scripta* **1987**, *27A*, 1-13.

(15) Ernster, L.; Danielson, L.; Ljunggren, M. DT diaphorase. I. Purification from the soluble fraction of rat-liver cytoplasm, and properties. *Biochim. Biophys. Acta.* **1962**, *58*, 171-188.

(16) Eliasson, M.; Bostrom, M.; DePierre, J. W. Levels and subcellular distributions of detoxifying enzymes in the ovarian corpus luteum of the pregnant and non-pregnant pig. *Biochem. Pharmacol.* **1999**, *58*, 1287-1292.

(17) Winski, S. L.; Koutalos, Y.; Bentley, D. L.; Ross, D. Subcellular localization of NAD(P)H:quinone oxidoreductase 1 in human cancer cells. *Cancer Res.* **2002**, *62*, 1420-1424.

(18) Ernster, L. DT Diaphorase. *Methods Enzymol.* **1967**, *10*, 309-317.

(19) Beall, H. D.; Liu, Y.; Siegel, D.; Bolton, E. M.; Gibson, N. W.; Ross, D. Role of NAD(P)H:quinone oxidoreductase (DT-diaphorase) in cytotoxicity and induction of DNA damage by streptonigrin. *Biochem. Pharmacol.* **1996**, *51*, 645-652.

(20) Sun, X.; Ross, D. Quinone-induced apoptosis in human colon adenocarcinoma cells via DT-diaphorase mediated bioactivation. *Chem. Biol. Interact.* **1996**, *100*, 267-276.

(21) Lewis, A. M.; Ough, M.; Du, J.; Tsao, M. S.; Oberley, L. W.; Cullen, J. J. Targeting NAD(P)H:Quinone oxidoreductase (NQO1) in pancreatic cancer. *Mol. Carcinog.* **2006**.

(22) Siegel, D.; Gibson, N. W.; Preusch, P. C.; Ross, D. Metabolism of mitomycin C by DT-diaphorase: Role in mitomycin C-induced DNA damage and cytotoxicity in human colon carcinoma cells. *Cancer Res.* **1990**, *50*, 7483-7489.

(23) Siegel, D.; Beall, H. D.; Senekowitsch, C.; Kasai, M.; Arai, H.; Gibson, N. W.; Ross, D. Bioreductive activation of mitomycin C by DT-diaphorase. *Biochemistry* **1992**, *31*, 7879-7885.

(24) Pink, J. J.; Planchon, S. M.; Tagliarino, C.; Varnes, M. E.; Siegel, D.; Boothman, D. A. NAD(P)H:Quinone oxidoreductase activity is the principal determinant of beta-lapachone cytotoxicity. *J. Biol. Chem.* **2000**, *275*, 5416-5424.

(25) Planchon, S. M.; Pink, J. J.; Tagliarino, C.; Bornmann, W. G.; Varnes, M. E.; Boothman, D. A. beta-Lapachone-induced apoptosis in human prostate cancer cells: Involvement of NQO1/xip3. *Exp. Cell Res.* **2001**, *267*, 95-106.

(26) Walton, M. I.; Smith, P. J.; Workman, P. The role of NAD(P)H: quinone reductase (EC 1.6.99.2, DT-diaphorase) in the reductive bioactivation of the novel indoloquinone antitumor agent EO9. *Cancer Commun.* **1991**, *3*, 199-206.

(27) Swann, E.; Barraja, P.; Oberlander, A. M.; Gardipee, W. T.; Hudnott, A. R.; Beall, H. D.; Moody, C. J. Indolequinone antitumor agents: Correlation between quinone structure and rate of metabolism by recombinant human NAD(P)H:quinone oxidoreductase. Part 2. *J. Med. Chem.* **2001**, *44*, 3311-3319.

(28) Beall, H. D.; Winski, S.; Swann, E.; Hudnott, A. R.; Cotterill, A. S.; O'Sullivan, N.; Green, S. J.; Bien, R.; Siegel, D.; Ross, D.; Moody, C. J. Indolequinone antitumor agents: Correlation between quinone structure, rate of metabolism by recombinant human NAD(P)H:quinone oxidoreductase, and in vitro cytotoxicity. *J. Med. Chem.* **1998**, *41*, 4755-4766.

(29) Nemeikaite-Ceniene, A.; Dringeliene, A.; Sarlauskas, J.; Cenas, N. Role of NAD(P)H:quinone oxidoreductase (NQO1) in apoptosis induction by aziridinylbenzoquinones RH1 and MeDZQ. *Acta Biochim. Pol.* **2005**, *52*, 937-941.

(30) Dehn, D. L.; Inayat-Hussain, S. H.; Ross, D. RH1 induces cellular damage in an NAD(P)H:quinone oxidoreductase 1-dependent manner: Relationship between DNA cross-linking, cell cycle perturbations, and apoptosis. *J. Pharmacol. Exp. Ther.* **2005**, *313*, 771-779.

(31) Dehn, D. L.; Winski, S. L.; Ross, D. Development of a new isogenic cell-xenograft system for evaluation of NAD(P)H:quinone oxidoreductase-directed antitumor quinones: evaluation of the activity of RH1. *Clin. Cancer Res.* **2004**, *10*, 3147-3155.

(32) Winski, S. L.; Hargreaves, R. H.; Butler, J.; Ross, D. A new screening system for NAD(P)H:quinone oxidoreductase (NQO1)-directed antitumor quinones: Identification of a new aziridinylbenzoquinone, RH1, as a NQO1-directed antitumor agent. *Clin. Cancer Res.* **1998**, *4*, 3083-3088.

(33) Ngo, E. O.; Nutter, L. M.; Sura, T.; Gutierrez, P. L. Induction of p53 by the concerted actions of aziridine and quinone moieties of diaziquone. *Chem. Res. Toxicol.* **1998**, *11*, 360-368.

(34) Siegel, D.; Gibson, N. W.; Preusch, P. C.; Ross, D. Metabolism of diaziquone by NAD(P)H:(quinone acceptor) oxidoreductase (DT-diaphorase): Role in diaziquone-induced DNA damage and cytotoxicity in human colon carcinoma cells. *Cancer Res.* **1990**, *50*, 7293-7300.

(35) Fisher, G. R.; Gutierrez, P. L. Free radical formation and DNA strand breakage during metabolism of diaziquone by NAD(P)H quinone-acceptor oxidoreductase (DT-diaphorase) and NADPH cytochrome c reductase. *Free Radic. Biol. Med.* **1991**, *11*, 597-607.

(36) Asher, G.; Dym, O.; Tsvetkov, P.; Adler, J.; Shaul, Y. The crystal structure of NAD(P)H quinone oxidoreductase 1 in complex with its potent inhibitor dicoumarol. *Biochemistry* **2006**, *45*, 6372-6378.

(37) Faig, M.; Bianchet, M. A.; Winski, S.; Hargreaves, R.; Moody, C. J.; Hudnott, A. R.; Ross, D.; Amzel, L. M. Structure-based development of anticancer drugs: Complexes of NAD(P)H:quinone oxidoreductase 1 with chemotherapeutic quinones. *Structure* **2001**, *9*, 659-667.

(38) Winski, S. L.; Faig, M.; Bianchet, M. A.; Siegel, D.; Swann, E.; Fung, K.; Duncan, M. W.; Moody, C. J.; Amzel, L. M.; Ross, D. Characterization of a mechanism-based inhibitor of NAD(P)H:quinone oxidoreductase 1 by biochemical, x-ray crystallographic, and mass spectrometric approaches. *Biochemistry* **2001**, *40*, 15135-15142.

(39) Hassani, M.; Cai, W.; Holley, D. C.; Lineswala, J. P.; Maharjan, B. R.; Ebrahimian, G. R.; Seradj, H.; Stocksdale, M. G.; Mohammadi, F.; Marvin, C. C.; Gerdes, J. M.; Beall, H. D.; Behforouz, M. Novel lavendamycin analogues as antitumor agents: synthesis, in vitro cytotoxicity, structure-metabolism, and computational molecular modeling studies with NAD(P)H:quinone oxidoreductase 1. *J. Med. Chem.* **2005**, *48*, 7733-7749.

(40) Zhou, Z.; Fisher, D.; Spidel, J.; Greenfield, J.; Patson, B.; Fazal, A.; Wigal, C.; Moe, O. A.; Madura, J. D. Kinetic and docking studies of the interaction of quinones with the quinone reductase active site. *Biochemistry* **2003**, *42*, 1985-1994.

(41) Cavelier, G.; Amzel, L. M. Mechanism of NAD(P)H:quinone reductase: Ab initio studies of reduced flavin. *Proteins: Struct. Funct. Genet.* **2001**, *43*, 420-432.

(42) Ross, D.; Beall, H.; Traver, R. D.; Siegel, D.; Phillips, R. M.; Gibson, N. W. Bioactivation of quinones by DT-diaphorase, molecular, biochemical, and chemical studies. *Oncol. Res.* **1994**, *6*, 493-500.

(43) Schlager, J. J.; Powis, G. Cytosolic NAD(P)H:(quinone-acceptor)oxidoreductase in human normal and tumor tissue: Effects of cigarette smoking and alcohol. *Int. J. Cancer* **1990**, *45*, 403-409.

(44) Malkinson, A. M.; Siegel, D.; Forrest, G. L.; Gazdar, A. F.; Oie, H. K.; Chan, D. C.; Bunn, P. A.; Mabry, M.; Dykes, D. J.; Harrison, S. D.; Ross, D. Elevated DT-diaphorase activity and messenger RNA content in human non-small cell lung carcinoma: Relationship to the response of lung tumor xenografts to mitomycin C. *Cancer Res.* **1992**, *52*, 4752-4757.

(45) Cresteil, T.; Jaiswal, A. K. High levels of expression of the NAD(P)H:quinone oxidoreductase (NQO1) gene in tumor cells compared to normal cells of the same origin. *Biochem. Pharmacol.* **1991**, *42*, 1021-1027.

(46) Mikami, K.; Naito, M.; Ishiguro, T.; Yano, H.; Tomida, A.; Yamada, T.; Tanaka, N.; Shirakusa, T.; Tsuruo, T. Immunological quantitation of DT-diaphorase in carcinoma cell lines and clinical colon cancers: Advanced tumors express greater levels of DT-diaphorase. *Jpn. J. Cancer Res.* **1998**, *89*, 910-915.

(47) Phillips, R. M.; Burger, A. M.; Fiebig, H. H.; Double, J. A. Genotyping of NAD(P)H:quinone oxidoreductase (NQO1) in a panel of human tumor xenografts: relationship between genotype status, NQO1 activity and the response of xenografts to Mitomycin C chemotherapy in vivo(1). *Biochem. Pharmacol.* **2001**, *62*, 1371-1377.

(48) Ross, D.; Siegel, D. NAD(P)H:quinone oxidoreductase 1 (NQO1, DT-diaphorase), functions and pharmacogenetics. *Methods Enzymol.* **2004**, *382*, 115-144.

(49) Jaiswal, A. K. Regulation of genes encoding NAD(P)H:quinone oxidoreductases. *Free Radic. Biol. Med.* **2000**, *29*, 254-262.

(50) Ross, D.; Kepa, J. K.; Winski, S. L.; Beall, H. D.; Anwar, A.; Siegel, D. NAD(P)H:quinone oxidoreductase 1 (NQO1): chemoprotection, bioactivation, gene regulation and genetic polymorphisms. *Chem. Biol. Interact.* **2000**, *129*, 77-97.

(51) Jaiswal, A. K. Human NAD(P)H:quinone oxidoreductase (NQO1) gene structure and induction by dioxin. *Biochemistry* **1991**, *30*, 10647-10653.

(52) Traver, R. D.; Siegel, D.; Beall, H. D.; Phillips, R. M.; Gibson, N. W.; Franklin, W. A.; Ross, D. Characterization of a polymorphism in NAD(P)H: quinone oxidoreductase (DT-diaphorase). *Br. J. Cancer* **1997**, *75*, 69-75.

(53) Traver, R. D.; Horikoshi, T.; Danenberg, K. D.; Stadlbauer, T. H.; Danenberg, P. V.; Ross, D.; Gibson, N. W. NAD(P)H:quinone oxidoreductase gene expression in human colon carcinoma cells: characterization of a mutation which modulates DT-diaphorase activity and mitomycin sensitivity. *Cancer Res.* **1992**, *52*, 797-802.

(54) Fleming, R. A.; Drees, J.; Loggie, B. W.; Russell, G. B.; Geisinger, K. R.; Morris, R. T.; Sachs, D.; McQuellon, R. P. Clinical significance of a NAD(P)H: quinone oxidoreductase 1 polymorphism in patients with disseminated peritoneal cancer

receiving intraperitoneal hyperthermic chemotherapy with mitomycin C. *Pharmacogenetics* **2002**, *12*, 31-37.

(55) Phillips, R. M. Bioreductive activation of a series of analogues of 5-aziridinyl-3-hydroxymethyl-1-methyl-2-[1H-indole-4, 7-dione] prop-beta-en-alpha-ol (EO9) by human DT-diaphorase. *Biochem. Pharmacol.* **1996**, *52*, 1711-1718.

(56) Beall, H. D.; Murphy, A. M.; Siegel, D.; Hargreaves, R. H.; Butler, J.; Ross, D. Nicotinamide adenine dinucleotide (phosphate): quinone oxidoreductase (DT-diaphorase) as a target for bioreductive antitumor quinones: Quinone cytotoxicity and selectivity in human lung and breast cancer cell lines. *Mol. Pharmacol.* **1995**, *48*, 499-504.

(57) Asche, C. Antitumour quinones. *Mini-Rev. Med. Chem.* **2005**, *5*, 449-467.

(58) Bolzan, A. D.; Bianchi, M. S. Genotoxicity of streptonigrin: A review. *Mutat. Res.* **2001**, *488*, 25-37.

(59) Begleiter, A. Clinical applications of quinone-containing alkylating agents. *Front. Biosci.* **2000**, *5*, E153-171.

(60) Balitz, D. M.; Bush, J. A.; Bradner, W. T.; Doyle, T. W.; O'Herron, F. A.; Nettleton, D. E. Isolation of lavendamycin, a new antibiotic from Streptomyces lavendulae. *J. Antibiot. (Tokyo)* **1982**, *35*, 259-265.

(61) Doyle, T. W.; Balitz, D. M.; Grulich, R. E.; Nettleton, D. E.; Gould, S. J.; Tann, C.; Moews, A. E. Structure determination of lavendamycin, a new antitumor antibiotic from Streptomyces lavendulae. *Tetrahedron Lett.* **1981**, *22*, 4595-4598.

(62) Abe, N.; Nakakita, Y.; Nakamura, T.; Enoki, N.; Uchida, H.; Takeo, S.; Munekata, M. Novel cytocidal compounds, oxopropalines from Streptomyces sp.

G324 producing lavendamycin. I. Taxonomy of the producing organism, fermentation, isolation and biological activities. *J. Antibiot. (Tokyo)* **1993**, *46*, 1672-1677.

(63) Boger, D. L.; Yasuda, M.; Mitscher, L. A.; Drake, S. D.; Kitos, P. A.; Thompson, S. C. Streptonigrin and lavendamycin partial structures. Probes for the minimum, potent pharmacophore of streptonigrin, lavendamycin, and synthetic quinoline-5,8-diones. *J. Med. Chem.* **1987**, *30*, 1918-1928.

(64) Behforouz, M.; Cai, W.; Mohammadi, F.; Stocksdale, M. G.; Gu, Z.; Ahmadian, M.; Baty, D. E.; Etling, M. R.; Al-Anzi, C. H.; Swiftney, T. M.; Tanzer, L. R.; Merriman, R. L.; Behforouz, N. C. Synthesis and evaluation of antitumor activity of novel N-acyllavendamycin analogues and quinoline-5,8-diones. *Bioorg. Med. Chem.* **2007**, *15*, 495-510.

(65) Fang, Y.; Linardic, C. M.; Richardson, D. A.; Cai, W.; Behforouz, M.; Abraham, R. T. Characterization of the cytotoxic activities of novel analogues of the antitumor agent, lavendamycin. *Mol. Cancer Ther.* **2003**, *2*, 517-526.

(66) Behforouz, M.; Cai, W.; Stocksdale, M. G.; Lucas, J. S.; Jung, J. Y.; Briere, D.; Wang, A.; Katen, K. S.; Behforouz, N. C. Novel lavendamycin analogues as potent HIV-reverse transcriptase inhibitors: Synthesis and evaluation of anti-reverse transcriptase activity of amide and ester analogues of lavendamycin. *J. Med. Chem.* **2003**, *46*, 5773-5780.

(67) Behforouz, M.; Merriman, R. L. Lavendamycin analogs and methods of making and using them. *U.S. Patent 5525611* **1996**.

(68) Davis, A. M.; Teague, S. J.; Kleywegt, G. J. Application and limitations of X-ray crystallographic data in structure-based ligand and drug design. *Angew. Chem. Int. Ed. Engl.* **2003**, *42*, 2718-2736.

(69) Erickson, J. A.; Jalaie, M.; Robertson, D. H.; Lewis, R. A.; Vieth, M. Lessons in molecular recognition: the effects of ligand and protein flexibility on molecular docking accuracy. *J. Med. Chem.* **2004**, *47*, 45-55.

(70) Glen, R. C.; Allen, S. C. Ligand-protein docking: cancer research at the interface between biology and chemistry. *Curr. Med. Chem.* **2003**, *10*, 763-767.

(71) Kroemer, R. T. Molecular modelling probes: docking and scoring. *Biochem. Soc. Trans.* **2003**, *31*, 980-984.

(72) Amzel, L. M.; Bryant, S. H.; Prochaska, H. J.; Talalay, P. Preliminary crystallographic X-ray data for an NAD(P)H:quinone reductase from mouse liver. *J. Biol. Chem.* **1986**, *261*, 1379.

(73) Ysern, X.; Prochaska, H. J. X-ray diffraction analyses of crystals of rat liver NAD(P)H:(quinone-acceptor) oxidoreductase containing cibacron blue. *J. Biol. Chem.* **1989**, *264*, 7765-7767.

(74) Phillips, R. M.; Naylor, M. A.; Jaffar, M.; Doughty, S. W.; Everett, S. A.; Breen, A. G.; Choudry, G. A.; Stratford, I. J. Bioreductive activation of a series of indolequinones by human DT-diaphorase: Structure-activity relationships. *J. Med. Chem.* **1999**, *42*, 4071-4080.

(75) Suleman, A.; Skibo, E. B. A comprehensive study of the active site residues of DT-diaphorase: Rational design of benzimidazolediones as DT-diaphorase substrates. *J. Med. Chem.* **2002**, *45*, 1211-1220.

(76) Lyne, P. D. Structure-based virtual screening: An overview. *Drug Discov. Today.* **2002**, *7*, 1047-1055.

(77) Joseph-McCarthy, D. Computational approaches to structure-based ligand design. *Pharmacol. Ther.* **1999**, *84*, 179-191.

(78) Frimurer, T. M.; Peters, G. H.; Iversen, L. F.; Andersen, H. S.; Moller, N. P. H.; Olsen, O. H. Ligand-induced conformational changes: Improved predictions of ligand binding conformations and affinities. *Biophys. J.* **2003**, *84*, 2273-2281.

(79) Ollinger, K.; Kagedal, K. Induction of apoptosis by redox-cycling quinones. *Subcell. Biochem.* **2002**, *36*, 151-170.

(80) Bolton, J. L.; Trush, M. A.; Penning, T. M.; Dryhurst, G.; Monks, T. J. Role of quinones in toxicology. *Chem. Res. Toxicol.* **2000**, *13*, 135-160.

(81) Cadenas, E. Antioxidant and prooxidant functions of DT-diaphorase in quinone metabolism. *Biochem. Pharmacol.* **1995**, *49*, 127-140.

(82) Gutierrez, P. L. The role of NAD(P)H oxidoreductase (DT-Diaphorase) in the bioactivation of quinone-containing antitumor agents: A review. *Free Radic. Biol. Med.* **2000**, *29*, 263-275.

(83) Ross, D. Quinone reductases multitasking in the metabolic world. *Drug Metab. Rev.* **2004**, *36*, 639-654.

(84) Opara, E. C. Oxidative stress. *Dis. Mon.* **2006**, *52*, 183-198.

(85) Engel, R. H.; Evens, A. M. Oxidative stress and apoptosis: a new treatment paradigm in cancer. *Front. Biosci.* **2006**, *11*, 300-312.

(86) Fisher, G. R.; Brown, J. R.; Patterson, L. H. Redox cycling in MCF-7 human breast cancer cells by antitumor agents based on mitozantrone. *Free Radic. Res. Commun.* **1989**, *7*, 221-226.

(87) Fisher, G. R.; Gutierrez, P. L. The reductive metabolism of diaziquone (AZQ) in the S9 fraction of MCF-7 cells: Free radical formation and NAD(P)H: quinone-acceptor oxidoreductase (DT-diaphorase) activity. *Free Radic. Biol. Med.* **1991**, *10*, 359-370.

(88) Fisher, G. R.; Patterson, L. H.; Gutierrez, P. L. A comparison of free radical formation by quinone antitumour agents in MCF-7 cells and the role of NAD(P)H (quinone-acceptor) oxidoreductase (DT-diaphorase). *Chem. Biol. Interact.* **1993**, *88*, 137-153.

(89) Fisher, G. R.; Gutierrez, P. L.; Oldcorne, M. A.; Patterson, L. H. NAD(P)H (quinone acceptor) oxidoreductase (DT-diaphorase)-mediated two-electron reduction of anthraquinone-based antitumour agents and generation of hydroxyl radicals. *Biochem. Pharmacol.* **1992**, *43*, 575-585.

(90) Bailey, S. M.; Lewis, A. D.; Knox, R. J.; Patterson, L. H.; Fisher, G. R.; Workman, P. Reduction of the indoloquinone anticancer drug EO9 by purified DT-diaphorase: A detailed kinetic study and analysis of metabolites. *Biochem. Pharmacol.* **1998**, *56*, 613-621.

(91) Shi, M. M.; Kugelman, A.; Iwamoto, T.; Tian, L.; Forman, H. J. Quinone-induced oxidative stress elevates glutathione and induces gamma-glutamylcysteine synthetase activity in rat lung epithelial L2 cells. *J. Biol. Chem.* **1994**, *269*, 26512-26517.

(92) Ordonez, I. D.; Cadenas, E. Thiol oxidation coupled to DT-diaphorase-catalysed reduction of diaziquone. Reductive and oxidative pathways of diaziquone semiquinone modulated by glutathione and superoxide dismutase. *Biochem. J.* **1992**, *286 (Pt 2)*, 481-490.

(93) May, J. M.; Qu, Z. C.; Li, X. Ascorbic acid blunts oxidant stress due to menadione in endothelial cells. *Arch. Biochem. Biophys.* **2003**, *411*, 136-144.

(94) Giulivi, C.; Cadenas, E. One- and two-electron reduction of 2-methyl-1,4-naphthoquinone bioreductive alkylating agents: Kinetic studies, free-radical production, thiol oxidation and DNA-strand-break formation. *Biochem. J.* **1994**, *301 (Pt 1)*, 21-30.

(95) Li, B.; Blough, N. V.; Gutierrez, P. L. Trace detection of hydroxyl radicals during the redox cycling of low concentrations of diaziquone: a new approach. *Free Radic. Biol. Med.* **2000**, *29*, 548-556.

(96) Wu, L. L.; Chiou, C. C.; Chang, P. Y.; Wu, J. T. Urinary 8-OHdG: a marker of oxidative stress to DNA and a risk factor for cancer, atherosclerosis and diabetics. *Clin. Chim. Acta.* **2004**, *339*, 1-9.

(97) Peoples, M. C.; Karnes, H. T. Recent developments in analytical methodology for 8-hydroxy-2'-deoxyguanosine and related compounds. *J. Chromatogr. B Analyt. Technol. Biomed. Life Sci.* **2005**, *827*, 5-15.

(98) Bolin, C.; Stedeford, T.; Cardozo-Pelaez, F. Single extraction protocol for the analysis of 8-hydroxy-2'-deoxyguanosine (oxo8dG) and the associated activity of 8-oxoguanine DNA glycosylase. *J. Neurosci. Methods* **2004**, *136*, 69-76.

(99) Pagano, G.; Degan, P.; De Biase, A.; Iaccarino, M.; Warnau, M. Diepoxybutane and mitomycin C toxicity is associated with the induction of oxidative DNA damage in sea urchin embryos. *Hum. Exp. Toxicol.* **2001***, 20*, 651-655.

(100) Norbury, C. J.; Zhivotovsky, B. DNA damage-induced apoptosis. *Oncogene* **2004***, 23*, 2797-2808.

(101) Meiler, J.; Schuler, M. Therapeutic targeting of apoptotic pathways in cancer. *Curr. Drug Targets* **2006***, 7*, 1361-1369.

(102) Laux, I.; Nel, A. Evidence that oxidative stress-induced apoptosis by menadione involves Fas-dependent and Fas-independent pathways. *Clin. Immunol.* **2001***, 101*, 335-344.

(103) Planchon, S. M.; Wuerzberger, S.; Frydman, B.; Witiak, D. T.; Hutson, P.; Church, D. R.; Wilding, G.; Boothman, D. A. Beta-lapachone-mediated apoptosis in human promyelocytic leukemia (HL-60) and human prostate cancer cells: A p53-independent response. *Cancer Res.* **1995***, 55*, 3706-3711.

(104) Wuerzberger, S. M.; Pink, J. J.; Planchon, S. M.; Byers, K. L.; Bornmann, W. G.; Boothman, D. A. Induction of apoptosis in MCF-7:WS8 breast cancer cells by beta-lapachone. *Cancer Res.* **1998***, 58*, 1876-1885.

(105) Sharp, S. Y.; Kelland, L. R.; Valenti, M. R.; Brunton, L. A.; Hobbs, S.; Workman, P. Establishment of an isogenic human colon tumor model for NQO1 gene expression: application to investigate the role of DT-diaphorase in bioreductive drug activation in vitro and in vivo. *Mol. Pharmacol.* **2000***, 58*, 1146-1155.

(106) Winski, S. L.; Swann, E.; Hargreaves, R. H.; Dehn, D. L.; Butler, J.; Moody, C. J.; Ross, D. Relationship between NAD(P)H:quinone oxidoreductase 1 (NQO1)

levels in a series of stably transfected cell lines and susceptibility to antitumor quinones. *Biochem. Pharmacol.* **2001**, *61*, 1509-1516.

Chapter 2

Novel Lavendamycin Antitumor Agents: Electrochemistry, Structure-metabolism Studies and *In Vitro* Cytotoxicity with NAD(P)H:Quinone Oxidoreductase 1 (NQO1)

2.1 Abstract

A series of novel lavendamycin analogues bearing various substituents were evaluated as potential NAD(P)H:quinone oxidoreductase (NQO1)-directed antitumor agents. The effects of substituents and functional group changes on the metabolism (reduction efficiency) of these analogues by recombinant human NQO1 were studied. Lavendamycin analogues reduction was monitored using a spectrophotometric assay in which the rate of reduction of cytochrome *c* was quantified at 550 nm. Structure-metabolism studies demonstrated that small to medium-size substituents at the quinolinedione-7-position were well tolerated whereas large, bulky substituents were not. Substituents at the quinolinedione-6-position of lavendamycins generally reduced rates of reduction compared to compounds with no substituents at this position. Small or large substituents at the indolopyridine-2'-position were tolerated. Addition of NH_2 and CH_2OH groups at the quinolinedione-7-position and indolopyridine-2'-position, respectively, had the greatest positive impact on substrate specificity. The best and poorest lavendamycin substrates were MB-353 (2′-CH_2OH-7-NH_2 derivative) and MB-323 (2′-$CONH_2$-7-$NHCOC_3H_7$-*n* derivative) with reduction rates of 263 ± 30 and 0.1 ± 0.1 μmol/min/mg NQO1, respectively. The electrochemical reduction potentials of the lavendamycin analogues were measured by cyclic voltammetry. The findings suggest a

more important role of lavendamycin substituent size and steric influence compared to electronic effects to determine the reduction efficiency of the compounds by NQO1. The cytotoxicity toward human colon adenocarcinoma cells with either no detectable NQO1 activity (BE) or with high NQO1 activity (BE-NQ) was determined in representative lavendamycin analogues. The best lavendamycin substrates for NQO1 were also the most selectively toxic to the NQO1-rich BE-NQ cell line compared to the NQO1-deficient BE cells with the 2′-CH_2OH-7-NH_2 derivative (MB-353) being 11 times more toxic to BE-NQ cells versus BE cells.

2.2 Introduction

A large number of antitumor agents have been discovered empirically without the theoretical understanding of the corresponding molecular targets or mechanisms of action.[1] A rational approach to chemotherapy, selective cancer therapy, takes advantage of molecular targets that are unique to cancer cells utilizing the differences existing between cancer and normal cells.[1,2] In selective cancer therapy antitumor agents are designed with pre-existing knowledge of the biochemical mechanism of the drug action.[3] This approach is aimed to destroy cancer cells via exclusive interaction of antitumor agents with unique tumor targets (selective toxicity) while posing minimal toxicity to normal cells.[2-5] One approach to achieve antitumor selectivity is enzyme-directed bioreductive drug development.[2,4,5] In this approach, selective toxicity can be obtained by identifying reductase enzymes that are overexpressed in tumor cells when compared to normal cells.[2,4-6] Then, bioreductive agents that are substrates for and bioactivated by the

related reductase can be designed to selectively target the tumors with the up-regulated reductase.[2,4-6]

One proper candidate for enzyme-directed bioreductive drug development is NAD(P)H:quinone oxidoreductase 1 (NQO1). NQO1 is a ubiquitous homodimeric flavoenzyme that possesses two closely associated monomers of 273 residues. Each monomer contains one molecule of the FAD prosthetic group that is required for NQO1 enzymatic activity.[7-11] This obligate two-electron reductase is a mainly cytosolic enzyme (> 90%),[12] although lower amounts of this reductase have been detected in nucleus, mitochondria and endoplasmic reticulum.[13] NQO1 catalyzes a nicotinamide nucleotide-dependent two-electron reduction[14,15] and the bioactivation of quinone anticancer compounds such as quinolinequinones, mitomycins, indoloquinones and aziridinylbenzoquinones.[16-20] In addition, marked elevations in NQO1 activity and mRNA content in primary tumors from lung, liver, colon and breast,[21] and lung,[22] liver,[23] brain[24] and colorectal[25] tumors have been reported. These suggest that antitumor compounds that are bioactivated by NQO1 can be selectively toxic to tumors that overexpress this enzyme.

Lavendamycin (Chart 2.1), a bacterially derived quinolinedione antibiotic, was isolated from the fermentation broth of *Streptomyces lavendulae* in 1981.[26] Lavendamycin is structurally[26,27] and biosynthetically[28-30] related to streptonigrin (SN) (Chart 2.1), another potent 7-aminoquinoline-5,8-dione antitumor antibiotic. Earlier work has shown that the use of both of these antitumor agents as potential drugs has been precluded due to their high degree of toxicity.[27,31,32] However, in contrast to the parent

compound, it has been found that a significant number of lavendamycin derivatives have low animal toxicity but exhibit strong antitumor activity.[33-35]

Bioreductive enzyme-directed antitumor agent development depends on identification of antitumor agents with high substrate specificity for target reductases.[36] Several approaches have been applied to identify efficient quinone-based substrates for NQO1, optimize the substrate specificity, and reduce the non-selective toxicity toward normal tissues. A large number of metabolism studies of quinone-based anticancer agents excluding lavendamycins with NQO1 have been performed during the last twenty years to identify the most efficient quinone substrates for NQO1. One common approach has been to investigate the effects of functional group alterations on reduction efficiency and bioactivation of antitumor quinones by NQO1.[36] This can assist in identification of the structural features that confer substrate specificity and are required for selective bioactivation of quinone compounds by NQO1 and their selective cytotoxicity.[36,37] Many studies reported that functional group changes in a series of indolequinone, 1,4-naphthoquinone and benzoquinone mustard analogues significantly affected the substrate specificity and selective cytotoxicity of the analogues towards NQO1-rich cell lines *in vitro*.[36-43]

Chart 2.1. Chemical structures of lavendamycin, streptonigrin and the lavendamycin analogues with substituent positions indicated by R^1, R^2, R^3 and R^4.

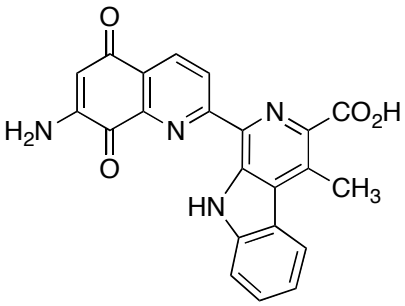

Lavendamycin

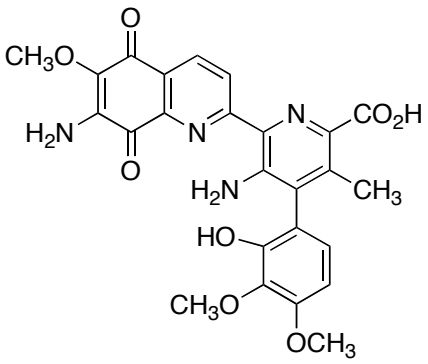

Streptonigrin

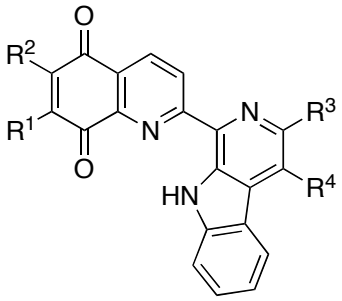

Lavendamycin analogues

This study was conducted to clarify the role of NQO1 in the bioactivation of lavendamycin analogues. Specifically, the objectives were to perform structure-activity relationship (SAR) studies to analyze the effects of functional group changes on the reduction efficiency of lavendamycin analogues by NQO1 and to verify whether activation by NQO1 resulted in selective cytotoxicity of these compounds toward NQO1-rich cells. This is the first study that has been performed to verify structural features of lavendamycin analogues that are required for their efficient reduction by NQO1 and the selective toxicity of these analogues toward human colon adenocarcinoma NQO1-rich BE-NQ cells compared to NQO1-deficient BE cells. In addition, there is currently no information on how electrochemical characteristics of lavendamycin analogues correlate with their substrate specificities for NQO1. Therefore, we also sought to determine the electrochemical ease of reduction of the lavendamycin analogues and to examine how the electronic features of these compounds impact their rate of reduction by NQO1.

2.3 Materials and Methods

2.3.1 Chemistry. Our studies have been possible through the success of Dr. Mohammad Behforouz's laboratory in developing short and efficient syntheses for a variety of variously substituted lavendamycin analogues (Chart 2.1) possessing the full pentacyclic structure. General Methods are described in the 2003 and 2005 papers by Behforouz et al. and Hassani et al.[44,45]

2.3.2 Electrochemistry. Cyclic voltammetry (CV) for lavendamycin analogues was conducted using a BAS CV-50W electrochemical analyzer equipped with a standard three-electrode cell. This cell was designed to allow the tip of the reference electrode to

approach closely to the working electrode. Voltammetric experiments were performed using Ag/AgCl as the reference electrode, a glossy carbon (GC) rod as the working electrode and a platinum (Pt) wire as the auxiliary electrode. Potential data are referred to the Ferrocene (0/+) couple, which is oxidized in dried dimethylsulfoxide (DMSO) at +0.52 V *vs.* Ag/AgCl. Positive-feedback *iR* compensation was routinely applied. The working electrode was regularly polished using alumina. Typically, a solution containing 1 mM of the lavendamycin analogues and 0.1 M supporting electrolyte, tetrabutylammonium hexafluorophosphate (Bu_4NPF_6), was prepared using dried DMSO. All samples were purged with argon prior to use and kept under a continuous flow of argon during the course of the experiments. All CV data were recorded at a potential range between 0.00 and -2.00 V and at potential sweep rates of 50 to 500 mV/s. All measurements were performed at 22 ± 1 °C.

2.3.3 Cell Culture. BE human colon adenocarcinoma cells and stably NQO1-transfected BE-NQ cells[46] were a gift from Dr. David Ross (University of Colorado Health Sciences Center, Denver, CO). Cells were grown in a minimum essential medium (MEM) with Earle's salts, non-essential amino acids, L-glutamine and penicillin/streptomycin, and supplemented with 10% fetal bovine serum (FBS), sodium bicarbonate and HEPES. Cell culture medium and supplements were obtained from Gibco, Invitrogen Co., Grand Island, NY. The cells were incubated at 37°C under a humidified atmosphere containing 5% CO_2.

2.3.4 Cytochrome *c* Assay. Lavendamycin analogue reduction was monitored using a spectrophotometric assay in which the rate of reduction of cytochrome *c* was quantified at 550 nm. Briefly, the assay mixture contained cytochrome *c* (70 μM),

NADH (1 mM), human recombinant NQO1 (0.1-3 μg) (gift from Dr. David Ross, University of Colorado Health Sciences Center, Denver, CO) and lavendamycins (25 μM) in a final volume of 1 mL Tris-HCl (25 mM, pH 7.4) containing 0.7 mg/mL BSA and 0.1% Tween-20. Reactions were carried out at room temperature and started by the addition of NADH. Rates of reduction were calculated from the initial linear part of the reaction curve (0-30 s), and results were expressed in terms of μmol of cytochrome *c* reduced/min/mg of NQO1 using a molar extinction coefficient of 21.1 mM^{-1} cm^{-1} for cytochrome *c*. All reactions were carried out at least in triplicate.

2.3.5 MTT Assay. Growth inhibition was determined using the MTT colorimetric assay. Cells were plated in 96-well plates at a density of 10,000 cells/mL and allowed to attach overnight (16 h). Lavendamycin analogue solutions were applied in medium for 2 hours. Lavendamycin analogue solutions were removed and replaced with fresh medium, and the plates were incubated at 37 °C under a humidified atmosphere containing 5% CO_2 for 4-5 days. MTT (50 μg) was added and the cells were incubated for another 4 hours. Medium/MTT solutions were removed carefully by aspiration, the MTT formazan crystals were dissolved in 100 μL DMSO, and absorbance was determined on a plate reader at 560 nm. IC_{50} values (concentration at which cell survival equals 50% of control) were determined from semi-log plots of percent of control *vs.* concentration. Selectivity ratios were defined as the IC_{50} value for the BE cell line divided by the IC_{50} value for the BE-NQ cell line.

2.3.6 Clonogenic Assay. Cells were harvested from logarithmic-phase growing cultures and plated at densities of 1000 cells per 100-mm dish to yield a readily quantifiable number of colonies at the end of the experiment. After 24 hours, cells were

treated with lavendamycin analogues, 2% DMSO (drug vehicle) or no treatment (control) for 2 hours at 37 °C. After 2 hours, drug-containing medium was replaced with fresh drug-free medium. Cells were incubated at 37 °C under a humidified atmosphere containing 5% CO_2 for 12 days. Then, the medium was removed and colonies were washed twice with PBS, fixed and stained with 0.1% (w/v) Coomassie Blue dye in 30% methanol and 10% acetic acid for 1-2 minutes. Surviving colonies (> 50 cells) were counted and the surviving fraction determined by dividing the number of colonies in a treatment dish by the number of colonies in the control dish. IC_{50} values (concentration at which cell survival equals 50% of control) were determined from semi-log plots of percent of control *vs.* concentration. Selectivity ratios were defined as the IC_{50} value for the BE cell line divided by the IC_{50} value for the BE-NQ cell line.

2.4 Results and Discussion

2.4.1 Electrochemistry. The aim of the electrochemical studies was to determine the relative ease of reduction of the lavendamycin analogues and to investigate how the electrochemical behavior of these compounds correlates with their reduction rate by NQO1. Electrochemical studies of a number of lavendamycin analogues were carried out. In these studies, dried DMSO and Bu_4NPF_6 were used as solvent and the supporting electrolyte, respectively. Cathodic and anodic peak potentials, E_{pc} and E_{pa}, respectively, were measured and the midpoint of the peak potentials was used to determine $E_{1/2}$ values, $E_{1/2} = (E_{pc} + E_{pa})/2$. $E_{1/2}$ values were consistent for the potential sweep rates in the range of 50 to 500 mV/s. The $E_{1/2}$ values determined from the recorded voltammograms at the

potential sweep rates of 50, 100, 200, 400 and 500 mV/s were averaged and reported with reference to Ferrocene ($Fc^{0/+}$) $E_{1/2}$ value (Table 2.1).

All of the lavendamycin analogues exhibited reversible electrochemistry. The analogues with electron-withdrawing groups at the R^1 position showed similar $E_{1/2}$ values, between -0.85 and -0.99 V, with the exception of compound MB-361 that exhibited a slightly more negative $E_{1/2}$ value (-1.13), which can be in part due to the presence of an electron-donating group at the R^2 position (Table 2.1). The lavendamycin analogues with electron-donating groups at the R^1 position showed slightly more negative $E_{1/2}$ values, between -1.01 and -1.09 V, compared to the former group (Table 2.1). In general, the lavendamycin analogues with electron-withdrawing groups at the R^1 position were easier to reduce electrochemically compared to the ones with electron-donating groups at this position (Table 2.1).

Table 2.1. Electrochemical reduction potentials[a] (in DMSO) of lavendamycin analogues (MB) versus Ferrocene.

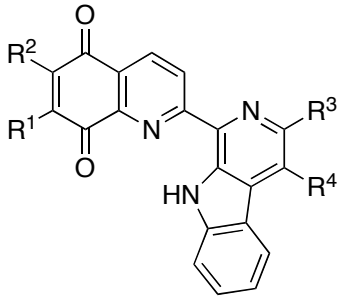

MB	R^1	R^2	R^3	R^4	E_{pc} (V)	E_{pa} (V)	$E_{1/2}$ (V) *vs* Fc
65	CH_3CONH	H	H	H	-0.95	-0.95	-0.95
47	CH_3CONH	H	CO_2CH_3	H	-0.92	-0.83	-0.88
361	CH_3CONH	$N(CH_2)_4$	CO_2CH_3	CH_3	-1.16	-1.10	-1.13
362	CH_3CONH	$N(CH_2)_2$	$CONH_2$	H	-0.99	-0.93	-0.96
21	CH_3CONH	H	CO_2CH_3	CH_3	-0.91	-0.85	-0.88
320	CH_3CONH	H	$CO_2(CH_2)_2OH$	H	-1.02	-0.95	-0.99
76	CH_3CONH	H	$CONH_2$	H	-0.88	-0.82	-0.85
323	*n*-C_3H_7CONH	H	$CONH_2$	H	-0.92	-0.89	-0.91
328	NH_2	Cl	CO_2CH_3	CH_3	-1.01	-1.01	-1.01

22	NH_2	H	CO_2CH_3	CH_3	-1.10	-1.04	-1.07
97	NH_2	H	$CONH_2$	H	-1.09	-1.05	-1.07
353	NH_2	H	CH_2OH	H	-1.11	-1.06	-1.09
348	NH_2	H	H	H	-1.12	-1.06	-1.09
355	H	H	H	H	-0.88	-0.85	-0.87

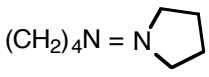

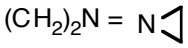

[a] $E_{1/2}$ values (± 0.005V) calculated as (E_{pc}+ E_{pa})/2 are averages of the values determined from voltammograms recorded at potential sweep rates of 50, 100, 200, 300, 400 and 500 mV/s; E_{pc} = Cathodic peak potential; E_{pa} = Anodic peak potential.

Although all of the investigated lavendamycin analogues possessed similar $E_{1/2}$ values (-0.85 to -1.13 V) (Table 2.1), the rate of reduction of these compounds by NQO1 differed dramatically (Table 2.2). Compounds MB-22, -97, -348 and -353 were among the good substrates for NQO1 (high rate of reduction by NQO1) (Table 2.2), but they exhibited the most negative $E_{1/2}$ values and were among the most difficult to reduce electrochemically (Table 2.1). This suggests that their substituent size and potential ability to form efficient interactions such as hydrogen bonds inside the active site of the enzyme may play a more important role than the electrochemical reduction potentials in their substrate specificity (See Chapter 3). Although, compound MB-323 possessed an $E_{1/2}$ value that is in the higher range of the observed $E_{1/2}$ values (-0.91) (Table 2.1), it displayed very poor substrate specificity for NQO1 (Table 2.2). This also indicates that other factors such as lavendamycin substituent size, steric influence and lack of formation of efficient interactions in the NQO1 active site may be more important than the electronic effects to determine the reduction efficiency of these compounds by NQO1 (See Chapter 3). In general, when the electrochemical reduction potential and rate of reduction of the lavendamycin analogues by NQO1 were compared, no overall linear correlation between the two factors was found ($r^2 = 0.029$, $P = 0.578$) (Figure 2.1). These findings imply that the reduction potentials of the lavendamycin analogues do not play a major role in determination of substrate specificity of these analogues for NQO1.

Electrochemical studies can be used to determine the ease of reduction of compounds, but there is often no overall or very small association between the rate of reductions by NQO1 and reduction potentials for quinones such as indolequinones[38,42,47] and quinolinequinones[48] as previously reported. In addition, Fourie et al. suggested the

more important role of steric effects of the functional groups of a series of benzoquinone mustard analogues rather than electronic effects on the reduction efficiency of these compounds by NQO1.[36,49] The lavendamycin analogues exhibited similar reduction potential values to the quinolinequinone compounds studied by Fryatt et al.[48] Also, they were easier to reduce ($E_{1/2}$ values = -0.85 to -1.13 V) than the indolequinones previously studied by Beall et al. and Swann et al. ($E_{1/2}$ values = -1.19 to -1.61 V).[38,42]

2.4.2 Metabolism and Structure-activity Relationship (SAR) Studies.

Metabolism of the novel lavendamycin analogues by recombinant human NQO1 was examined. The effect of functional group changes on reduction efficiency and rate of reduction by NQO1 was studied using a spectrophotometic assay that employs cytochrome *c* as the terminal electron acceptor[37] and gives initial rates of lavendamycin analogues reduction (Table 2.2). The initial reduction rates (μmol cytochrome *c* reduced/min/mg NQO1) were calculated from the linear portion (0-30 s) of the reaction graphs.

Table 2.2. Metabolism of lavendamycin analogues (MB) by recombinant human NQO1 monitored by spectrophotometric cytochrome *c* assay.

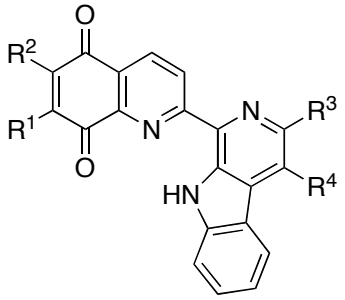

MB	R^1	R^2	R^3	R^4	Metabolism by NQO1 (μmol/min/mg) (Cytochrome *c* Reduction)
65	CH_3CONH	H	H	H	2.7 ± 1.2
47	CH_3CONH	H	CO_2CH_3	H	0.9 ± 0.2
302	CH_3CONH	H	$CO_2C_4H_9$-*n*	H	8.6 ± 2.6
303	CH_3CONH	H	$CO_2C_5H_{11}$-*n*	H	9.2 ± 6.6
50	CH_3CONH	H	$CO_2C_5H_{11}$-*i*	H	35.4 ± 6.9
304	CH_3CONH	H	$CO_2C_6H_{13}$-*n*	H	11.7 ± 5.3
120	CH_3CONH	H	$CON(CH_2)_5$	H	15.2 ± 11.5

118	CH_3CONH	H	$CON[(CH_2)_2O(CH_2)_2]$	H	7.5 ± 1.5
69	$ClCH_2CONH$	H	$CO_2C_5H_{11}$-*i*	H	9.9 ± 5.6
361	CH_3CONH	$N(CH_2)_4$	CO_2CH_3	CH_3	1 ± 1
362	CH_3CONH	$N(CH_2)_2$	$CONH_2$	H	0.2 ± 0.2
21	CH_3CONH	H	CO_2CH_3	CH_3	1.9 ± 1.7
51	CH_3CONH	H	$CO_2C_8H_{17}$-*n*	H	1.5 ± 0.8
320	CH_3CONH	H	$CO_2(CH_2)_2OH$	H	11.0 ± 2.5
344	CH_3CONH	H	$CO_2(CH_2)_2OPO_3H_2$	H	15.4 ± 0.9
76	CH_3CONH	H	$CONH_2$	H	33 ± 12
323	*n*-C_3H_7CONH	H	$CONH_2$	H	0.1 ± 0.1
328	NH_2	Cl	CO_2CH_3	CH_3	0.9 ± 0.8
22	NH_2	H	CO_2CH_3	CH_3	21 ± 12
366	Br	H	CO_2CH_3	CH_3	0.7 ± 0.3
83	NH_2	H	$CO_2C_8H_{17}$-*n*	H	106 ± 15
97	NH_2	H	$CONH_2$	H	18.3 ± 13.6
353	NH_2	H	CH_2OH	H	263 ± 30

348	NH_2	H	H	H	24.0 ± 6.5
355	H	H	H	H	3.4 ± 1.2

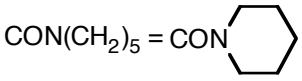

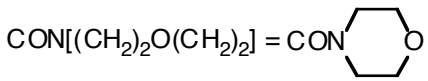

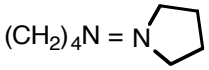

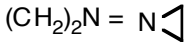

Figure 2.1. Correlation of the reduction potential values and rate of reduction of lavendamycin analogues by NQO1.

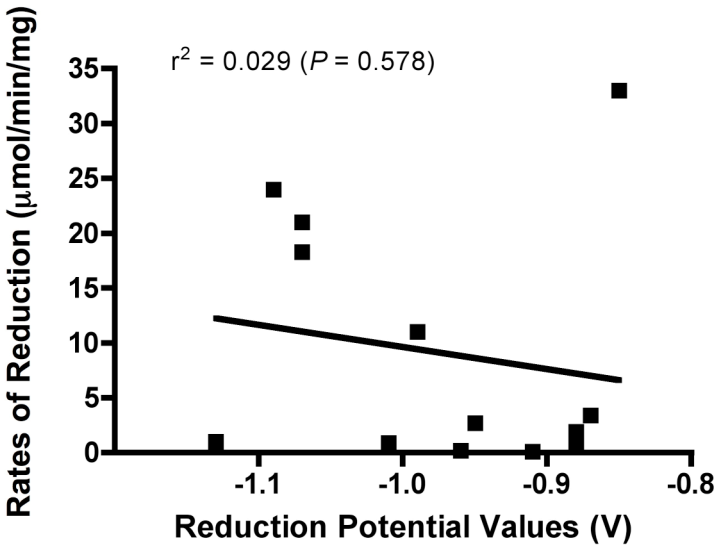

Figure 2.1. Correlation of the reduction potential values and rate of reduction of lavendamycin analogues by NQO1. The reduction potential values of lavendamycin analogues were plotted along the horizontal axis and rates of reduction of lavendamycin analogues by NQO1 were plotted along the vertical axis. $r^2 = 0.029$ ($P = 0.578$).

Our SAR studies determined that large substituents at the quinolinedione-7-position (R^1) of the lavendamycin analogues were poorly tolerated and greatly reduced the metabolism rate of the analogues by NQO1 compared to smaller substituents (MB-97 *vs.* MB-323, MB-50 *vs.* MB-69, MB-51 *vs.* MB-83 and MB-76 *vs.* MB-323) (Table 2.2). Large substituents such as $NHCOC_3H_7$-*n* in MB-323 at the 7-position had the most negative impact on the rate of reduction by NQO1 whereas NH_2 followed by the $NHCOCH_3$ group were the best substituents for this position (Table 2.2). This could partly be due to steric hindrance between the quinolinedione moiety (5,8- dione ring enters the active site first) and NQO1 active site that results in unfavorable positioning of the lavendamycin analogues for hydride ion reception from $FADH_2$ and quinone reduction. Our molecular modeling studies have also demonstrated that placing a small substituent at the R^1 position that is capable of hydrogen bonding with key residues of the active site could be a contributing factor to substrate specificity of these analogues (See Chapter 3). Faig et al. determined that positions of RH1, 2,5-diaziridinyl-3-(hydroxymethyl)-6-methyl-1,4-benzoquinone,[50] that point to the inner part of the NQO1 active site could accommodate only small substituents.[51] Furthermore, 1,4-naphthoquinones with small substituents such as an aziridine ring or CH_3 at C2 and no substituents at C3 were reported to be good substrates for NQO1.[52] Dipyrroloimidazobenzimidazole compounds with both pyrrolo rings bearing bulky substituents were determined to be poor substrates for NQO1 due to steric interactions with residues of the NQO1 active site.[53]

Comparison of analogues MB-328 *vs.* MB-22 and MB-362 *vs.* MB-76 determined that 6-unsubstituted (R^2) lavendamycin analogues are far better substrates for NQO1 than

the corresponding 6-substituted counterparts (Table 2.2). This is likely due to active site constraints and steric effects caused by substituents that hinder entrance or proper positioning of the 5,8-dione moiety of the analogues toward the key residues of the active site and the FAD isoalloxazine ring for hydride ion reception and quinone reduction. This finding is consistent with other studies that previously showed that increased bulkiness of the substituents at C5 position on EO9, 3-hydroxy-5-aziridinyl-1-methyl-2-(1H-indole-4,7-dione)-propenol,[54] dramatically reduced rates of reduction by NQO1.[37,51] Another study determined that indolequinones and mitosenes with bulky amine substituents at C5 and C7 positions, respectively, are not substrates for NQO1 due to steric effects.[38]

A number of substituents at the 2'-position of the fused indolopyridine moiety (R^3) were also investigated. Among the analogues that shared an NH_2 group at the R^1 position and had no substituent at R^2, 2'-CH_2OH derivative (MB-353) was the best substrate followed by the 2'-$CO_2C_8H_{17}$-*n* derivative (MB-83) (Table 2.2). Also, our molecular modeling studies have demonstrated that the CH_2OH group at R^3 was capable of hydrogen bond formation with the key residues of the NQO1 active site and therefore could be an important contributing factor to substrate specificity (See Chapter 3). A CH_2OH group at the C6 position of a series of substituted 1,4-naphthoquinones also contributed the most to substrate specificity for NQO1.[52] Phillips et al. determined that some of the good indolequinone substrates for NQO1 including EO9 possessed a CH_2OH group at the analogous C3 position.[37] Furthermore, RH1, which is an excellent substrate for NQO1, possesses a CH_2OH group at C3 position.[8,50]

2.4.3 *In Vitro* Cytotoxicity. Cytotoxicity studies were also performed on

representative lavendamycin analogues with cell survival being determined by the colorimetric MTT and clonogenic assays. We used the BE human colon adenocarcinoma cells stably transfected with human NQO1 cDNA.[50] The BE cells had no measurable NQO1 activity whereas activity in the transfected cells (BE-NQ) was greater than 660 nmol/min/mg total cell protein using dichlorophenolindophenol (DCPIP) as the standard electron acceptor. We also evaluated the correlation between the chemosensitivity results of clonogenic and MTT assays in both cell lines for three lavendamycin analogues, MB-22, MB-323 and MB-353. There was an excellent positive linear correlation between the IC_{50} values of the two assays for the three lavendamycins for BE ($r^2 = 0.999$, $P = 0.03$), BE-NQ ($r^2 = 0.999$, $P = 0.025$) and both cell lines ($r^2 = 0.990$, $P = 0.0001$) (Figure 2.2). In this study the cytotoxicity of representative lavendamycin analogues (Table 2.3) has been compared using these cell lines.

Figure 2.2. Correlation of the mean IC_{50} values obtained by MTT and clonogenic assays.

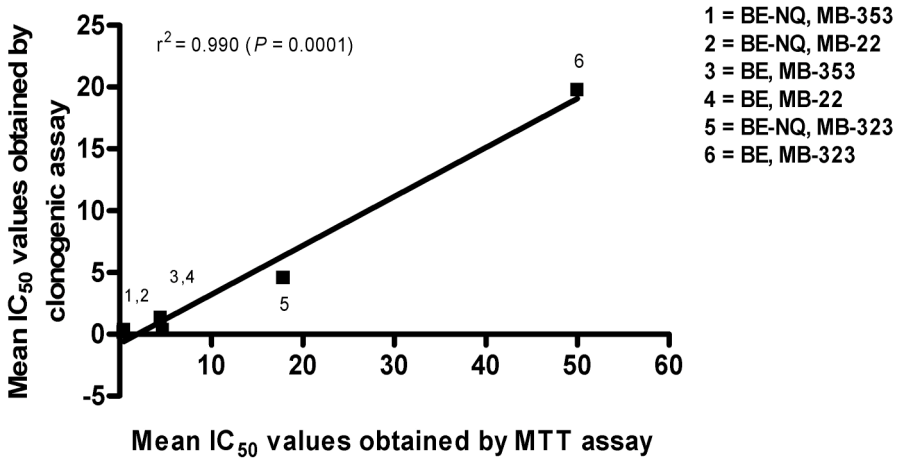

Figure 2.2. Correlation of the mean IC_{50} values obtained by MTT and clonogenic assays. The mean IC_{50} values obtained by MTT assay were plotted along the horizontal axis and mean IC_{50} values obtained by clonogenic assay were plotted along the vertical axis. $r^2 = 0.990$ ($P = 0.0001$).

Table 2.3. Cytotoxicity of lavendamycin analogues (MB) towards BE (NQO1-deficient) and BE-NQ (NQO1-rich) human colon adenocarcinoma cell lines.

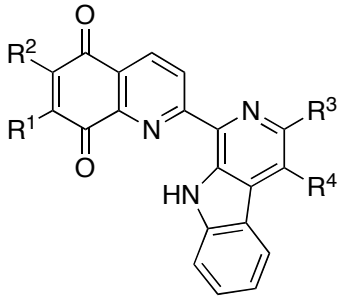

MB	R^1	R^2	R^3	R^4	Cytotoxicity IC_{50} (μM)		Selectivity Ratio [IC_{50} (BE-WT) / IC_{50} (BE-NQ)]
					BE-NQ	BE	
302	CH_3CONH	H	$CO_2C_4H_9$-*n*	H	20.5 ± 0.6	20.0 ± 2.3	1.0
21	CH_3CONH	H	CO_2CH_3	CH_3	13.2 ± 0.7	19.3 ± 4.3	1.5
51	CH_3CONH	H	$CO_2C_8H_{17}$-*n*	H	>50	>50	-
344	CH_3CONH	H	$CO_2(CH_2)_2OPO_3H_2$	H	6.8 ± 0.6	8.1 ± 0.5	1.2
76	CH_3CONH	H	$CONH_2$	H	0.8 ± 0.0	3.5 ± 0.7	4.4
323	*n*-C_3H_7CONH	H	$CONH_2$	H	21.4 ± 1.2	>50	2.3
22	NH_2	H	CO_2CH_3	CH_3	0.5 ± 0.1	4.7 ± 0.7	9.4
366	Br	H	CO_2CH_3	CH_3	>50	>50	-
83	NH_2	H	$CO_2C_8H_{17}$-*n*	H	3.4 ± 0.7	35.0 ±3.4	10.3

97	NH_2	H	$CONH_2$	H	0.2 ± 0.0	1.8 ± 0.1	9.0
353	NH_2	H	CH_2OH	H	0.4 ± 0.1	4.5 ± 0.2	11.3
348	NH_2	H	H	H	8.0 ± 0.5	16.8 ± 1.0	2.1
355	H	H	H	H	12.4 ± 1.0	9.3 ± 1.2	0.8

Lavendamycin analogues such as MB-22, -76, -83, -97 and -353 that were good substrates for NQO1 (Table 2.2) were also more toxic to the NQO1-rich BE-NQ cell line than the NQO1-deficient BE cell line (Table 2.3). Compound MB-353, the best substrate for NQO1 (Table 2.2), had the greatest differential toxicity with a selectivity ratio [IC_{50} (BE) / IC_{50} (BE-NQ)] of 11 (Table 2.3). Antitumor and antiproliferative activity of lavendamycin against implanted leukemia cells in BDF1 mice and three other cancer cell lines has been previously reported.[27,55] A recent study investigating cytotoxic activities of a series of lavendamycin analogues against A549 human lung carcinoma cells indicated that compounds with an amide or amine substituent at the R^3 position displayed the most potent colony formation inhibitory effects.[35] At a concentration of 10 nM, the most potent compound of this group, MB-97, reduced the colony outgrowth of A549 cells by 70%.[35] Since MB-97 also displayed promising cytotoxic and antitumor activities in the National Cancer Institute's (NCI) 60-cell line panel and *in vivo* hollow fiber tumorigenesis assay, it has been considered for *in vivo* testing against tumor xenografts in mice.[35] Our study also determined that lavendamycin analogue MB-97 showed highly selective toxicity toward BE-NQ cells (selectivity ratio = 9).

Lavendamycin analogues such as MB-21, -51, -323, -366 and -355 that were poor substrates for NQO1 demonstrated no selective toxicity toward BE-NQ cells or had no measurable cytotoxicity (IC_{50} > 50 μM) (Table 2.3). Although compound MB-348 was a rather good substrate for NQO1, it displayed only minimal selective toxicity toward BE-NQ cells. This could be due to the less toxic nature of MB-348 (high IC_{50} values for both cell lines) compared to other good substrates such as MB-76, -22 and -97 that have lower IC_{50} values (Table 2.3). Overall, our results determined that the best lavendamycin

substrates for NQO1 were also the most selectively toxic to the high NQO1 BE-NQ cell line.

2.5 Conclusions

Large substituents at the quinolinedione-7-position (R^1) of the lavendamycin analogues were poorly tolerated and greatly decreased the rate of reduction of the analogues by NQO1. Absence of substituents at the quinolinedione-6-position (R^2) was highly preferred. Small or large substituents were well tolerated at the 2'-position of the fused indolopyridine moiety (R^3). Addition of an NH_2 group at R^1 and CH_2OH or $CO_2C_8H_{17}$-*n* groups at the R^3 position had the greatest positive impact on substrate specificity compared to other substituents at these positions. The best substrate was the 2'-CH_2OH-7-NH_2 derivative (MB-353) with a reduction rate of 263 ± 30 μmol/min/mg NQO1 and selectivity ratio of 11. The best lavendamycin substrates for NQO1 were also the most selectively toxic to the NQO1-rich BE-NQ cell line compared to NQO1-deficient BE cells. Lavendamycin substituent size and steric influence compared to electronic effects had a greater impact on determination of the reduction efficiency of the compounds by NQO1. These SAR findings greatly enhance our understanding of the required structural features for lavendamycin analogue substrate specificity for NQO1. Performance of molecular docking studies will assist us to better understand and explain the observed SAR data. These studies can be used for the purpose of structure-based design of novel lavendamycin agents with improved NQO1 substrate specificity.

2.6 References

(1) Rooseboom, M.; Commandeur, J. N.; Vermeulen, N. P. Enzyme-catalyzed activation of anticancer prodrugs. *Pharmacol. Rev.* **2004**, *56*, 53-102.

(2) Phillips, R. M. Prospects for bioreductive drug development. *Exp. Opin. Invest. Drugs* **1998**, *7*, 905-928.

(3) Palumbo, M. Anticancer agents: towards the future. *Curr. Med. Chem. Anticancer Agents* **2004**, *4*, 425-427.

(4) Beall, H. D.; Winski, S. I. Mechanisms of action of quinone-containing alkylating agents. I: NQO1-directed drug development. *Front. Biosci.* **2000**, *5*, 639-648.

(5) Workman, P. Keynote address: Bioreductive mechanisms. *Int. J. Radiat. Oncol. Biol. Phys.* **1992**, *22*, 631-637.

(6) Workman, P. Enzyme-directed bioreductive drug development revisited: A commentary on recent progress and future prospects with emphasis on quinone anticancer agents and quinone metabolizing enzymes, particularly DT-diaphorase. *Oncol. Res.* **1994**, *6*, 461-475.

(7) Skelly, J. V.; Sanderson, M. R.; Suter, D. A.; Baumann, U.; Read, M. A.; Gregory, D. S.; Bennett, M.; Hobbs, S. M.; Neidle, S. Crystal structure of human DT-diaphorase: A model for interaction with the cytotoxic prodrug 5-(aziridin-1-yl)-2,4-dinitrobenzamide (CB1954). *J. Med. Chem.* **1999**, *42*, 4325-4330.

(8) Danson, S.; Ward, T. H.; Butler, J.; Ranson, M. DT-diaphorase: A target for new anticancer drugs. *Cancer Treat. Rev.* **2004**, *30*, 437-449.

(9) Lind, C.; Cadenas, E.; Hochstein, P.; Ernster, L. DT-diaphorase: Purification, properties, and function. *Methods Enzymol.* **1990**, *186*, 287-301.

(10) Faig, M.; Bianchet, M. A.; Talalay, P.; Chen, S.; Winski, S.; Ross, D.; Amzel, L. M. Structures of recombinant human and mouse NAD(P)H:quinone oxidoreductases: Species comparison and structural changes with substrate binding and release. *Proc. Natl. Acad. Sci. U. S. A.* **2000**, *97*, 3177-3182.

(11) Li, R.; Bianchet, M. A.; Talalay, P.; Amzel, L. M. The three-dimensional structure of NAD(P)H:quinone reductase, a flavoprotein involved in cancer chemoprotection and chemotherapy: Mechanism of the two-electron reduction. *Proc. Natl. Acad. Sci. U. S. A.* **1995**, *92*, 8846-8850.

(12) Eliasson, M.; Bostrom, M.; DePierre, J. W. Levels and subcellular distributions of detoxifying enzymes in the ovarian corpus luteum of the pregnant and non-pregnant pig. *Biochem. Pharmacol.* **1999**, *58*, 1287-1292.

(13) Winski, S. L.; Koutalos, Y.; Bentley, D. L.; Ross, D. Subcellular localization of NAD(P)H:quinone oxidoreductase 1 in human cancer cells. *Cancer Res.* **2002**, *62*, 1420-1424.

(14) Ernster, L. DT Diaphorase. *Methods Enzymol.* **1967**, *10*, 309-317.

(15) Ernster, L. DT Diaphorase: A historical review. *Chem. Scripta* **1987**, *27A*, 1-13.

(16) Siegel, D.; Gibson, N. W.; Preusch, P. C.; Ross, D. Metabolism of mitomycin C by DT-diaphorase: Role in mitomycin C-induced DNA damage and cytotoxicity in human colon carcinoma cells. *Cancer Res.* **1990**, *50*, 7483-7489.

(17) Walton, M. I.; Smith, P. J.; Workman, P. The role of NAD(P)H: quinone reductase (EC 1.6.99.2, DT-diaphorase) in the reductive bioactivation of the novel indoloquinone antitumor agent EO9. *Cancer Commun.* **1991**, *3*, 199-206.

(18) Siegel, D.; Beall, H. D.; Senekowitsch, C.; Kasai, M.; Arai, H.; Gibson, N. W.; Ross, D. Bioreductive activation of mitomycin C by DT-diaphorase. *Biochemistry* **1992**, *31*, 7879-7885.

(19) Naylor, M. A.; Swann, E.; Everett, S. A.; Jaffar, M.; Nolan, J.; Robertson, N.; Lockyer, S. D.; Patel, K. B.; Dennis, M. F.; Stratford, M. R.; Wardman, P.; Adams, G. E.; Moody, C. J.; Stratford, I. J. Indolequinone antitumor agents: Reductive activation and elimination from (5-methoxy-1-methyl-4,7-dioxoindol-3-yl)methyl derivatives and hypoxia-selective cytotoxicity in vitro. *J. Med. Chem.* **1998**, *41*, 2720-2731.

(20) Siegel, D.; Gibson, N. W.; Preusch, P. C.; Ross, D. Metabolism of diaziquone by NAD(P)H:(quinone acceptor) oxidoreductase (DT-diaphorase): Role in diaziquone-induced DNA damage and cytotoxicity in human colon carcinoma cells. *Cancer Res.* **1990**, *50*, 7293-7300.

(21) Schlager, J. J.; Powis, G. Cytosolic NAD(P)H:(quinone-acceptor)oxidoreductase in human normal and tumor tissue: Effects of cigarette smoking and alcohol. *Int. J. Cancer* **1990**, *45*, 403-409.

(22) Malkinson, A. M.; Siegel, D.; Forrest, G. L.; Gazdar, A. F.; Oie, H. K.; Chan, D. C.; Bunn, P. A.; Mabry, M.; Dykes, D. J.; Harrison, S. D.; Ross, D. Elevated DT-diaphorase activity and messenger RNA content in human non-small cell lung

carcinoma: Relationship to the response of lung tumor xenografts to mitomycin C. *Cancer Res.* **1992**, *52*, 4752-4757.

(23) Cresteil, T.; Jaiswal, A. K. High levels of expression of the NAD(P)H:quinone oxidoreductase (NQO1) gene in tumor cells compared to normal cells of the same origin. *Biochem. Pharmacol.* **1991**, *42*, 1021-1027.

(24) Rampling, R.; Cruickshank, G.; Lewis, A. D.; Fitzsimmons, S. A.; Workman, P. Direct measurement of pO2 distribution and bioreductive enzymes in human malignant brain tumors. *Int. J. Radiat. Oncol. Biol. Phys.* **1994**, *29*, 427-431.

(25) Mikami, K.; Naito, M.; Ishiguro, T.; Yano, H.; Tomida, A.; Yamada, T.; Tanaka, N.; Shirakusa, T.; Tsuruo, T. Immunological quantitation of DT-diaphorase in carcinoma cell lines and clinical colon cancers: Advanced tumors express greater levels of DT-diaphorase. *Jpn. J. Cancer Res.* **1998**, *89*, 910-915.

(26) Doyle, T. W.; Balitz, D. M.; Grulich, R. E.; Nettleton, D. E.; Gould, S. J.; Tann, C.; Moews, A. E. Structure determination of lavendamycin, a new antitumor antibiotic from Streptomyces lavendulae. *Tetrahedron Lett.* **1981**, *22*, 4595-4598.

(27) Balitz, D. M.; Bush, J. A.; Bradner, W. T.; Doyle, T. W.; O'Herron, F. A.; Nettleton, D. E. Isolation of lavendamycin, a new antibiotic from Streptomyces lavendulae. *J. Antibiot. (Tokyo)* **1982**, *35*, 259-265.

(28) Erickson, W. R.; Gould, S. J. Streptonigrin biosynthesis. 7. Incorporation of oxygen from $^{18}O_2$: Evidence for an oxidative β-carboline cleavage. *J. Am. Chem. Soc.* **1985**, *107*, 5831-5832.

(29) Erickson, W. R.; Gould, S. J. Streptonigrin Biosynthesis. 8. Evidence for the involvement of a new Shikimate pathway product and a new route to quinolines. *J. Am. Chem. Soc.* **1987**, *109*, 620-621.

(30) Rao, K. V.; Biemann, K.; Woodward, R. B. The structure of streptonigrin. *J. Am. Chem. Soc.* **1963**, *85*, 2532-2533.

(31) Boger, D. L.; Yasuda, M.; Mitscher, L. A.; Drake, S. D.; Kitos, P. A.; Thompson, S. C. Streptonigrin and lavendamycin partial structures. Probes for the minimum, potent pharmacophore of streptonigrin, lavendamycin, and synthetic quinoline-5,8-diones. *J. Med. Chem.* **1987**, *30*, 1918-1928.

(32) Hackethal, C. A.; Golbey, R. B.; Tan, C. T.; Karnofsky, D. A.; Burchenal, J. H. Clinical observations on the effects of streptonigrin in patients with neoplastic disease. *Antibiot. Chemother.* **1961**, *11*, 178-183.

(33) Behforouz, M.; Merriman, R. L. Lavendamycin analogs and methods of making and using them. *U.S. Patent 5525611* **1996**.

(34) Behforouz, M.; Cai, W.; Mohammadi, F.; Stocksdale, M. G.; Gu, Z.; Ahmadian, M.; Baty, D. E.; Etling, M. R.; Al-Anzi, C. H.; Swiftney, T. M.; Tanzer, L. R.; Merriman, R. L.; Behforouz, N. C. Synthesis and evaluation of antitumor activity of novel N-acyllavendamycin analogues and quinoline-5,8-diones. *Bioorg. Med. Chem.* **2007**, *15*, 495-510.

(35) Fang, Y.; Linardic, C. M.; Richardson, D. A.; Cai, W.; Behforouz, M.; Abraham, R. T. Characterization of the cytotoxic activities of novel analogues of the antitumor agent, lavendamycin. *Mol. Cancer Ther.* **2003**, *2*, 517-526.

(36) Fourie, J.; Oleschuk, C. J.; Guziec, F., Jr.; Guziec, L.; Fiterman, D. J.; Monterrosa, C.; Begleiter, A. The effect of functional groups on reduction and activation of quinone bioreductive agents by DT-diaphorase. *Cancer Chemother. Pharmacol.* **2002**, *49*, 101-110.

(37) Phillips, R. M.; Naylor, M. A.; Jaffar, M.; Doughty, S. W.; Everett, S. A.; Breen, A. G.; Choudry, G. A.; Stratford, I. J. Bioreductive activation of a series of indolequinones by human DT-diaphorase: Structure-activity relationships. *J. Med. Chem.* **1999**, *42*, 4071-4080.

(38) Beall, H. D.; Winski, S.; Swann, E.; Hudnott, A. R.; Cotterill, A. S.; O'Sullivan, N.; Green, S. J.; Bien, R.; Siegel, D.; Ross, D.; Moody, C. J. Indolequinone antitumor agents: Correlation between quinone structure, rate of metabolism by recombinant human NAD(P)H:quinone oxidoreductase, and in vitro cytotoxicity. *J. Med. Chem.* **1998**, *41*, 4755-4766.

(39) Beall, H. D.; Hudnott, A. R.; Winski, S.; Siegel, D.; Swann, E.; Ross, D.; Moody, C. J. Indolequinone antitumor agents: Relationship between quinone structure and rate of metabolism by recombinant human NQO1. *Bioorg. Med. Chem. Lett.* **1998**, *8*, 545-548.

(40) Jaffar, M.; Phillips, R. M.; Williams, K. J.; Mrema, I.; Cole, C.; Wind, N. S.; Ward, T. H.; Stratford, I. J.; Patterson, A. V. 3-substituted-5-aziridinyl-1-methylindole-4,7-diones as NQO1-directed antitumour agents: Mechanism of activation and cytotoxicity in vitro. *Biochem. Pharmacol.* **2003**, *66*, 1199-1206.

(41) Phillips, R. M. Bioreductive activation of a series of analogues of 5-aziridinyl-3-hydroxymethyl-1-methyl-2-[1H-indole-4, 7-dione] prop-beta-en-alpha-ol (EO9) by human DT-diaphorase. *Biochem. Pharmacol.* **1996**, *52*, 1711-1718.

(42) Swann, E.; Barraja, P.; Oberlander, A. M.; Gardipee, W. T.; Hudnott, A. R.; Beall, H. D.; Moody, C. J. Indolequinone antitumor agents: Correlation between quinone structure and rate of metabolism by recombinant human NAD(P)H:quinone oxidoreductase. Part 2. *J. Med. Chem.* **2001**, *44*, 3311-3319.

(43) Buffinton, G. D.; Ollinger, K.; Brunmark, A.; Cadenas, E. DT-diaphorase-catalysed reduction of 1,4-naphthoquinone derivatives and glutathionyl-quinone conjugates. *Biochem. J.* **1989**, *257*, 561-571.

(44) Behforouz, M.; Cai, W.; Stocksdale, M. G.; Lucas, J. S.; Jung, J. Y.; Briere, D.; Wang, A.; Katen, K. S.; Behforouz, N. C. Novel lavendamycin analogues as potent HIV-reverse transcriptase inhibitors: Synthesis and evaluation of anti-reverse transcriptase activity of amide and ester analogues of lavendamycin. *J. Med. Chem.* **2003**, *46*, 5773-5780.

(45) Hassani, M.; Cai, W.; Holley, D. C.; Lineswala, J. P.; Maharjan, B. R.; Ebrahimian, G. R.; Seradj, H.; Stocksdale, M. G.; Mohammadi, F.; Marvin, C. C.; Gerdes, J. M.; Beall, H. D.; Behforouz, M. Novel lavendamycin analogues as antitumor agents: synthesis, in vitro cytotoxicity, structure-metabolism, and computational molecular modeling studies with NAD(P)H:quinone oxidoreductase 1. *J. Med. Chem.* **2005**, *48*, 7733-7749.

(46) Winski, S. L.; Swann, E.; Hargreaves, R. H.; Dehn, D. L.; Butler, J.; Moody, C. J.; Ross, D. Relationship between NAD(P)H:quinone oxidoreductase 1 (NQO1)

levels in a series of stably transfected cell lines and susceptibility to antitumor quinones. *Biochem. Pharmacol.* **2001**, *61*, 1509-1516.

(47) Cotterill, A. S.; Moody, C. J.; Mortimer, R. J.; Norton, C. L.; O'Sullivan, N.; Stephens, M. A.; Stradiotto, N. R.; Swann, E.; Stratford, I. J. Cyclopropamitosenes, novel bioreductive anticancer agents. Synthesis, electrochemistry, and biological activity of 7-substituted cyclopropamitosenes and related indolequinones. *J. Med. Chem.* **1994**, *37*, 3834-3843.

(48) Fryatt, T.; Pettersson, H. I.; Gardipee, W. T.; Bray, K. C.; Green, S. J.; Slawin, A. M.; Beall, H. D.; Moody, C. J. Novel quinolinequinone antitumor agents: Structure-metabolism studies with NAD(P)H:quinone oxidoreductase (NQO1). *Bioorg. Med. Chem.* **2004**, *12*, 1667-1687.

(49) Fourie, J.; Guziec, F., Jr.; Guziec, L.; Monterrosa, C.; Fiterman, D. J.; Begleiter, A. Structure-activity study with bioreductive benzoquinone alkylating agents: Effects on DT-diaphorase-mediated DNA crosslink and strand break formation in relation to mechanisms of cytotoxicity. *Cancer Chemother. Pharmacol.* **2004**, *53*, 191-203.

(50) Winski, S. L.; Hargreaves, R. H.; Butler, J.; Ross, D. A new screening system for NAD(P)H:quinone oxidoreductase (NQO1)-directed antitumor quinones: Identification of a new aziridinylbenzoquinone, RH1, as a NQO1-directed antitumor agent. *Clin. Cancer Res.* **1998**, *4*, 3083-3088.

(51) Faig, M.; Bianchet, M. A.; Winski, S.; Hargreaves, R.; Moody, C. J.; Hudnott, A. R.; Ross, D.; Amzel, L. M. Structure-based development of anticancer drugs:

Complexes of NAD(P)H:quinone oxidoreductase 1 with chemotherapeutic quinones. *Structure* **2001***, 9*, 659-667.

(52) Phillips, R. M.; Jaffar, M.; Maitland, D. J.; Loadman, P. M.; Shnyder, S. D.; Steans, G.; Cooper, P. A.; Race, A.; Patterson, A. V.; Stratford, I. J. Pharmacological and biological evaluation of a series of substituted 1,4-naphthoquinone bioreductive drugs. *Biochem. Pharmacol*. **2004***, 68*, 2107-2116.

(53) Suleman, A.; Skibo, E. B. A comprehensive study of the active site residues of DT-diaphorase: Rational design of benzimidazolediones as DT-diaphorase substrates. *J. Med. Chem*. **2002***, 45*, 1211-1220.

(54) Hendriks, H. R.; Pizao, P. E.; Berger, D. P.; Kooistra, K. L.; Bibby, M. C.; Boven, E.; Dreef-van der Meulen, H. C.; Henrar, R. E. C.; Fiebig, H. H.; Double, J. A.; Hornstra, H. W.; Pinedo, H. M.; Workman, P.; Schwartsmann, G. EO9: A novel bioreductive alkylating indoloquinone with preferential solid tumour activity and lack of bone marrow toxicity in preclinical models. *Eur. J. Cancer* **1993***, 29A*, 897-906.

(55) Abe, N.; Nakakita, Y.; Nakamura, T.; Enoki, N.; Uchida, H.; Takeo, S.; Munekata, M. Novel cytocidal compounds, oxopropalines from Streptomyces sp. G324 producing lavendamycin. I. Taxonomy of the producing organism, fermentation, isolation and biological activities. *J. Antibiot. (Tokyo)* **1993***, 46*, 1672-1677.

Chapter 3

Development of an *In Silico* Model of the NAD(P)H:Quinone Oxidoreductase 1 (NQO1) Active Site and Computational Molecular Docking Studies on Lavendamycin Antitumor Agents

3.1 Abstract

To facilitate NAD(P)H:quinone oxidoreductase 1 (NQO1)-directed lavendamycin antitumor agent development and perform corresponding docking studies, our laboratory developed a 1H69 crystal structure-based *in silico* (computer-generated) model of the NQO1 active site. The coordinates of the crystal structure of the NQO1 complex with the indolequinone ARH019 obtained from the Protein Data Bank (PDB ID code: 1H69) was used as a reference structure. In order to develop the *in silico* model, the energy-minimized compound MB-353 was superposed to the coordinates of the original reference ligand ARH019. FAD was introduced to the active site of NQO1 as a heteroatom file. Computational molecular docking studies were performed on two lavendamycin analogues, MB-353 and MB-323, good and poor substrates for NQO1, respectively. The molecular docking was performed using the FlexX module of SYBYL 6.9.1 software suite. FlexX used MB-353 as the reference ligand for docking experiments. The docked conformations (poses) of ligands were evaluated using the CSCORE module in SYBYL. Geometric post-docking analyses that determine hydrogen-bonding interactions of the ligands with the key residues of the active site and FAD and hydride ion transfer from the flavin to the ligands were performed. Of thirty

possible docked poses of MB-353, nineteen had CSCORE ≥ 4 indicating that this ligand was a good substrate. All of the nineteen poses were capable of forming effective hydrogen-bonding interactions and hydride ion transfer. However, none of the MB-323 poses had a CSCORE = 5 nor was capable of hydrogen bond formation and hydride ion transfer. Molecular docking supported a model in which the good (MB-353) versus poor NQO1 substrate (MB-323) was capable of effective hydrogen-bonding interactions with FAD and the key amino acid residues of the active site along with hydride ion reception.

3.2 Introduction

Molecular docking was first introduced in the early 1980s and since then has become a useful tool and a principal component in the field of drug development and discovery.[1,2] Protein-ligand docking as a subcategory of the general field of molecular docking has received enormous attention from the scientific community due to its application in many fields of research including medicinal chemistry and cancer studies.[1,3] This approach has emerged as a powerful tool in the design of selective substrates for validated targets in cancer therapy.[3]

Molecular docking is defined as computational methods that predict binding orientations of ligands in the active site of the target.[4-6] This approach consists of utilizing a computer program to generate an *in silico* model of the target based on the available three-dimentional (3D) crystal structure.[1,2] There are two major components to protein-ligand docking protocols including docking and scoring.[1-3] Docking, which is also known as searching/search algorithm/posing/pose prediction, is the placement of

ligands in the target binding site. Docking makes it possible to search for and correctly predict the ligand conformations and binding orientations.[1-3] A search algorithm should be fast and capable of effective coverage of the relevant search space.[1]

The prediction of binding affinities and how well ligands bind to the protein are performed by scoring.[1,2] The scoring function should distinguish the correct binding mode (pose) among others explored through the search algorithm , and evaluate and rank the search results accordingly.[1,3] The computed interaction energy of ligand-protein (score) of a pose determines its final rank-ordering.[2] One proper scoring approach - consensus score - employs several scoring functions to rank different poses.[2] For a pose to be selected and kept based on this approach , it has to be assigned high scores by a number of different component scoring functions.[2]

Molecular docking methods need to utilize three-dimensional protein structures to investigate protein-ligand molecular recognitions and binding events.[2] Today, there are more than 35,000 structures of proteins and nucleic acids stored in the Protein Data Bank (PDB).[1] This wealth of the available three-dimensional structures of proteins and protein-ligand structural data has highly contributed to the field of molecular docking and subsequently to the drug development process.[6]

When the target binding site has been already determined, one way to perform a ligand-protein fit search is the manual docking of the corresponding ligand into the active site.[3] However, manual docking requires a great expertise and is a very labor intensive and time consuming practice.[3] Therefore, development of a general *in silico* model of the target protein active site that can be used in automatic docking processes can greatly facilitate and accelerate these processes. Several modeling studies of NQO1-quinone

substrates have been performed to identify key components of quinone compounds, which confer high substrate specificity.[7-10] However, there has not been any systematic attempt to develop an *in silico* general model of the NQO1 active site as a predictive tool. An active site model can be utilized for docking studies and prediction of the substrate specificity of a series of structurally related antitumor quinone compounds.[9]

To facilitate NQO1-directed lavendamycin antitumor agent development, we developed an *in silico* model of the NQO1 active site. This model served to gain insights into the details of molecular basis of lavendamycin binding events at the NQO1 active site that would be used along with our structure-activity relationship (SAR) data for structure-based design of novel lavendamycin substrates (See Chapter 4). Development of this model will also enable rapid docking of a large number of lavendamycin substrates into the NQO1 active site without bearing the extra effort and expense of synthesizing and testing all the analogues. This will provide a useful tool, which is capable of accurate prediction of the best potential lavendamycin substrates for NQO1 with high preferential toxicity towards cancer cells that overexpress this enzyme.

3.3 Materials and Methods

3.3.1 Coordinates Preparation. The coordinates of the crystal structure of human NQO1 complex with bound FAD and the indolequinone ARH019, 3-(Hydroxymethyl)-5-(2-methylaziridin-1-yl)-1-methyl-2-phenylindole-4,7-dione,[11] were obtained from the Protein Data Bank (PDB ID code: 1H69[12]). This structure was used as a reference structure for the docking experiments and compound ARH019 served as the

original reference ligand. The physiological dimer in the crystal unit was used for docking purposes.

3.3.2 Development of *In Silico* Model of the NQO1 Active Site. The molecular modeling studies were performed using SYBYL 6.9.1 software suite[13] (Tripos, Inc.; St. Louis, MO). The coordinates of the crystal structure of human NQO1 complex with bound FAD and ARH019, obtained from the Protein Data Bank (PDB ID code: 1H69[12]), were utilized to develop the *in silico* model of the NQO1 active site.[14] In order to develop the model, the energy-minimized compound MB-353 was superposed to the coordinates of the original reference ligand ARH019 such that overlap was optimal. Ligand MB-353 was again energy minimized in the context of the active site and therefore the position of the ligand within the pocket was considered optimized for the purpose of this study. The active site was then defined as all the amino acid residues confined within 6.5 Å radius sphere centered on the superposed ligand MB-353. The coordinates were locally minimized and subjected to energy minimization with minimal iterations (100) by Powell minimization standard method using Minimize Subset option within SYBYL. This option automatically selected 24 seed amino acid residues surrounding the superposed ligand MB-353 to perform the local minimization. Default parameters and values within the minimization dialog were used except where otherwise mentioned. This procedure yielded a weighted root-mean-square distance of 0.26 Å between the 24 corresponding non-minimized and minimized residues in the structures. The file of the composite structure containing ligand MB-353 and FAD was saved. The composite structure without MB-353 utilized as the *in silico* model of the NQO1 active site for docking studies. Ligand MB-353 served as the reference ligand for the docking

studies. Docking calculations were performed using one of the two identical active sites.

3.3.3 Ligand Preparation. The structures of ligands were sketched and prepared as MOL2 files employing the Sketch Molecule module of SYBYL 6.9.1 software suite[13] (Tripos, Inc.; St. Louis, MO). Initially sketched Ligands were subjected to energy minimization (10,000 iterations) by Powell minimization standard method. Initial Optimization and Termination parameters were set to None and Energy Change options, respectively. Default parameters and values within the minimization dialog (Minimize Details) were used except where otherwise noted. The final ligand conformational coordinates were stored as MOL2 files within the database.

3.3.4 Docking. Flexible docking was performed using the FlexX module of SYBYL 6.9.1 software suite.[13] FlexX is an automatic docking program for conformationaly flexible ligands that employs the 3D structure of the target protein in PDB format, and is capable of determining 30 possible conformations for each docked ligand. The final rank order of the conformations is based on the free binding energy. This program automatically selects the base fragment of a ligand (the ligand core). The base fragment is then placed into the active site of the target protein using the algorithmic approach called pose clustering that is based upon a pattern recognition paradigm. Subsequent incremental reconstruction of the complete ligand molecule is then performed by linking the remaining components.[15,16] For the *in silico* model, the active site was defined as all the amino acid residues confined within 6.5 Å radius sphere centered on the superposed ligand MB-353. FAD was introduced to the active site as a heteroatom file in MOL2 format.

3.3.5 Scoring Functions. The docked conformations of ligands were evaluated

and ranked using FlexX and four scoring functions implemented in the CSCORE module in SYBYL. CSCORE is a consensus scoring program that integrates multiple well-known scoring functions such as FlexX, ChemScore,[17] D-Score,[18] G-Score[19] and PMF-Score[20] to evaluate docked conformations. Individual scoring functions are used to predict the affinity of the ligand binding to a target protein. CSCORE creates columns in a molecular spreadsheet that contains raw scores for each individual scoring function. The consensus column contains integers that range from 0 to 5; where 5 is the best fit to the model. Docked conformations whose scores exceed the threshold for a particular function contribute one to the value of the consensus, whereas those with scores below the threshold add a zero.

3.3.6 Molecular Graphics System. The molecular graphics images and surface representations were prepared with PyMOL molecular graphics system version PyMOLX11Hybrid 0.97[21] (Delano Scientific, San Carlos, CA, USA). The data of the coordinates of the NQO1 complex with bound FAD and docked conformations of ligands were prepared in PDB format as PyMOL input files. PyMOL session files of the NQO1 active site with docked conformations of ligands and the superimposition of clustered conformations were created. The images were then stored as graphic files.

3.4 Results and Discussion

3.4.1 Development of *In Silico* Model of the NQO1 Active Site. The molecular modeling and docking studies were performed using SYBYL 6.9.1 software suite[13] (Tripos, Inc.; St. Louis, MO). The crystal structure of human NQO1 complex

with bound FAD and ARH019 (Chart 3.1) (PDB ID code: 1H69[12]) has been suggested as an appropriate model for molecular docking studies of other quinone compounds such as streptonigrin (SN).[12] Therefore, the coordinates of this crystal structure were used as the reference structure to develop an *in silico* model of the NQO1 active site for docking studies. To develop the *in silico* model that can be used in lavendamycin docking studies we introduced a reference ligand into the active site that could be recognized by the FlexX docking program. Since FlexX could not recognize ARH019 as the reference ligand, compound MB-353 (Chart 3.1) was used as the reference ligand for lavendamycin docking studies. MB-353 was superposed to the coordinates of ARH019 such that overlap was optimal. ARH019 served as the reference of location for MB-353. The active site was then defined as all the amino acid residues confined within 6.5 Å radius sphere centered on the superposed ligand MB-353. The file of the composite structure containing ligand MB-353 and FAD was saved. This composite structure without MB-353 utilized as the *in silico* model of the NQO1 active site for automatic docking studies (Figure 3.1). FlexX used MB-353 as the reference ligand in automatic docking processes and FAD was introduced to the active site as a heteroatom file in MOL2 format.

Chart 3.1. Chemical structures of the indolequinone ARH019 and lavendamycin analogue MB-353.

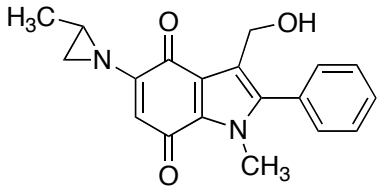

ARH019

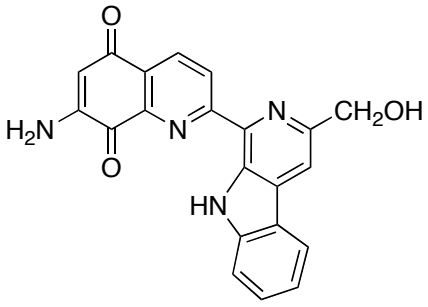

MB-353

Figure 3.1. The developed *in silico* model of the NQO1 active site.

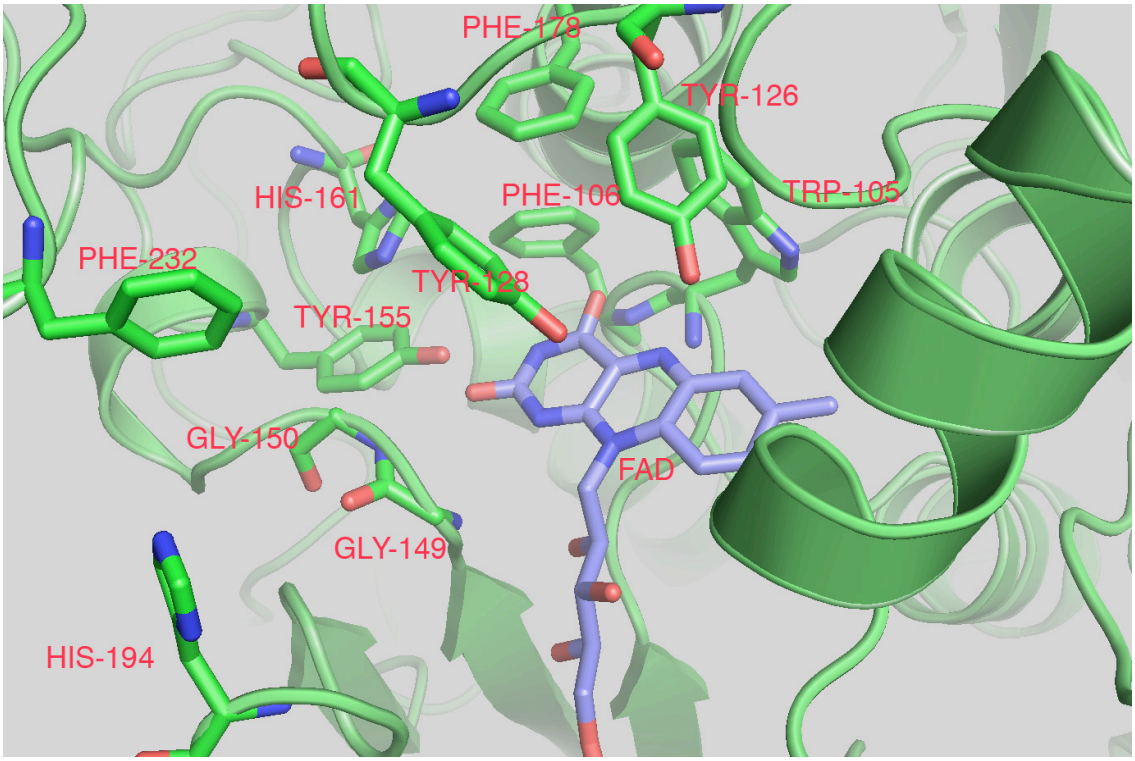

Figure 3.1. The developed *in silico* model of the NQO1 active site. The coordinates of the crystal structure of human NQO1 complex with bound FAD and ARH019 (PDB ID code: 1H69) were utilized to develop the *in silico* model of the NQO1 active site. To develop the model, the energy-minimized compound MB-353 was superposed to the coordinates of the ligand ARH019. The active site was then defined as all the amino acid residues confined within 6.5 Å radius sphere centered on the superposed ligand MB-353. The composite structure containing ligand MB-353 and FAD was saved. The composite structure without MB-353 was utilized as the *in silico* model of the NQO1 active site for lavendamycin docking studies. Residues of the active site (lime) and FAD (blue) are represented as stick models. The rest of the structure is represented as a secondary structure cartoon. The atoms are colored: red, oxygen atoms; blue, nitrogen atoms; orange, phosphorus atoms and white, hydrogen atoms.

3.4.2 Docking Studies. Computational and comparative molecular docking studies were performed on two lavendamycin analogues, MB-323 and MB-353, poor and good substrates for NQO1, respectively. Flexible docking was performed using the FlexX module of SYBYL that is capable of determining 30 possible poses for each docked ligand.[15,16] The docked conformations of ligands MB-323 and MB-353 were evaluated and ranked using FlexX and four scoring functions implemented in the CSCORE module in SYBYL. CSCORE is the consensus score computed from FlexX, ChemScore,[17] D-Score,[18] G-Score[19] and PMF-Score[20] scoring functions, in which docked poses are evaluated and ranked from 0 to 5; where 5 is the best fit to the model. Table 3.1 displays the number of poses of ligands MB-323 and MB-353 in each score group of CSCORE function.

Table 3.1. Number of poses of ligands MB-323 and MB-353 in each score group of CSCORE function.

Compound	MB-323						MB-353					
CSCORE	0	1	2	3	4	5	0	1	2	3	4	5
Number of Poses	18	8	-	-	4	-	3	3	1	4	15	4

Ligand MB-353 possessed a higher number of poses with more optimal CSCORE values compared to MB-323 (Table 3.1). To minimize the number of false positives and/or negatives, visual screening of the binding orientations of the poses and geometric post-docking analyses were performed. The analyses included distance measurements and poses geometries that determined: a) hydrogen-bonding interactions of the ligand poses with the key amino acid residues of the NQO1 active site including Tyr-126, -128, Gly-149 and His-161, b) hydride ion transfer from the N5 of the FAD isoalloxazine ring to the ligands at either carbonyl oxygens (O5 or O8) or at a ring carbon, and c) the angle between the quinone-moiety plane of the ligands and the FAD isoalloxazine ring. Residue numbers in this study are those used in the Protein Data Bank coordinates, PDB ID code: 1H69.[12]

Of the thirty possible docked conformations of ligand MB-353, twenty-four poses (CSCORE ≥ 2) displayed binding orientations similar to that of the original reference ligand ARH019. Compound ARH019 has been shown to enter the active site by the 4,7-dione moiety where the plane of the indolequinone forms a partial aromatic-ring parallel stacking with the FAD isoalloxazine ring, and the corresponding plane-to-plane angle is 16°.[12] The methyl-aziridinyl group of ARH019 stacks against the Trp-105 indole and 2-phenyl group stacks over Gly-149 and Gly-150 and points toward the outside of NQO1 active site.[12] The binding orientation of ARH019, and ligands MB-323 and MB-353 in the NQO1 active site were similarly determined by the positioning of quinone carbonyl oxygens and atoms toward the isoalloxazine ring atoms of FAD and residues of the active site. Compound ARH019 carbonyl oxygen O4 in comparison to O7 is positioned closer to Tyr-126, -128 and the N5 of FAD.[12]

Nineteen poses of ligand MB-353 had CSCORE ≥ 4 (Table 3.1). Poses with CSCORE ≥ 4 fell into four clusters, where a cluster is defined as a group of poses that gives a root mean square deviation (RMSD) less than 0.8 Å for the quinolinedione and indolopyridine moieties atoms. Poses 1, 9 and 15 (Figure 3.2a) and 20, 24 and 27 (Figure 3.2b) fell into two clusters in which the RMS deviation of the poses equaled zero and the difference was in the binding orientation of the CH_2OH group in the NQO1 active site (Figures 3.2a and 3.2b). Poses 3, 4, 5, 6, 7, 11 and 12 (Figure 3.2c) and 8, 10, 18, 19 and 26 (Figure 3.2d) were clustered into two groups that yielded RMS deviations of < 0.8 Å. All of the clustered poses of MB-353 entered the active site by the 5,8-dione moiety similar to ARH019, where the departure of the planes of most of these poses from a complete aromatic-ring parallel stacking with the FAD isoalloxazine ring closely resembled that of ARH019 (Figure 3.2) (Table 3.2).

The purpose of pose clustering is to determine the preferred binding orientation of ligands.[10] The carbonyl oxygen O5 of the clustered poses compared to O8 was positioned closer to Tyr-126, -128 and the FAD N5 (Table 3.2) resembling compound ARH019 binding orientation, suggesting that this could be the preferred binding orientation for ligand MB-353 (Figure 3.2). Also, the departure of the planes of the most of these poses from an exact aromatic parallel stacking with FAD closely resembled that for the reference ligand ARH019 (Table 3.2).

Figure 3.2. View of the superposition of the docked poses of MB-353 (CSCORE ≥ 4) in the NQO1 active site.

a) **b)**

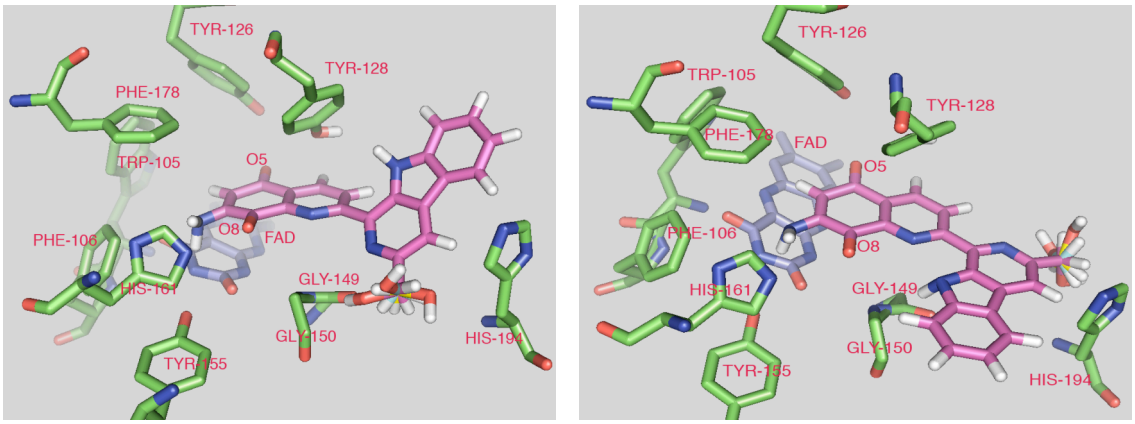

c) **d)**

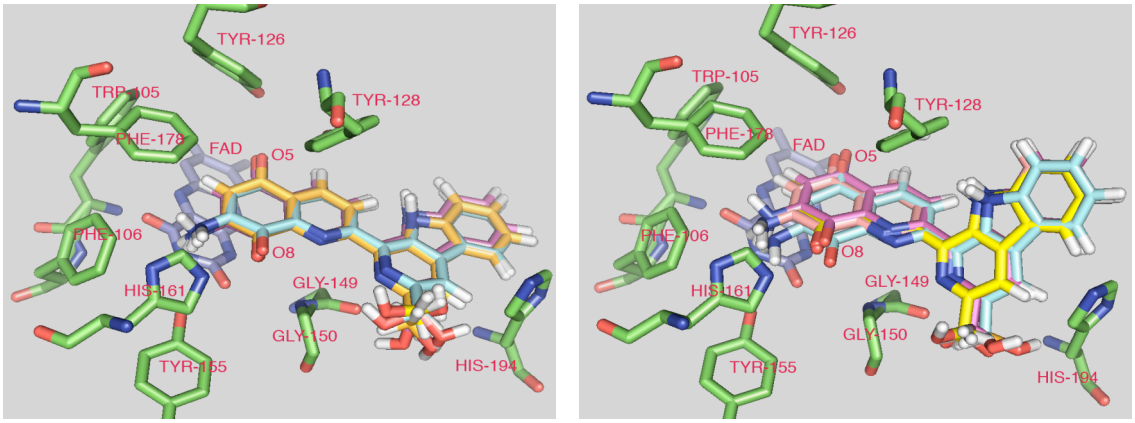

Figure 3.2. View of the superposition of the docked poses of MB-353 (CSCORE ≥ 4) in the NQO1 active site. **a)** View of the superposition of the docked poses 1, 9 and 15 of ligand MB-353 (magenta, cyan and yellow) (CSCORE = 5, 4 and 4) in the NQO1 active site (RMSD = 0 Å). **b)** View of the superposition of the docked poses 20, 24 and 27 of MB-353 (magenta, cyan and yellow) (CSCORE = 4) in the NQO1 active site (RMSD = 0 Å). **c)** View of the superposition of the docked poses 3, 4, 5, 6, 7, 11 and 12 of MB-353 (magenta, cyan, yellow, salmon, blue, orange and green) (CSCORE = 4) in the NQO1 active site (RMSD < 0.8 Å). **d)** View of the superposition of the docked poses 8, 10, 18, 19 and 26 of MB-353 (yellow, salmon, magenta, cyan and orange) (CSCORE = 5, 5, 4, 4 and 4) in the NQO1active site (RMSD < 0.8 Å). Residues of the active site (lime), FAD (blue), and MB-353 are represented as stick models. The atoms are colored: red, oxygen atoms; blue, nitrogen atoms and white, hydrogen atoms.

Table 3.2. Geometric post-docking analysis, measurements and calculations of the thirty possible poses of ligand MB-353 in the NQO1 active site.

P[a]	C[b]	O5 - Tyr126 (Å)	O5 - Tyr128 (Å)	O8 - Tyr126 (Å)	O8 - Tyr128 (Å)	N5 - O5 (Å)	N5 - O8 (Å)	N5 - C6 (Å)	N5 - C7 (Å)	Angle[c] (°)
2	5	3.960	2.051	9.165	6.132	4.515	7.382	4.310	5.198	24.96
1	5	3.705	2.055	8.743	5.774	4.359	7.053	4.044	4.893	18.18
10	5	3.865	2.190	9.015	6.199	4.355	7.133	4.122	4.988	21.29
8	5	3.822	2.142	8.849	6.061	4.311	7.004	3.963	4.820	21.63
27	4	3.880	1.842	8.853	5.678	4.609	7.331	4.296	5.146	16.87
24	4	3.880	1.842	8.853	5.678	4.609	7.331	4.296	5.146	16.87
19	4	4.240	1.991	9.437	6.419	4.693	7.522	4.451	5.326	25.87
18	4	3.635	1.752	8.682	5.783	4.674	7.032	4.148	4.897	21.04
9	4	3.705	2.055	8.743	5.774	4.359	7.053	4.044	4.893	18.18
26	4	4.240	1.991	9.437	6.419	4.693	7.522	4.451	5.326	25.87
15	4	3.705	2.055	8.743	5.774	4.359	7.053	4.044	4.893	18.18
7	4	3.896	2.100	9.008	6.017	4.379	7.271	4.261	5.146	15.40
12	4	3.760	2.257	8.976	6.058	4.237	6.934	4.009	4.848	18.33
6	4	3.896	2.100	9.008	6.017	4.379	7.271	4.261	5.146	15.40
5	4	3.896	2.100	9.008	6.017	4.379	7.271	4.261	5.146	15.40
4	4	3.896	2.100	9.008	6.017	4.379	7.271	4.261	5.146	15.40
3	4	3.760	2.257	8.976	6.058	4.237	6.934	4.009	4.848	18.33
11	4	3.842	1.981	9.071	6.159	4.593	7.066	4.265	5.026	18.88
20	4	3.880	1.842	8.853	5.678	4.609	7.331	4.296	5.146	16.87
21	3	4.273	2.592	9.493	6.405	4.138	7.517	4.302	5.322	27.95

13	3	3.792	1.704	9.022	6.026	4.952	7.154	4.555	5.219	18.25
16	3	3.826	1.724	8.924	5.918	4.714	7.092	4.314	5.048	13.46
14	3	3.792	1.704	9.022	6.026	4.952	7.154	4.555	5.219	18.25
22	2	3.853	1.690	8.916	5.976	4.753	6.996	4.262	4.960	14.29
28	1	6.654	4.783	9.874	7.394	7.306	12.051	9.310	10.551	102.72
29	1	9.117	6.163	4.100	1.869	7.306	4.653	5.502	4.735	11.76
23	1	7.305	5.108	2.521	2.661	7.690	6.728	5.708	5.376	114.20
30	0	6.654	4.783	9.874	7.394	7.306	12.051	9.310	10.551	102.72
17	0	6.458	4.530	9.980	7.878	6.974	12.182	9.198	10.491	108.29
25	0	7.027	4.920	9.890	7.543	7.699	12.561	10.035	11.223	98.04

[a] P = Pose

[b] C = CSCORE

[c] Plane-to-plane angle between the isoaloxazine ring of FAD and the quinolinequinone moiety of ligand MB-353

In the NQO1 active site, the hydroxyl groups of Tyr-126 and -128 and/or the N or NH of His-161 can form hydrogen bonds with carbonyl oxygens and/or other atoms of quinone substrates.[10,12,22] One crucial determining factor of quinone substrate binding strength in the NQO1 active site is the quinone oxygens capability of forming hydrogen-bonding interactions with Tyr-126 and -128.[10] The carbonyl oxygens O4 and O7 of the quinone nucleus of ARH019 form hydrogen bonds with the OH of Tyr-126 and NH of His-161, respectively.[12] Good substrates for NQO1 such as RH1 and EO9 are capable of forming hydrogen-bonding interactions with the key residues of the NQO1 active site.[12] The carbonyl oxygens O1 and O4 of RH1 also form hydrogen bonds with the NH of His-161 and the hydroxyl group of Tyr-128, respectively.[12] The O4 and O7 of EO9 is capable of hydrogen-bonding interaction formation with the Tyr-126 OH and NH of His-161, respectively.[12]

Although all of the clustered poses of MB-353 were capable of forming hydrogen-bonding interactions and hydride ion reception from the FAD N5, these poses differed in the number of and ability to form hydrogen bonds with FAD and the residues of the NQO1 active site (Table 3.2). Among the poses of ligand MB-353, poses 1 and 2 formed the highest number of hydrogen bonds in the active site of the enzyme. The 5,8-dione moiety of pose 1 with CSCORE = 5 stacked over the isoalloxazine ring of FAD and the NH_2 group at the quinolinedione-7-position was placed close to His-161 (Figures 3.3a and 3.3b). The fused three-ring indolopyridine moiety pointed toward the outside of the active site. The CH_2OH group at the indolopyridine -2'-position was placed close to Gly-149 (Figures 3.3a and 3.3b). Pose 2 (CSCORE = 5) also positioned in the NQO1 active site in a very similar way to pose 1 (Figure 3.3c) (Table 3.2). The carbonyl oxygen

O5 of MB-353 poses 1 and 2 formed a hydrogen bond with the Tyr-128 OH and one hydrogen atom of the NH_2 substituent formed a hydrogen bond with the N of His-161 (Figures 3.3b and 3.3c). Another hydrogen atom of the NH_2 substituent was capable of forming hydrogen-binding interactions with the O2 and N3 of FAD (Figures 3.3b and 3.3c). The CH_2OH group of the indolopyridine moiety further stabilized the binding by making a hydrogen bond to the carbonyl oxygen of Gly-149 (Figures 3.3b and 3.3c). Poses 1 and 2 of ligand MB-353 with high CSCORE of 5 made the highest number of hydrogen-bonding interactions in the active site resulting in favorable binding orientation for efficient hydride ion reception and quinone reduction.

Figure 3.3. Molecular model of the poses of MB-353 (CSCORE = 5) docked into the NQO1 active site.

a)

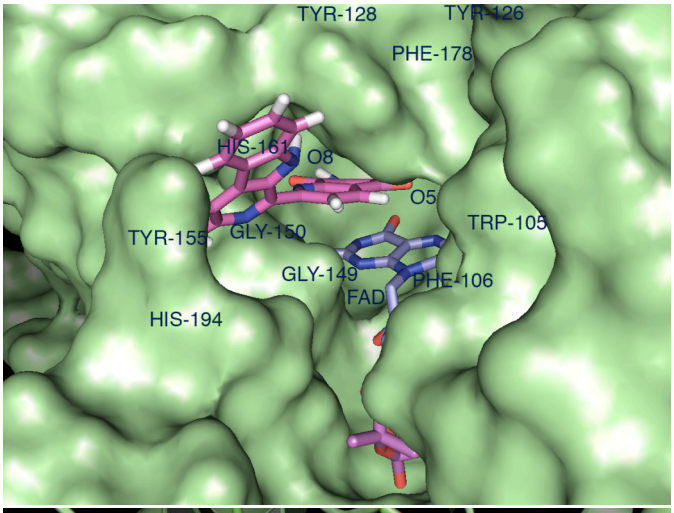

b)

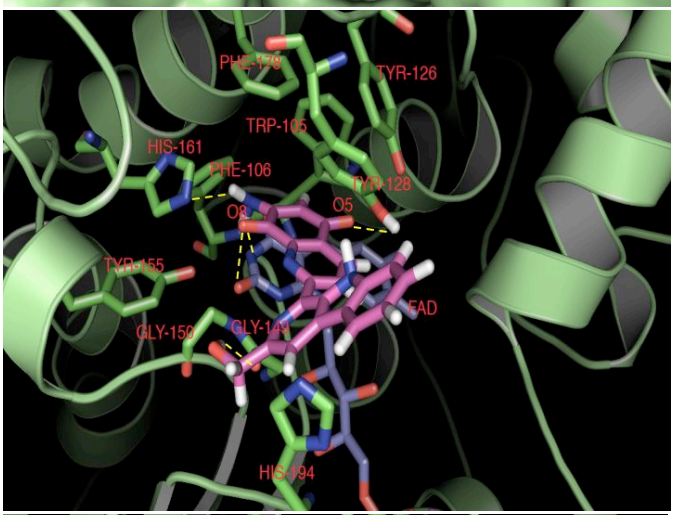

c)

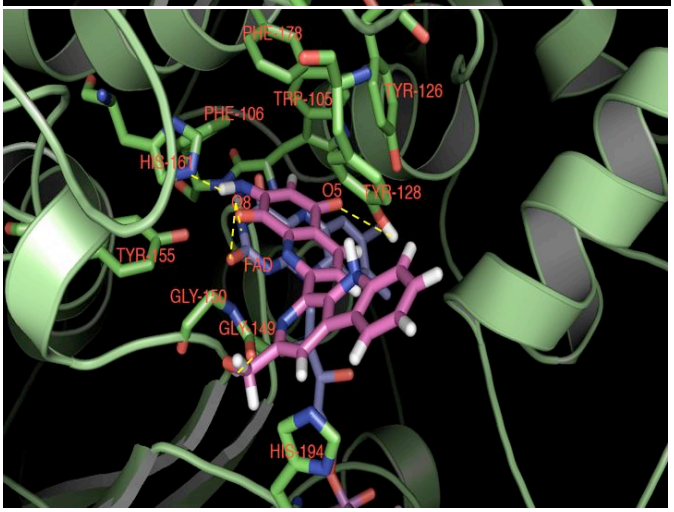

Figure 3.3. Molecular model of the poses of MB-353 (CSCORE = 5) docked into the NQO1 active site. **a)** Depiction of the molecular surface of the NQO1 active site region. The surface of the pocket is colored lime with FAD (blue) and the docked pose 1 of MB-353 (magenta) (CSCORE = 5) represented as stick models. **b)** Molecular model of the pose 1 of MB-353 docked into the NQO1 active site. **c)** Molecular model of the pose 2 of MB-353 (CSCORE = 5) docked into the NQO1 active site. In (b) and (c) the carbonyl oxygen O5 of MB-353 poses 1 and 2 formed a hydrogen bond with the Tyr-128 OH and one hydrogen atom of the NH_2 substituent formed a hydrogen bond with the N of His-161. Another hydrogen atom of the NH_2 substituent was capable of forming hydrogen-binding interactions with the O2 and N3 of FAD. The CH_2OH group of the indolopyridine moiety further stabilized the binding by making a hydrogen bond to the carbonyl oxygen of Gly-149. In (b) and (c) residues of the active site (lime), FAD (blue), and MB-353 (magenta) are represented as stick models and the rest of the structure is represented as a secondary structure cartoon. The atoms are colored: red, oxygen atoms; blue, nitrogen atoms and white, hydrogen atoms. Hydrogen bonds are represented as yellow dashed lines.

However, of the thirty possible docked conformations of ligand MB-323, twenty-six poses possessed CSCORE ≤ 1 and no conformation had a CSCORE = 5 (Table 3.1). None of the thirty poses had a binding orientation similar to that of the ligand ARH019. Pose 12 with CSCORE = 4 had a binding orientation opposite that of the original reference ligand where carbonyl oxygen O8 of pose 12 compared to O5 was positioned closer to Tyr-126, -128 and the FAD N5 (Figure 3.4a) (Table 3.3). The quinone nucleus partially stacked over the isoalloxazine ring of FAD and the $NHCOC_3H_7$-*n* group at the quinolinedione-7-position stacked over the isoalloxazine ring of FAD (Figure 3.4a). The fused three-ring indolopyridine moiety pointed toward the outside of the active site (Figure 3.4a). Neither of the carbonyl oxygens O5 and O8 of pose 12 was capable of forming hydrogen bonds with the residues of the active site unlike poses 1 and 2 of ligand MB-353 (Figure 3.4a) (Table 3.3). The other three poses (11, 26 and 28) of MB-323 with CSCORE = 4 entered the active site of NQO1 with the fused three-ring indolopyridine moiety where the quinolinedione moiety pointed toward the outside of the active site (Figures 3.4b and 3.4c) (Table 3.3). Compound ES1340, 5-Methoxy-3-(phenyloxymethyl)-1,2-dimethylindole-4,7-dione,[23] which is a poor substrate for NQO1[24] has been shown to position in the NQO1 active site such that the 4,7-dione moiety points to the outside of the active site.[25] The binding orientations of the poses of ligand MB-323 were not favorable for formation of hydrogen-bonding interactions, hydride ion reception and quinone reduction. The remaining twenty-six poses with CSCORE of 0 or 1 did not merit further considerations.

Figure 3.4. Molecular model of the poses of MB-323 (CSCORE = 4) docked into the NQO1 active site.

a)

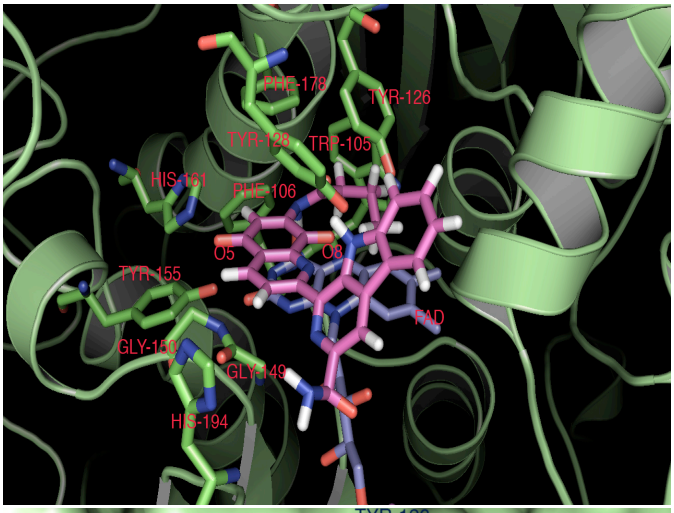

b)

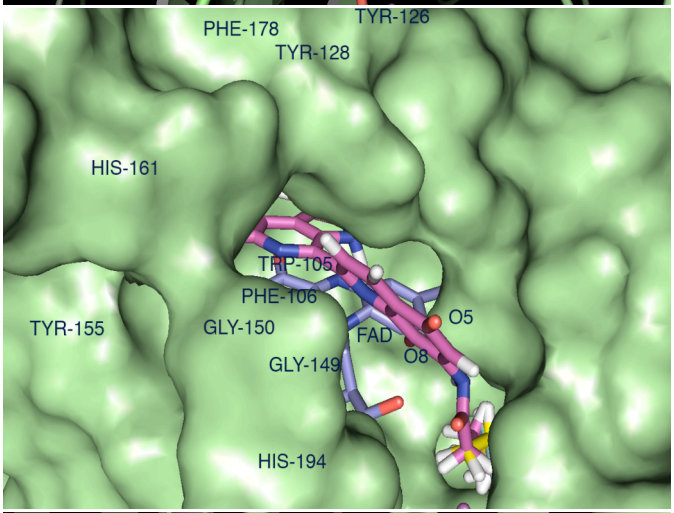

c)

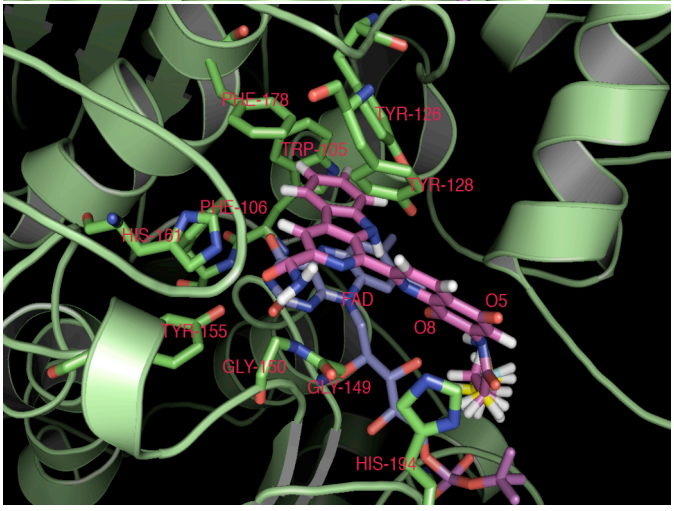

Figure 3.4. Molecular model of the poses of MB-323 (CSCORE = 4) docked into the NQO1 active site. **a)** Molecular model of the pose 12 of MB-323 (CSCORE = 4) docked into the NQO1 active site. Residues of the active site (lime), FAD (blue) and MB-323 (magenta) are represented as stick models and the rest of the structure is represented as a secondary structure cartoon. **b)** Depiction of the molecular surface of the NQO1 active site region. The surface of the pocket is colored lime with FAD (blue) and the docked poses 11, 26 and 28 of MB-323 (magenta, yellow and cyan) (CSCORE = 4) represented as stick models. **c)** Molecular model of the poses 11, 26 and 28 of MB-323 docked into the NQO1 active site. Residues of the active site (lime), FAD (blue) and MB-323 (magenta, yellow and cyan) are represented as stick models and the rest of the structure is represented as a secondary structure cartoon. The atoms are colored: red, oxygen atoms; blue, nitrogen atoms and white, hydrogen atoms.

Table 3.3. Geometric post-docking analysis, measurements and calculations of the thirty possible poses of ligand MB-323 in the NQO1 active site.

P[a]	C[b]	O5 - Tyr126 (Å)	O5 - Tyr128 (Å)	O8 - Tyr126 (Å)	O8 - Tyr128 (Å)	N5 - O5 (Å)	N5 - O8 (Å)	N5 - C6 (Å)	N5 - C7 (Å)	Angle[c] (º)
12	4	9.319	6.115	4.323	2.240	7.734	4.353	5.656	4.654	14.40
28	4	9.370	6.589	6.388	4.844	11.373	6.612	10.068	8.941	126.44
11	4	9.370	6.589	6.388	4.844	11.373	6.612	10.068	8.941	126.44
26	4	9.370	6.589	6.388	4.844	11.373	6.612	10.068	8.941	126.44
6	1	10.425	6.678	12.527	8.753	12.363	12.173	11.541	11.479	60.59
1	1	11.846	8.005	10.778	7.183	13.405	10.639	11.401	10.625	102.20
7	1	11.071	7.388	11.834	8.090	13.141	11.655	11.761	11.346	74.51
2	1	11.908	8.587	11.246	7.419	14.621	11.760	12.892	12.120	76.63
8	1	11.923	8.076	10.816	7.209	13.458	10.666	11.461	10.680	14.40
3	1	13.915	10.623	11.791	7.979	16.582	12.726	14.711	13.699	88.98
4	1	11.170	7.359	10.354	6.787	12.889	10.205	10.834	10.072	100.03
5	1	11.170	7.359	10.354	6.787	12.889	10.205	10.834	10.072	100.03
14	0	11.447	7.608	10.606	7.033	13.048	10.448	11.055	10.320	100.79
15	0	11.071	7.388	11.834	8.090	13.141	11.655	11.761	11.346	74.51
9	0	10.165	6.251	13.341	9.635	11.525	12.845	11.364	11.705	52.13
16	0	10.425	6.678	12.527	8.753	12.363	12.173	11.541	11.479	60.59
30	0	11.337	7.502	10.537	6.955	12.963	10.324	10.955	10.209	99.90
17	0	10.871	7.155	11.727	8.000	12.878	11.491	11.508	11.119	74.88
18	0	11.173	7.319	10.679	7.120	12.740	10.390	10.811	10.143	98.05
19	0	12.336	8.994	11.705	7.877	14.986	12.213	13.341	12.597	76.96

20	0	10.165	6.251	13.341	9.635	11.525	12.845	11.364	11.705	52.13
21	0	13.563	10.281	11.495	7.696	16.260	12.419	14.341	13.329	87.30
22	0	10.165	6.251	13.341	9.635	11.525	12.845	11.364	11.705	52.13
23	0	11.071	7.388	11.834	8.090	13.141	11.655	11.761	11.346	74.51
24	0	11.739	7.899	10.741	7.147	13.314	10.592	11.320	10.556	101.46
25	0	10.165	6.251	13.341	9.635	11.525	12.845	11.364	11.705	52.13
10	0	11.189	7.511	11.583	7.840	13.268	11.425	11.750	11.237	78.19
27	0	10.988	7.331	11.648	7.940	13.110	11.514	11.640	11.193	76.02
13	0	11.897	8.049	10.812	7.209	13.430	10.658	11.436	10.661	102.26
29	0	12.218	8.847	11.761	7.939	14.825	12.200	13.213	12.507	76.35

[a] P = Pose

[b] C = CSCORE

[c] Plane-to-plane angle between the isoaloxazine ring of FAD and the quinolinequinone moiety of ligand MB-323

3.5 Conclusions

The developed *in silico* model served to gain insights into the details of molecular basis of lavendamycin binding events in the NQO1 active site. The molecular modeling and docking studies demonstrated that ligand MB-353 possessed an increased number of possible poses with favorable binding orientations to promote hydrogen bonding interactions, hydride ion reception and quinone reduction compared to ligand MB-323. Ligand MB-353 due to the small hydrogen bond-forming substituents possessed structural characteristics for favorable positioning in the NQO1 active site for reduction. Conversely, the unfavorable structural characteristics of ligand MB-323 excluded it from proper positioning in the NQO1 active site for reduction. These findings suggest that active site positioning contributes to the much greater substrate specificity observed for ligand MB-353 compared to ligand MB-323. The docking studies greatly contributed to understanding of our structure-activity relationship (SAR) data and the observed different substrate specificity of the ligands. The use of molecular modeling and docking techniques can contribute to future structure-based design of good NQO1 substrates for NQO1-directed lavendamycin antitumor agent development. Therefore, the data obtained from the molecular docking in conjunction with the SAR studies will be utilized for the structure-based design of novel improved lavendamycin substrates for NQO1.

3.6 References

(1) Sousa, S. F.; Fernandes, P. A.; Ramos, M. J. Protein-ligand docking: current status and future challenges. *Proteins* **2006**, *65*, 15-26.

(2) Kroemer, R. T. Molecular modelling probes: docking and scoring. *Biochem. Soc. Trans.* **2003**, *31*, 980-984.

(3) Glen, R. C.; Allen, S. C. Ligand-protein docking: cancer research at the interface between biology and chemistry. *Curr. Med. Chem.* **2003**, *10*, 763-767.

(4) Erickson, J. A.; Jalaie, M.; Robertson, D. H.; Lewis, R. A.; Vieth, M. Lessons in molecular recognition: the effects of ligand and protein flexibility on molecular docking accuracy. *J. Med. Chem.* **2004**, *47*, 45-55.

(5) Taylor, R. D.; Jewsbury, P. J.; Essex, J. W. A review of protein-small molecule docking methods. *J. Comput.-Aided Mol. Des.* **2002**, *16*, 151-166.

(6) Fradera, X.; Mestres, J. Guided docking approaches to structure-based design and screening. *Curr. Top. Med. Chem.* **2004**, *4*, 687-700.

(7) Chen, S.; Wu, K.; Zhang, D.; Sherman, M.; Knox, R.; Yang, C. S. Molecular characterization of binding of substrates and inhibitors to DT-diaphorase: Combined approach involving site-directed mutagenesis, inhibitor-binding analysis, and computer modeling. *Mol. Pharmacol.* **1999**, *56*, 272-278.

(8) Phillips, R. M.; Naylor, M. A.; Jaffar, M.; Doughty, S. W.; Everett, S. A.; Breen, A. G.; Choudry, G. A.; Stratford, I. J. Bioreductive activation of a series of indolequinones by human DT-diaphorase: Structure-activity relationships. *J. Med. Chem.* **1999**, *42*, 4071-4080.

(9) Suleman, A.; Skibo, E. B. A comprehensive study of the active site residues of DT-diaphorase: Rational design of benzimidazolediones as DT-diaphorase substrates. *J. Med. Chem.* **2002**, *45*, 1211-1220.

(10) Zhou, Z.; Fisher, D.; Spidel, J.; Greenfield, J.; Patson, B.; Fazal, A.; Wigal, C.; Moe, O. A.; Madura, J. D. Kinetic and docking studies of the interaction of quinones with the quinone reductase active site. *Biochemistry* **2003**, *42*, 1985-1994.

(11) Beall, H. D.; Winski, S.; Swann, E.; Hudnott, A. R.; Cotterill, A. S.; O'Sullivan, N.; Green, S. J.; Bien, R.; Siegel, D.; Ross, D.; Moody, C. J. Indolequinone antitumor agents: Correlation between quinone structure, rate of metabolism by recombinant human NAD(P)H:quinone oxidoreductase, and in vitro cytotoxicity. *J. Med. Chem.* **1998**, *41*, 4755-4766.

(12) Faig, M.; Bianchet, M. A.; Winski, S.; Hargreaves, R.; Moody, C. J.; Hudnott, A. R.; Ross, D.; Amzel, L. M. Structure-based development of anticancer drugs: Complexes of NAD(P)H:quinone oxidoreductase 1 with chemotherapeutic quinones. *Structure* **2001**, *9*, 659-667.

(13) *SYBYL molecular modeling software*; SYBYL 6.9.1 ed.; Tripos Inc.: St. Louis, MO.

(14) Hassani, M.; Cai, W.; Holley, D. C.; Lineswala, J. P.; Maharjan, B. R.; Ebrahimian, G. R.; Seradj, H.; Stocksdale, M. G.; Mohammadi, F.; Marvin, C. C.; Gerdes, J. M.; Beall, H. D.; Behforouz, M. Novel lavendamycin analogues as antitumor agents: synthesis, in vitro cytotoxicity, structure-metabolism, and

computational molecular modeling studies with NAD(P)H:quinone oxidoreductase 1. *J. Med. Chem.* **2005**, *48*, 7733-7749.

(15) Lemmen, C.; Lengauer, T. Time-efficient flexible superposition of medium-sized molecules. *J. Comput.-Aided Mol. Des.* **1997**, *11*, 357-368.

(16) Rarey, M.; Kramer, B.; Lengauer, T.; Klebe, G. A fast flexible docking method using an incremental construction algorithm. *J. Mol. Biol.* **1996**, *261*, 470-489.

(17) Eldridge, M. D.; Murray, C. W.; Auton, T. R.; Paolini, G. V.; Mee, R. P. Empirical scoring functions: I. The development of a fast empirical scoring function to estimate the binding affinity of ligands in receptor complexes. *J. Comput.-Aided Mol. Des.* **1997**, *11*, 425-445.

(18) Kuntz, I. D.; Blaney, J. M.; Oatley, S. J.; Langridge, R.; Ferrin, T. E. A geometric approach to macromolecule-ligand interactions. *J. Mol. Biol.* **1982**, *161*, 269-288.

(19) Jones, G.; Willett, P.; Glen, R. C.; Leach, A. R.; Taylor, R. Development and validation of a genetic algorithm for flexible docking. *J. Mol. Biol.* **1997**, *267*, 727-748.

(20) Muegge, I.; Martin, Y. C. A general and fast scoring function for protein-ligand interactions: A simplified potential approach. *J. Med. Chem.* **1999**, *42*, 791-804.

(21) DeLano, W. L. *The PyMOL molecular graphics system*; PyMOLX11Hybrid ed.; DeLano Scientific: San Carlos, CA.

(22) Li, R.; Bianchet, M. A.; Talalay, P.; Amzel, L. M. The three-dimensional structure of NAD(P)H:quinone reductase, a flavoprotein involved in cancer chemoprotection and chemotherapy: Mechanism of the two-electron reduction. *Proc. Natl. Acad. Sci. U. S. A.* **1995**, *92*, 8846-8850.

(23) Naylor, M. A.; Swann, E.; Everett, S. A.; Jaffar, M.; Nolan, J.; Robertson, N.; Lockyer, S. D.; Patel, K. B.; Dennis, M. F.; Stratford, M. R.; Wardman, P.; Adams, G. E.; Moody, C. J.; Stratford, I. J. Indolequinone antitumor agents: Reductive activation and elimination from (5-methoxy-1-methyl-4,7-dioxoindol-3-yl)methyl derivatives and hypoxia-selective cytotoxicity in vitro. *J. Med. Chem.* **1998**, *41*, 2720-2731.

(24) Swann, E.; Barraja, P.; Oberlander, A. M.; Gardipee, W. T.; Hudnott, A. R.; Beall, H. D.; Moody, C. J. Indolequinone antitumor agents: Correlation between quinone structure and rate of metabolism by recombinant human NAD(P)H:quinone oxidoreductase. Part 2. *J. Med. Chem.* **2001**, *44*, 3311-3319.

(25) Winski, S. L.; Faig, M.; Bianchet, M. A.; Siegel, D.; Swann, E.; Fung, K.; Duncan, M. W.; Moody, C. J.; Amzel, L. M.; Ross, D. Characterization of a mechanism-based inhibitor of NAD(P)H:quinone oxidoreductase 1 by biochemical, x-ray crystallographic, and mass spectrometric approaches. *Biochemistry* **2001**, *40*, 15135-15142.

Chapter 4

Lavendamycin Antitumor Agents: Structure-based Design, Validation of *In Silico* Model of the NAD(P)H:Quinone Oxidoreductase 1 (NQO1) Active Site, and Molecular Docking and Biological Studies

4.1 Abstract

A 1H69 crystal structure-based *in silico* model of the NAD(P)H:quinone oxidoreductase 1 (NQO1) active site has been developed in our laboratory to facilitate NQO1-directed lavendamycin antitumor agent development. Lavendamycin analogues were designed as NQO1 substrates utilizing our structure-activity relationship (SAR) and molecular docking data as structure-based design criteria. Docking studies of the designed analogues were performed using the *in silico* model to predict their NQO1 substrate specificity. The molecular docking was performed using the FlexX module of SYBYL 7.0 software suite. Metabolism and cytotoxicity studies on the analogues with recombinant human NQO1 and human colon adenocarcinoma cells (NQO1-deficient BE and NQO1-rich BE-NQ) were also performed. Docking and biological data were consistent suggesting that there was an excellent association between the docking and biological data. Analogues MB-116, -340, -100, -137 and -73 with reduction rates of 143 ± 11, 60 ± 8, 7.0 ± 1.5, 4.9 ± 2.9 and 3.4 ± 1.7 μmol/min/mg NQO1 were categorized as good, good, poor, poor and poor NQO1 substrates, respectively, by docking and metabolism data. Analogues MB-116, -340 and -100 exhibited selectivity ratios [IC_{50} (BE) / IC_{50} (BE-NQ)] of 30, 7 and 1, respectively, while no measurable cytotoxicity for

MB-137 and -73 was found. Overall, our results suggest practicality of the design criteria resulting in the discovery of two good NQO1 substrates with high selectivity ratios. The observed consistency between the docking and biological data determines that the *in silico* model of the NQO1 active site possesses practical predictive power. Therefore, this model can be utilized as a cost- and time-efficient tool to facilitate and accelerate NQO1-directed lavendamycin antitumor agent development. The acquired docking data can further be used for future structure-based design of lavendamycins to result in discovery of optimized ligands as potential novel bioreductive drugs.

4.2 Introduction

Bioreductive enzyme-directed antitumor agent development depends on identification of chemotherapeutic agents with high substrate specificity for target reductases.[1] Structure-based ligand design is an efficient approach in modern drug development for targets with resolved three-dimensional (3D) structures.[2-4] This field was evolved more than two decades ago as an approach to take advantage of the increasing number of protein crystal structures being added to the database.[5] Workman et al. suggested that the concept of enzyme-directed bioreductive drug development can be utilized in the structure-based design of improved bioreductive anticancer drugs.[6,7]

In structure-based design the information obtained from the interactions and composite structure of the target protein-ligand is utilized to design improved ligands with high binding affinity for target proteins implicated in diseases.[2-4,8] A profound understanding of ligand-protein interactions in the active site of the target greatly

contributes to the corresponding structure-activity relationship (SAR) studies, which in turn are the crucial components in the context of structure-based ligand design.[9] Computer-aided docking techniques serve as time- and cost-efficient tools for structure-based design and decrease efforts of synthesis and biological testing of compounds.[3,10] These techniques greatly contribute to this field since they facilitate extraction of information on binding events and the molecular basis of ligand-protein interactions as well as prediction of binding orientations and affinities of candidate compounds.[2-4,11] This information then is utilized to design improvements to existing ligands.[3] Another major element in computer-aided structure-based design is the ability to quickly screen designed ligands against a target protein via docking methods and accurately rank them for the binding affinity.[3] At the end of the process, a small group of the most promising designed ligands is synthesized and considered for biological tests.[3]

Suleman et al. rationally designed a series of benzimidazolediones and performed molecular modeling studies on the compounds with NQO1.[8] Correlation of the modeling data with the substrate specificity of the compounds for NQO1 determined the structural features required for high affinity of the compounds for NQO1, the enzymatic mechanism of NQO1 and the role of amino acid residues in the active site.[8] They performed docking studies via manual docking of each compound into the active site and considered each NQO1-compound complex as a separate model to gain insight to binding events of that specific compound.[8] However, they did not develop a general model of the NQO1 active site that could be used in an automatic docking process.[8] They suggested that the developed models will be used to develop novel NQO1-activated antitumor agents and to predict the substrate specificity of the compounds.[8]

This present study was conducted to design more optimal lavendamycin substrates for NQO1 with increased selective cytotoxicity towards NQO1-rich cells using our obtained SAR and docking data (See Chapters 2 and 3). Furthermore, the objective was to determine whether our design criteria were fruitful and whether docking studies performed using our recently developed *in silico* model of the NQO1 active site were consistent with the biological results. We also sought to investigate the predictive power of the model to correctly distinguish between good and poor NQO1 substrates. This is the first study that attempts to perform structure-based lavendamycin design using SAR and docking data and to relate the developed model and docking studies of lavendamycin analogues with data from biological studies.

4.3 Materials and Methods

4.3.1 Chemistry. Designed *N*-acyllavendamycin esters and amides were synthesized in Dr. Mohammad Behforouz's laboratory at Ball State University.

4.3.2 *In Silico* Model of the NQO1 Active Site. The coordinates of the crystal structure of human NQO1 complex with bound FAD and the indolequinone ARH019, obtained from the Protein Data Bank (PDB ID code: 1H69[12]), were previously utilized as a reference structure to develop the *in silico* model of the NQO1 active site (See Chapter 3).[13] Briefly, the physiological dimer in the crystal unit was used for docking purposes. In order to develop the model, we previously superposed the energy-minimized compound MB-353 to the coordinates of the original reference ligand ARH019 such that overlap was optimal. Ligand MB-353 was again energy minimized in the context of the

active site and therefore the position of the ligand within the pocket was considered optimized for the purpose of this study. The active site was then defined as all the amino acid residues confined within 6.5 Å radius sphere centered on the superposed ligand MB-353. The coordinates were locally minimized and subjected to energy minimization with minimal iterations (100) by Powell minimization standard method using Minimize Subset option within SYBYL. This option automatically selected 24 seed amino acid residues surrounding the superposed ligand MB-353 to perform the local minimization. Default parameters and values within the minimization dialog were used except where otherwise mentioned. This procedure yielded a weighted root-mean-square distance of 0.26 Å between the 24 corresponding non-minimized and minimized residues in the structures. The file of the composite structure containing ligand MB-353 and FAD was saved. The composite structure without MB-353 utilized as the *in silico* model of the NQO1 active site for docking studies. Ligand MB-353 served as the reference ligand for the docking studies. Docking calculations were performed using one of the two identical active sites.

4.3.3 Ligand Preparation. The structures of ligands were sketched and prepared as MOL2 files employing the Sketch Molecule module of SYBYL 7.0 software suite[14] (Tripos, Inc.; St. Louis, MO). Initially sketched Ligands were subjected to energy minimization (10,000 iterations) by Powell minimization standard method. Initial Optimization and Termination parameters were set to None and Energy Change options, respectively. Default parameters and values within the minimization dialog (Minimize Details) were used except where otherwise noted. The final ligand conformational coordinates were stored as MOL2 files within the database.

4.3.4 Docking. Flexible docking was performed using the FlexX module of

SYBYL 7.0 software suite.[14] FlexX is an automatic docking program for conformationaly flexible ligands that employs the 3D structure of the target protein in PDB format, and is capable of determining 30 possible conformations for each docked ligand. The final rank order of the conformations is based on the free binding energy. This program automatically selects the base fragment of a ligand (the ligand core). The base fragment is then placed into the active site of the target protein using the algorithmic approach called pose clustering that is based upon a pattern recognition paradigm. Subsequent incremental reconstruction of the complete ligand molecule is then performed by linking the remaining components.[15,16] For the *in silico* model, the active site was defined as all the amino acid residues confined within 6.5 Å radius sphere centered on the superposed ligand MB-353. FAD was introduced to the active site as a heteroatom file in MOL2 format.

4.3.5 Scoring Functions. The docked conformations of ligands were evaluated and ranked using FlexX and four scoring functions implemented in the CSCORE module in SYBYL. CSCORE is a consensus scoring program that integrates multiple well-known scoring functions such as FlexX, ChemScore,[17] D-Score,[18] G-Score[19] and PMF-Score[20] to evaluate docked conformations. Individual scoring functions are used to predict the affinity of the ligand binding to a target protein. CSCORE creates columns in a molecular spreadsheet that contain raw scores for each individual scoring function. The consensus column contains integers that range from 0 to 5; where 5 is the best fit to the model. Docked conformations whose scores exceed the threshold for a particular function contribute one to the value of the consensus, whereas those with scores below the threshold add a zero.

4.3.6 Molecular Graphics System. The molecular graphics images and surface representations were prepared with PyMOL molecular graphics system version PyMOLX11Hybrid 0.97[21] (Delano Scientific, San Carlos, CA, USA). The data of the coordinates of the NQO1 complex with bound FAD and docked conformations of ligands were prepared in PDB format as PyMOL input files. PyMOL session files of the NQO1 active site with docked conformations of ligands and the superimposition of clustered conformations were created. The images were then stored as graphic files.

4.3.7 Cell Culture. BE human colon adenocarcinoma cells and stably NQO1-transfected BE-NQ cells[22] were a gift from Dr. David Ross (University of Colorado Health Sciences Center, Denver, CO). Cells were grown in a minimum essential medium (MEM) with Earle's salts, non-essential amino acids, L-glutamine and penicillin/streptomycin, and supplemented with 10% fetal bovine serum (FBS), sodium bicarbonate and HEPES. Cell culture medium and supplements were obtained from Gibco, Invitrogen Co., Grand Island, NY. The cells were incubated at 37°C under a humidified atmosphere containing 5% CO_2.

4.3.8 Cytochrome *c* Assay. Lavendamycin analogue reduction was monitored using a spectrophotometric assay in which the rate of reduction of cytochrome *c* was quantified at 550 nm. Briefly, the assay mixture contained cytochrome *c* (70 μM), NADH (1 mM), human recombinant NQO1 (0.1-3 μg) (gift from Dr. David Ross, University of Colorado Health Sciences Center, Denver, CO) and lavendamycins (25 μM) in a final volume of 1 mL Tris-HCl (25 mM, pH 7.4) containing 0.7 mg/mL BSA and 0.1% Tween-20. Reactions were carried out at room temperature and started by the addition of NADH. Rates of reduction were calculated from the initial linear part of the

reaction curve (0-30 s), and results were expressed in terms of μmol of cytochrome *c* reduced/min/mg of NQO1 using a molar extinction coefficient of 21.1 mM^{-1} cm^{-1} for cytochrome *c*. All reactions were carried out at least in triplicate.

4.3.9 MTT Assay. Growth inhibition was determined using the MTT colorimetric assay. Cells were plated in 96-well plates at a density of 10,000 cells/mL and allowed to attach overnight (16 h). Lavendamycin analogue solutions were applied in medium for 2 hours. Lavendamycin analogue solutions were removed and replaced with fresh medium, and the plates were incubated at 37 °C under a humidified atmosphere containing 5% CO_2 for 4-5 days. MTT (50 μg) was added and the cells were incubated for another 4 hours. Medium/MTT solutions were removed carefully by aspiration, the MTT formazan crystals were dissolved in 100 μL DMSO, and absorbance was determined on a plate reader at 560 nm. IC_{50} values (concentration at which cell survival equals 50% of control) were determined from semi-log plots of percent of control *vs.* concentration. Selectivity ratios were defined as the IC_{50} value for the BE cell line divided by the IC_{50} value for the BE-NQ cell line.

4.4 Results and Discussion

4.4.1 Structure-based Design. Lavendamycin analogues MB-116, -137, -100 and -340 (Chart 4.1) were designed utilizing the criteria obtained from our SAR and docking study (See Chapters 2 and 3),[13] and other recent NQO1-related literature. The structure-based design criteria for substituent features at key positions are detailed in the following sections.

Quinolinedione-7-position (R^1) (Chart 4.1): (1) Small to medium size substituents, preferably NH_2 or $NHCOCH_3$ group[13] that do not produce steric interactions with the key residues of the active site including the internal wall (Trp-105/Phe-106) (applied to MB-116, -137 and -340).[8,23,24] The substituents should also be capable of hydrogen bond formation with the FAD cofactor and/or the key amino acid residues of the active site including Tyr-126, -128 and His-161.[13] Faig et al. determined that positions of the aziridinylbenzoquinone RH1 that point to the inner part of the NQO1 active site could accommodate only small substituents.[12] (2) Substituents that can intercalate between and/or form van der Waals interactions with the Trp-105/Phe-106 mini-pocket (applied to MB-100).[8,23] A previous study demonstrated that an aziridinyl group at C5 position of EO9 can form favorable van der Waals interactions with Trp-106.[23] Another study determined that van der Waals interactions between the C5 aziridine ring of CB1954, 5-aziridinyl-2,4-dinitrobenzamide,[25] and Trp-105 is an important factor in the binding of this prodrug.[25] Unsubstituted pyrrolo rings in dipyrroloimidazobenzimidazole and dipyridoimidazobenzimidazole compounds can sandwich between the Trp-105/Phe-106 residues and form van der Waals interactions to increase NQO1 substrate specificity.[8] (3) No large substituents are allowed due to increased steric hindrance with the internal wall that can result in unfavorable positioning of the quinoline-5,8-dione moiety of lavendamycin analogues for hydride ion reception from $FADH_2$ and quinone reduction (applied to MB-116, -137, -100 and -340).[8,13] A study by Suleman et al. demonstrated that dipyrroloimidazobenzimidazole compounds with both pyrrolo rings bearing bulky substituents were excluded from the active site due to steric interactions.[8]

Chart 4.1. Chemical structures of the lavendamycin analogues MB-73, -100, -116, -137, and -340 and with substituent positions indicated by R^1, R^2 and R^3.

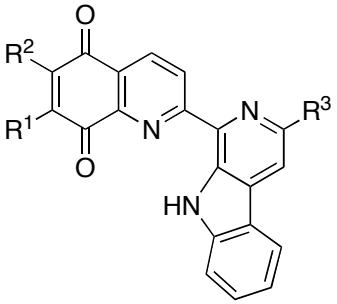

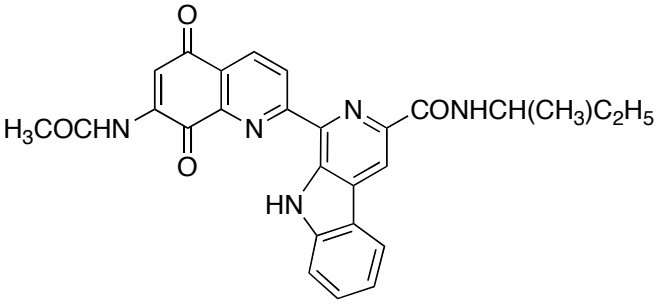

MB-137

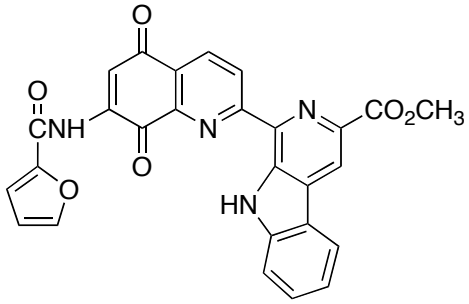

MB-100

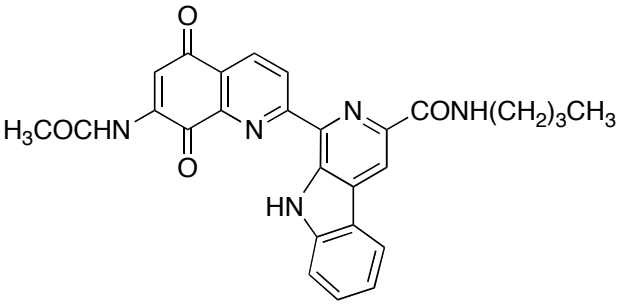

MB-116

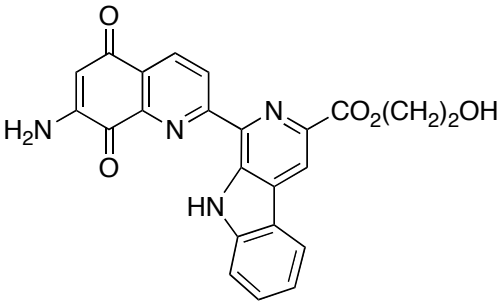

MB-340

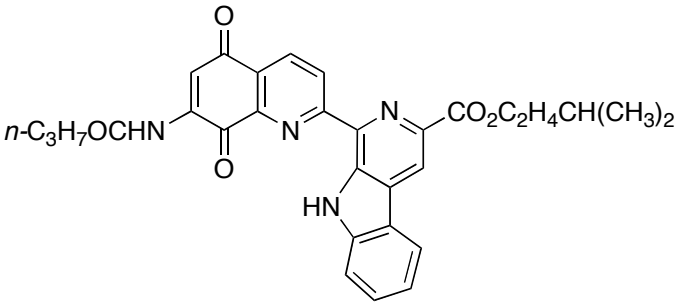

MB-73

Quinolinedione-6-position (R^2) (Chart 4.1): Absence of substituents in this position is highly preferred. Simultaneous placing of substituents at both R^1 and R^2 increases steric interactions of lavendamycin ligands with the internal wall of the active site.[13] It has been reported that 1,4-naphthoquinones with small substituents such as an aziridine ring or CH_3 at C2 and no substituents at C3 (C2 and C3 positions point to the inside of the active side) are good substrates for NQO1.[26] Increased bulkiness of substituents at the C5 position of indolequinones dramatically reduced rates of reduction by NQO1.[12,23] Previous SAR studies have demonstrated that 7-aminoquinoline-5,8-dione is an essential moiety in determining the cytotoxic and antitumor activity of quinolinedione antibiotics.[27,28] Therefore, substituent placement at the R^1 position over R^2 is highly desirable (applied to MB-116, -137, -100 and -340).

Indolopyridine-2'-position (R^3) (Chart 4.1): (1) Substituents that are capable of hydrogen bond formation with the FAD cofactor and/or the key residues of the active site including Gly-149 and Gly-150 (applied to MB-100 and -340).[13] The 3-hydroxymethyl group of ARH019 that points towards the outside of the active site forms a hydrogen bond with the Tyr-128 OH.[12] (2) Substituents (including aliphatic chains) that are capable of formation of van der Waals interactions with the key residues of the NQO1 active site (applied to MB-116 and -137). Compound MB-83 (See Chapter 2), demethyllavendamycin *n*-octyl ester,[29] possesses a large *n*-octyl ester substituent at the R^3 position and is a good NQO1 substrate with high selective toxicity towards NQO1-rich cancer cells.[13]

Utilizing the design criteria we designed compounds MB-116, -137, -100 and -340 with small or medium size substituents at R^1, no substituent at R^2 and small to large

substituents at R^3. The substituents at R^1 and R^3 are expected to form hydrogen bond and/or van der Waals interactions with FAD and/or the amino acid residues of the active site such as Trp-105, Phe-106, Tyr-126, -128, -Gly-149, -150 and His-161. The docking studies of the compounds using the *in silico* model were performed to predict the substrate specificity of the compounds for NQO1, to examine the predictive power of the model, to relate the model and docking studies with the metabolism and cytotoxicity results, and to gain further insight into the binding events and the molecular basis of lavendamycin agent-NQO1 interactions.

4.4.2 Docking Studies. Our laboratory recently developed a 1H69 crystal structure-based *in silico* model of the NQO1 active site (See Chapter 3). In order to further determine the predictive power of the model and correlation of the docking data with biological results, we performed computational and comparative docking studies on the structure-based designed lavendamycin analogues and the previously synthesized compound MB-73. A practical model should be able to correctly predict the substrate specificity of the docked compounds. The molecular modeling studies were performed using SYBYL 7.0 software suite[14] (Tripos, Inc.; St. Louis, MO). Flexible docking was performed using the FlexX module of SYBYL that is capable of determining 30 possible poses for each docked ligand.[15,16] The docked conformations of ligands MB-116, -137, -73, -100 and -340 were evaluated and ranked using the CSCORE module in SYBYL, from 0 to 5; where 5 was the best fit to the model. Table 4.1 displays the number of conformations of the ligands in each score group of CSCORE function.

Ligands MB-116 and -340 possessed higher number of poses with optimal CSCORE values compared to MB-73, -100 and -137 (Table 4.1). Visual screening of

binding orientations of the poses and geometric post-docking analyses were performed. The analyses included distance measurements and pose geometries that determined: (a) hydrogen-bonding and van der Waals interactions of ligand poses with FAD and the key residues of the NQO1 active site including Trp-105, Phe-106, Tyr-126, -128, -Gly-149, -150, His-161 and Phe-232 and (b) hydride ion transfer from the N5 of the FAD isoalloxazine ring to the ligands at carbonyl oxygens (O5 or O8), ring carbon or substituent atoms. Residue numbers in this report are those used in the Protein Data Bank coordinates, PDB ID code: 1H69.[12]

The binding orientations of the ligands in the NQO1 active site were determined by the positioning of quinone carbonyl oxygens towards the isoalloxazine ring atoms of FAD and residues of the active site. Quinone substrates can bind to the NQO1 active site in more than one orientation, and homologous compounds with different substituents may bind to the NQO1 active site in different orientations.[12,30] Only poses of the ligands with CSCORE ≥ 4 were considered for further detailed post-docking analyses.

Table 4.1. Number of poses of ligands MB-116, -137, -73, -100 and -340 in each score group of CSCORE function.

MB	116	137	73	100	340
CSCORE	Number of Poses				
0	7	6	5	9	5
1	4	9	10	9	3
2	5	1	6	7	2
3	5	11	4	3	5
4	4	3	5	1	10
5	5	0	0	1	5

Ligands MB-116 and -137 were designed to possess highly similar chemical structures with only a minor difference in the substituents at R^3 (R^3 substituents of MB-116 and -137 are structural isomers). The purpose was to examine the role that R^3 substituents play to impact the affinity of lavendamycin substrates for NQO1. Nine poses of ligand MB-116 possessed CSCORE ≥ 4 compared to three poses of MB-137 (Table 4.1). None of the poses of MB-137 had a CSCORE = 5 (Table 4.1). Poses 1, 2, 4, 5 and 6 (CSCORE = 5) of MB-116 fell into one cluster in which the root mean square deviation (RMSD) of the poses equaled zero for the quinolinedione and indolopyridine moieties atoms, and the difference was in the binding orientation of the $CONH(CH_2)_3CH_3$ group in the NQO1 active site (Figure 4.1a). All of the poses of MB-116 entered the active site by the 5,8-dione moiety where the carbonyl oxygen O8 compared to O5 was positioned closer to Tyr-126, -128 and FAD similar to the binding orientation of indolequinone EO9 (Figure 4.1a and Table 4.2).[12,23] The binding orientations of the MB-116 poses in the cluster are considered as preferred binding orientations of MB-116 since these are the binding orientations of the poses with high CSCORE of 5 (Figure 4.1a).

One crucial determining factor of NQO1 substrate binding strength in the NQO1 active site is the capability to form hydrogen-bonding and/or van der Waals interactions with FAD and/or residues of the active site.[8,12,25,30] Good substrates for NQO1 such as RH1, EO9 and CB1954 are capable of hydrogen-bonding interactions with the key residues of the NQO1 active site.[12,25] Duroquinone, a tetramethyl analogue of benzoquinone, binds to the NQO1 active site through interactions with FAD and several hydrophilic and hydrophobic residues.[31]

Figure 4.1. Molecular models of the poses of ligand MB-116 docked into the NQO1 active site.

a)

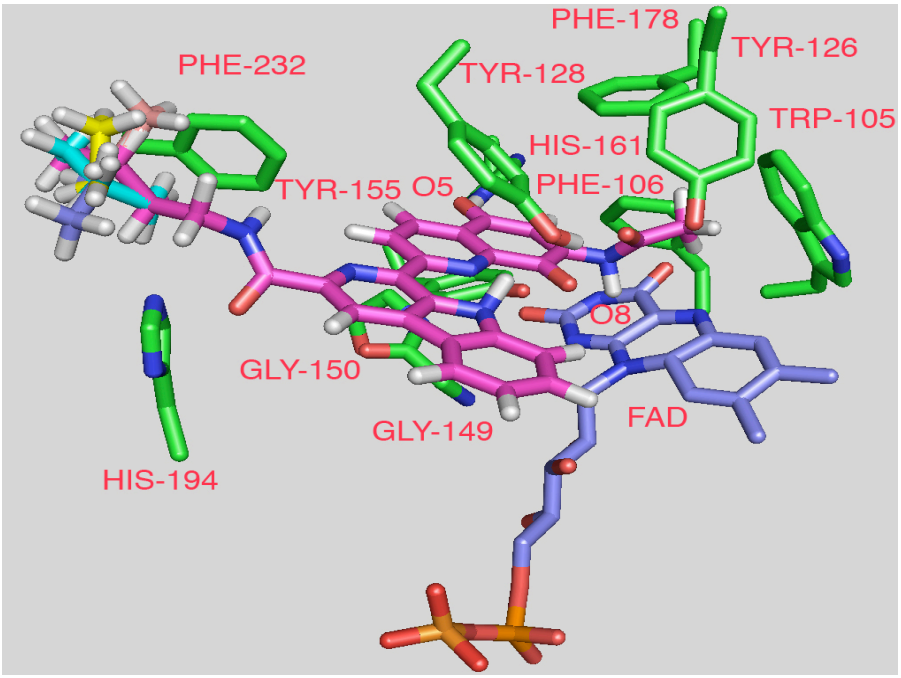

b)

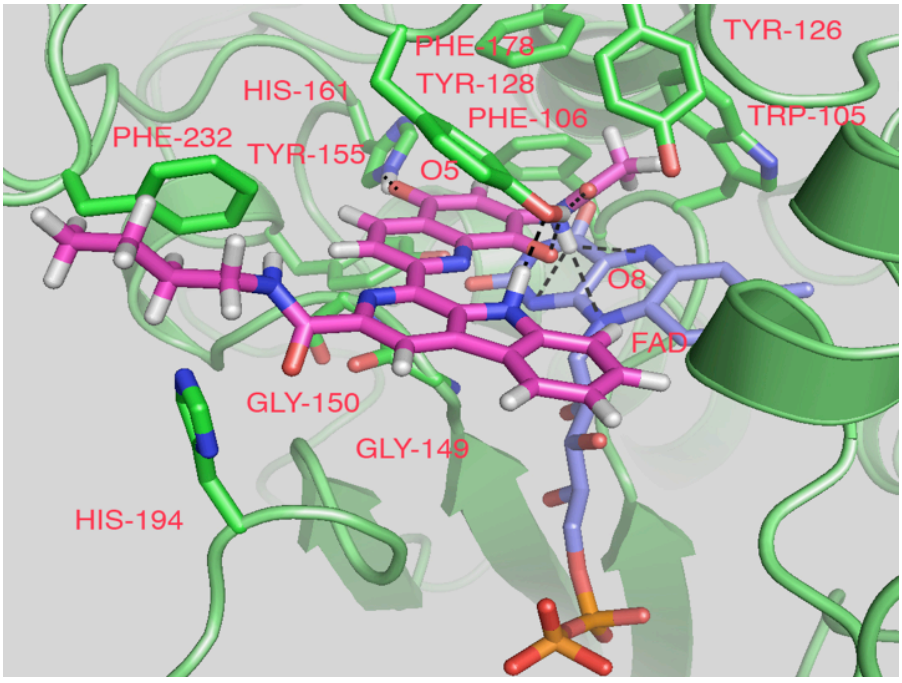

Figure 4.1. Molecular models of the poses of ligand MB-116 docked into the NQO1 active site. **a)** View of the superposition of the docked poses 1, 2, 4, 5 and 6 of MB-116 (magenta, cyan, yellow, salmon and blue) (CSCORE = 5) in the NQO1 active site. **b)** Molecular model of the pose 1 of MB-116 (magenta) (CSCORE = 5) docked into the NQO1 active site. In (b) the Tyr-128 OH formed hydrogen bonds with the carbonyl oxygen O8, the NH of the indole ring of the indolopyridine moiety and the carbonyl oxygen of the quinolinedione-7-position substituent. The carbonyl oxygen O5 formed a hydrogen bond with the NH of His 161. The NH of the quinolinedione-7-position substituent also formed hydrogen bonds with the N1, N5 and N10 of FAD. The $CONH(CH_2)_3CH_3$ group of the indolopyridine moiety further stabilized the binding by forming van der Waals interactions with Phe-232. In (a) and (b) residues of the active site (green), FAD (blue), and MB-116 are represented as stick models. In (b) the rest of the structure is represented as a secondary structure cartoon. The atoms are colored: red, oxygen atoms; blue, nitrogen atoms; orange, phosphorus atoms and white, hydrogen atoms. Hydrogen bonds are represented as black dashed lines.

Table 4.2. Geometric post-docking analysis and measurements of five poses (CSCORE = 5) and four poses (CSCORE = 4) of ligand MB-116 in the NQO1 active site.

P[a]	C[b]	O5 - Tyr126 (Å)	O5 - Tyr128 (Å)	O8 - Tyr126 (Å)	O8 - Tyr128 (Å)	N5 - O5 (Å)	N5 - O8 (Å)	N5 - C6 (Å)	N5 - C7 (Å)
1	5	9.174	6.143	4.862	2.077	7.786	5.006	5.515	4.622
2	5	9.174	6.143	4.862	2.077	7.786	5.006	5.515	4.622
4	5	9.174	6.143	4.862	2.077	7.786	5.006	5.515	4.622
5	5	9.174	6.143	4.862	2.077	7.786	5.006	5.515	4.622
6	5	9.174	6.143	4.862	2.077	7.786	5.006	5.515	4.622
3	4	9.417	6.196	4.804	1.802	7.953	5.281	5.714	4.863
7	4	9.260	6.085	4.774	1.899	7.772	5.187	5.532	4.697
14	4	9.180	6.242	4.878	2.123	7.618	4.960	5.375	4.515
25	4	9.167	6.198	4.882	2.081	7.692	5.016	5.427	4.560

[a] P = Pose

[b] C = CSCORE

Among the poses of ligand MB-116, poses 1, 2, 4, 5 and 6 formed the highest number of hydrogen bonds and van der Waals interactions in the active site of the enzyme. For pose 1 of MB-116, the Tyr-128 OH formed hydrogen bonds with the carbonyl oxygen O8, the NH of the indole ring of the indolopyridine moiety and the carbonyl oxygen of the quinolinedione-7-position substituent (Figure 4.1b). The carbonyl oxygen O5 formed a hydrogen bond with the NH of His 161 (Figure 4.1b). The NH of the quinolinedione-7-position substituent also formed hydrogen bonds with the N1, N5 and N10 of FAD (Figure 4.1b). The $CONH(CH_2)_3CH_3$ group of the indolopyridine moiety further stabilized the binding by forming van der Waals interactions with Phe-232 (Figure 4.1b). Poses 2, 4, 5 and 6 displayed the same interactions as pose 1 (Table 4.2). The model determined high number of poses of MB-116 with optimum CSCORE (≥ 4) that are capable of hydrogen bond and van der Waals formation in the NQO1 active site suggesting that this compound is a good substrate for NQO1.

However, of thirty poses of MB-137 only poses 1, 2 and 4 merited further considerations (CSCORE = 4) and the rest possessed CSCORE ≤ 3. None of the poses of MB-137 had a CSCORE = 5 (Table 4.1). Poses 1, 2 and 4 of MB-137 entered the active site by the 5,8-dione moiety similar to the poses of MB-116 (Figure 4.2a and Table 4.3). Although these poses formed hydrogen bonds with FAD and the residues of the NQO1 active site, the number of total hydrogen bonds was lower than that for the poses of MB-116 (hydrogen bonds not shown). Furthermore, none of poses 1, 2 and 4 of MB-137 formed van der Waals interactions with Phe-232 compared to the poses of MB-116 suggesting lower binding affinity of MB-137 compared to MB-116 in the NQO1 active site (Figures 4.2a and 4.2b). These docking studies performed using the *in silico* model ranked MB-137 as a poor substrate for NQO1.

Figure 4.2. Molecular models of the poses of ligand MB-137 docked into the NQO1 active site.

a)

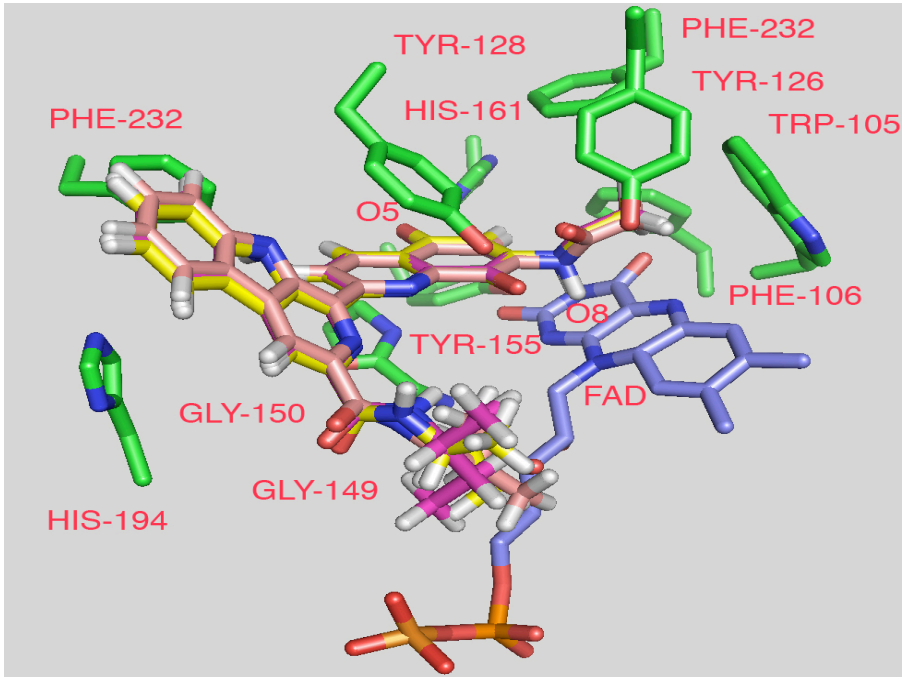

b)

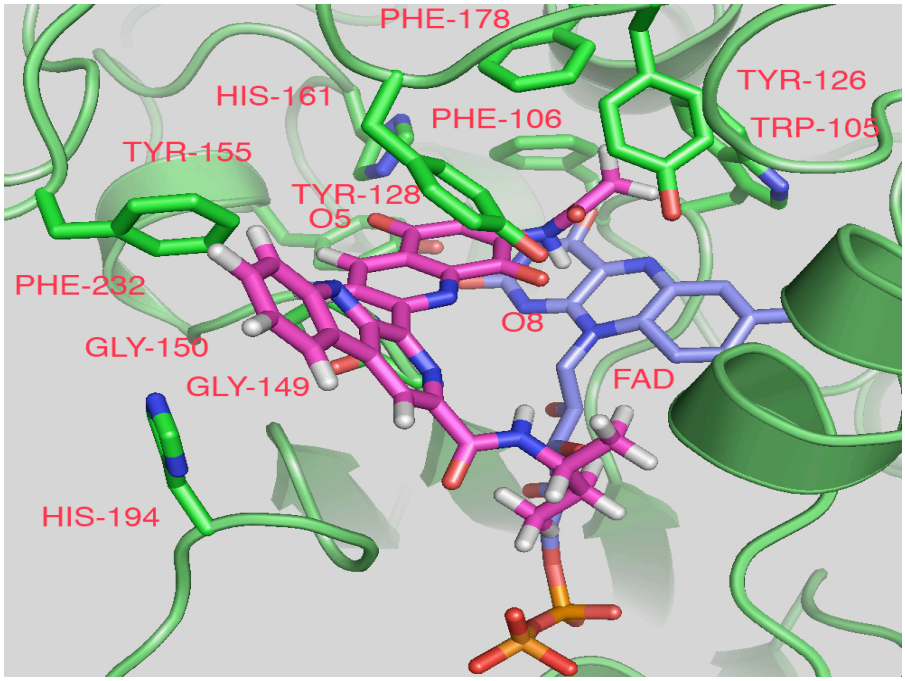

Figure 4.2. Molecular models of the poses of ligand MB-137 docked into the NQO1 active site. **a)** View of the superposition of the docked poses 1, 2 and 4 of MB-137 (magenta, yellow and salmon) (CSCORE = 4) in the NQO1 active site. **b)** Molecular model of the pose 1 of MB-137 (magenta) (CSCORE = 4) docked into the NQO1 active site. In (a) and (b) residues of the active site (green), FAD (blue), and MB-137 are represented as stick models. In (b) the rest of the structure is represented as a secondary structure cartoon. The atoms are colored: red, oxygen atoms; blue, nitrogen atoms; orange, phosphorus atoms and white, hydrogen atoms.

Table 4.3. Geometric post-docking analysis and measurements of three poses of ligand MB-137 (CSCORE = 4) in the NQO1 active site.

P[a]	C[b]	O5 - Tyr126 (Å)	O5 - Tyr128 (Å)	O8 - Tyr126 (Å)	O8 - Tyr128 (Å)	N5 - O5 (Å)	N5 - O8 (Å)	N5 - C6 (Å)	N5 - C7 (Å)
1	4	9.402	6.193	4.802	1.828	7.933	5.246	5.689	4.831
2	4	9.402	6.193	4.802	1.828	7.933	5.246	5.689	4.831
4	4	9.268	6.084	4.692	1.770	7.739	5.240	5.504	4.691

[a] P = Pose

[b] C = CSCORE

The important role that residue Phe-232 plays in contributing to the binding affinity of NQO1 substrates has been further emphasized in recent studies.[32,33] One study indicated that the distance between Tyr-128 and Phe-232 residues in the NQO1 active site increases dramatically from 4 Å in apo human NQO1 (PDB ID code: 1D4A[31]) and NQO1-duroquinone complex (PDB ID code: 1DXO[31]) crystal structures to 12 Å in the NQO1 complex with dicoumarol (NQO1 inhibitor) crystal structure.[32] Another study also determined that upon binding of the NQO1 inhibitor ES936, 5- methoxy-1,2-dimethyl-3-(4-nitrophenoxymethyl)indole-4,7- dione,[33] to the NQO1 active site, Tyr-128 and Phe-232 exhibit the largest displacement.[33] These studies suggest that proper positioning of phe-232 could contribute to binding affinity of NQO1 substrates which is disturbed upon binding of inhibitors. Overall, a higher number of poses of ligand MB-116 compared to MB-137 possessed optimum CSCORE, formed hydrogen bonding interactions (van der Waals interactions only in poses of MB-116) and had favorable binding orientation for hydride ion reception and quinone reduction (Tables 4.1, 4.2 and 4.3). The *in silico* model distinguished the two highly similar analogues MB-116 and MB-137 as the good and poor substrates, respectively.

Compound MB-100 was designed to investigate whether an aromatic amide group at R^1 is capable of intercalating between Trp-105 and Phe-106 residues and forming van der Waals interactions to increase NQO1 substrate specificity. Docking studies of MB-100 were performed to observe how the model would rank this compound as an NQO1 substrate. Only two poses 7 and 30 of ligand MB-100 possessed CSCORE ≥ 4 (Table 4.1). These poses entered the active site by the 5,8-dione moiety similar to the poses of MB-116 and MB-137 (Figure 4.3a and Table 4.4).

Figure 4.3. Molecular models of the poses of ligand MB-100 docked into the NQO1 active site.

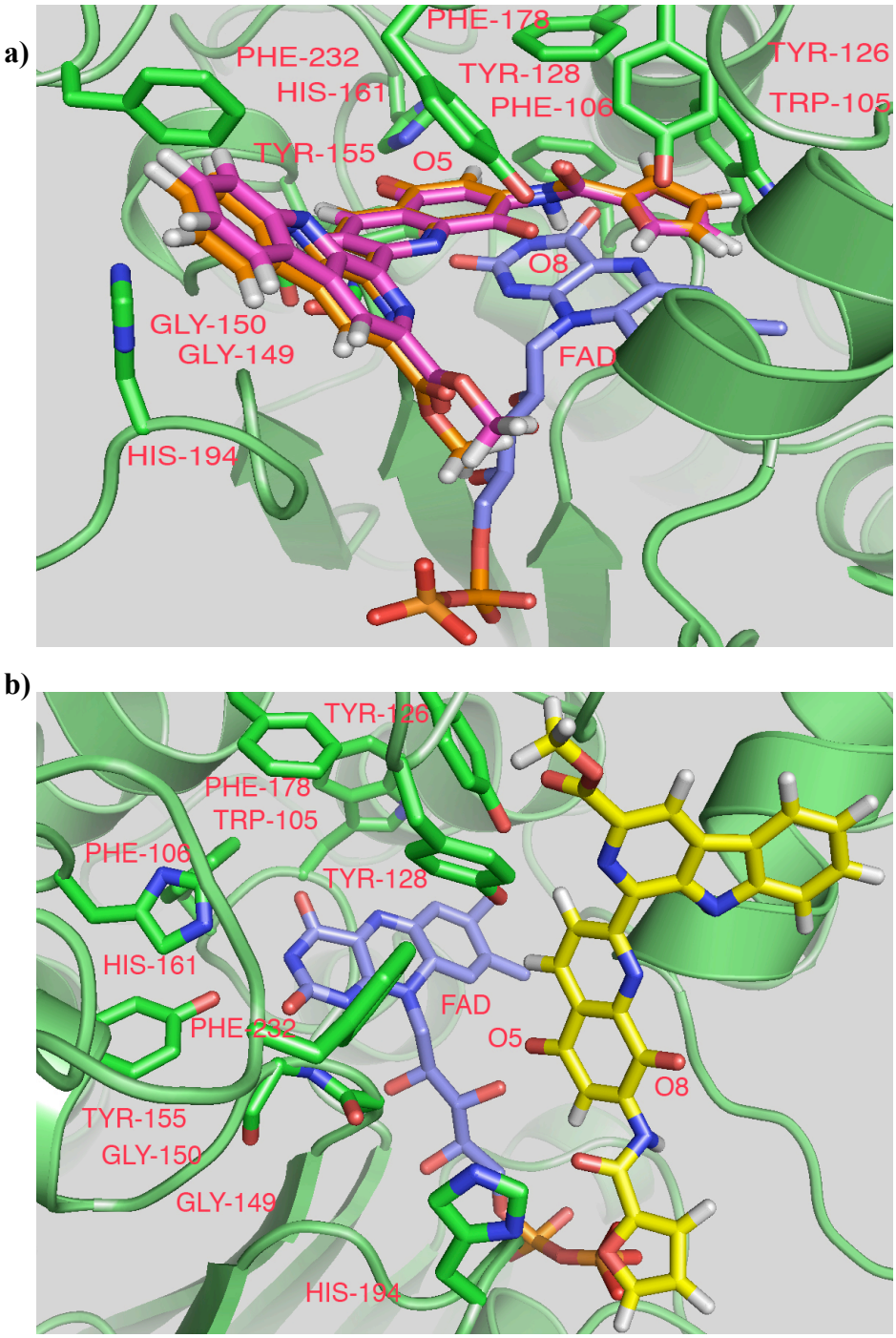

Figure 4.3. Molecular models of the poses of ligand MB-100 docked into the NQO1 active site. **a)** View of the superposition of the docked poses 7 and 30 of MB-100 (orange and magenta) (CSCORE = 5 and 4) in the NQO1 active site. **b)** Molecular model of the pose 2 of MB-100 (yellow) (CSCORE = 3) docked into the NQO1 active site. In (a) and (b) residues of the active site (green), FAD (blue), and MB-100 are represented as stick models and the rest of the structure is represented as a secondary structure cartoon. The atoms are colored: red, oxygen atoms; blue, nitrogen atoms; orange, phosphorus atoms and white, hydrogen atoms.

Table 4.4. Geometric post-docking analysis and measurements of two poses of ligand MB-100 (CSCORE = 4 and 5) in the NQO1 active site.

P[a]	C[b]	O5 - Tyr126 (Å)	O5 - Tyr128 (Å)	O8 - Tyr126 (Å)	O8 - Tyr128 (Å)	N5 - O5 (Å)	N5 - O8 (Å)	N5 - C6 (Å)	N5 - C7 (Å)
7	5	9.585	6.455	4.785	1.780	7.759	5.236	5.664	4.873
30	4	9.454	6.273	4.610	1.639	7.669	5.247	5.562	4.793

[a] P = Pose

[b] C = CSCORE

The two poses of MB-100 (7 and 30) formed few hydrogen bonds with FAD and the residues of the NQO1 active site (hydrogen bonds not shown). The other twenty-eight poses with CSCORE ≤ 3 were excluded from the NQO1 active site including pose 2 (CSCORE = 3) (Figure 4.3b). The NHCO-2-furyl group of poses 7 and 30 did not intercalate between the Trp-105 and Phe-106 residues, suggesting the lack of Van der Waals interactions with the Trp-105/Phe-106 mini-pocket and presence of possible steric interactions with the residues Trp-105 and Phe-106 (Figure 4.3a). Previous studies have indicated that the Trp-105/Phe-106 mini-pocket can play a crucial role in impacting the substrate specificity of NQO1 ligands.[8,23,34] If the corresponding substituent is able to intercalate between Trp-105 and Phe-106 and form van der Waals interactions with these residues, the binding affinity of the quinone substrate in the NQO1 active site will increase.[8,23] Our model ranked ligand MB-100 as a poor substrate for NQO1.

Compound MB-340 was designed after MB-353, a good NQO1 lavendamycin substrate, to create another good substrate. Fifteen poses of ligand MB-340 possessed CSCORE ≥ 4 (Table 4.1). Poses 1, 2, 4 and 7 (CSCORE = 5) of MB-340 entered the active site by the 5,8-dione moiety where the carbonyl oxygen O8 compared to O5 was positioned closer to Tyr-126, -128 and FAD (Figure 4.4a and Table 4.5). Among five poses of MB-340 with CSCORE = 5, pose 8 entered the active site in a different orientation compared to poses 1, 2, 4 and 7 where carbonyl oxygen O5 compared to O8 was positioned closer to Tyr-126, -128 and FAD (Figure 4.4b and Table 4.5). Different binding orientations of quinone substrates that can facilitate hydride ion reception from the FAD N5 to the substrates can be tolerated in the active site.[12,30]

Figure 4.4. Molecular models of the poses of ligand MB-340 docked into the NQO1 active site.

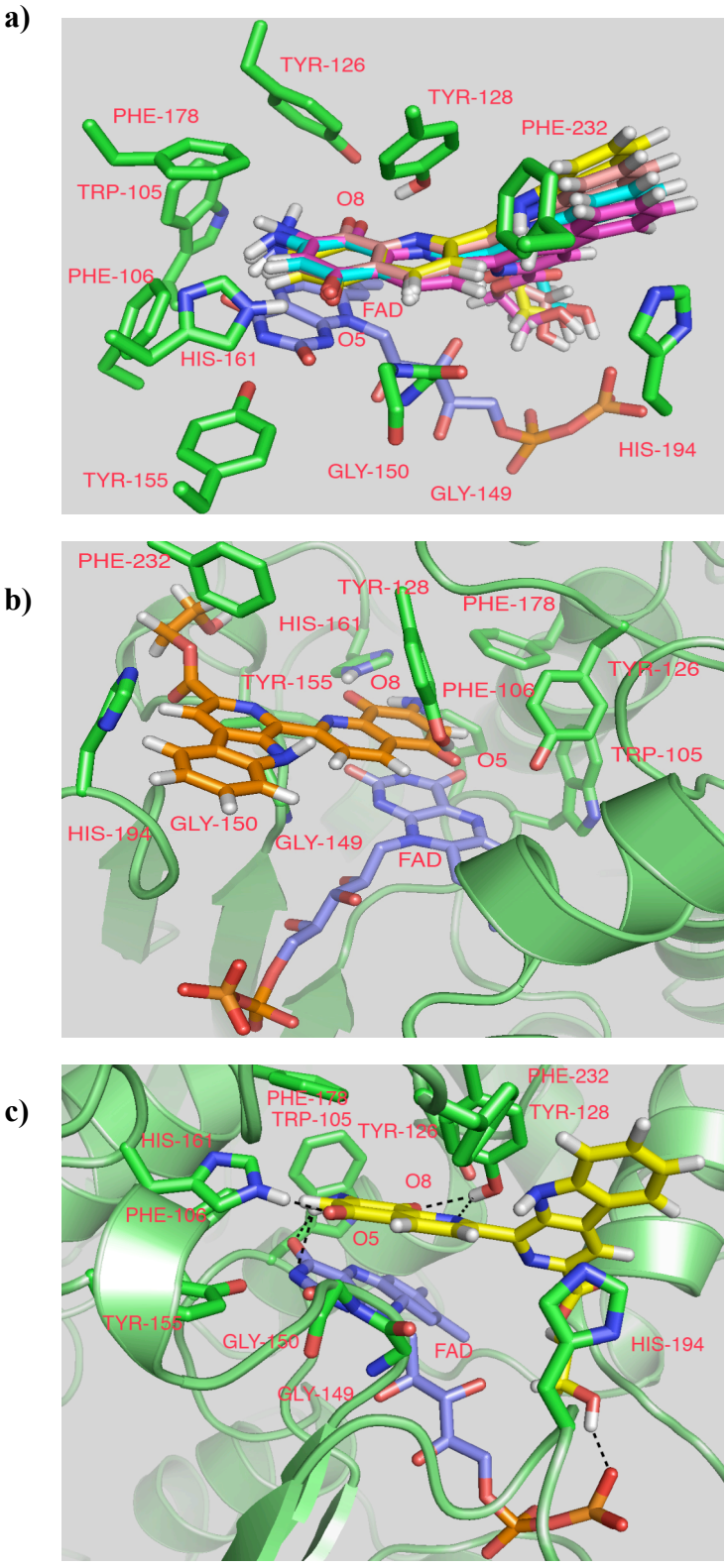

Figure 4.4. Molecular models of the poses of ligand MB-340 docked into the NQO1 active site. **a)** View of the superposition of the docked poses 1, 2, 4 and 7 of MB-340 (cyan, magenta, yellow and salmon) (CSCORE = 5) in the NQO1 active site. **b)** Molecular model of the pose 8 of MB-340 (orange) (CSCORE = 5) docked into the NQO1 active site. **c)** Molecular model of the pose 4 of MB-340 (yellow) (CSCORE = 5) docked into the NQO1 active site. In (c) the Tyr-128 OH formed hydrogen bonds with the carbonyl oxygen O8 and the N1 of the quinoline ring of the pose 4 of MB-340. One hydrogen atom of the NH_2 substituent also formed hydrogen bonds with the N3 and O4 of FAD. The carbonyl oxygen O5 formed a hydrogen bond with the NH of His 161. The OH of $CO_2(CH_2)_2OH$ at R^3 further stabilized the binding by making a hydrogen bond to one oxygen atom of the adenine phosphate of FAD. In (a), (b) and (c) residues of the active site (green), FAD (blue), and MB-340 are represented as stick models. In (b) and (c) the rest of the structure is represented as a secondary structure cartoon. The atoms are colored: red, oxygen atoms; blue, nitrogen atoms; orange, phosphorus atoms and white, hydrogen atoms. Hydrogen bonds are represented as black dashed lines.

Table 4.5. Geometric post-docking analysis and measurements of five poses of ligand MB-340 (CSCORE = 5) in the NQO1 active site.

P[a]	C[b]	O5 - Tyr126 (Å)	O5 - Tyr128 (Å)	O8 - Tyr126 (Å)	O8 - Tyr128 (Å)	N5 - O5 (Å)	N5 - O8 (Å)	N5 - C6 (Å)	N5 - C7 (Å)
1	5	9.662	6.593	4.421	2.243	7.925	4.627	5.978	5.027
2	5	9.519	6.480	4.375	1.917	7.800	4.829	5.854	4.977
4	5	9.631	6.564	4.374	2.281	7.774	4.533	5.705	4.738
7	5	9.597	6.568	4.597	2.177	7.787	4.692	5.816	4.904
8	5	3.767	1.862	8.938	5.903	4.596	7.253	4.557	5.355

[a] P = Pose

[b] C = CSCORE

Among the poses of ligand MB-340, poses 1, 2, 4 and 7 formed the highest number of hydrogen bonds in the active site of the enzyme. The Tyr-128 OH formed hydrogen bonds with the carbonyl oxygen O8 and the N1 of the quinoline ring of pose 4 of MB-340 (Figure 4.4c). One hydrogen atom of the R^1 NH_2 substituent also formed hydrogen bonds with the N3 and O4 of FAD. The carbonyl oxygen O5 formed a hydrogen bond with the NH of His 161 (Figure 4.4c). The OH of $CO_2(CH_2)_2OH$ at R^3 further stabilized the binding by making a hydrogen bond to one oxygen atom of the adenine phosphate of FAD (Figure 4.4c). However, pose 8 among poses of MB-340 with CSCORE = 5, formed the lowest number of hydrogen bonds. This suggests that the binding orientations of poses 1, 2, 4 and 7 are the preferred binding orientations for ligand MB-340 over that for pose 8 (Figures 4.4a and 4.4b). The *in silico* model recognized MB-340 as a good substrate for NQO1.

Compound MB-73 was selected from previously synthesized lavendamycin analogues. According to our SAR studies this compound should be a poor substrate for NQO1 due to the presence of the large $NHCOC_3H_7$-*n* group at the R^1 position that could create steric interactions inside the NQO1 active site. Therefore, this compound was selected for docking studies to observe how the model would rank it as an NQO1 substrate. None of the MB-73 conformations had a CSCORE = 5 (Table 4.1). All of the poses of MB-73 including poses 2, 5, 6, 21 and 25 (CSCORE = 4) fell into one cluster that yielded an RMSD equal to 0 Å for the quinolinedione and indolopyridine moieties atoms (Figure 4.5a). The difference was in the binding orientations of the $NHCOC_3H_7$-*n* and $CO_2C_2H_4CH(CH_3)_2$ groups (Figure 4.5a). All thirty poses of MB-73 including 2 were excluded from the NQO1 active site (Only pose 2 is shown) (Figure 4.5b). This

exclusion could be related to the steric hindrance produced by the large $NHCOC_3H_7$-*n* substituent against the Trp-105/Phe-106 wall that could be further enhanced by the contributing steric effect produced by the large $CO_2C_2H_4CH(CH_3)_2$ group. Ligand MB-73 was ranked as a poor substrate for NQO1.

The molecular docking studies demonstrated that Ligands MB-116 and MB-340 possessed an increased number of possible poses with optimum CSCORE and favorable binding orientations to promote hydrogen bonding and van der Waals interactions, hydride ion reception and quinone reduction compared to ligands MB-137, -100 and -73.

Figure 4.5. Molecular models of the poses of ligand MB-73 docked into the NQO1 active site.

a)

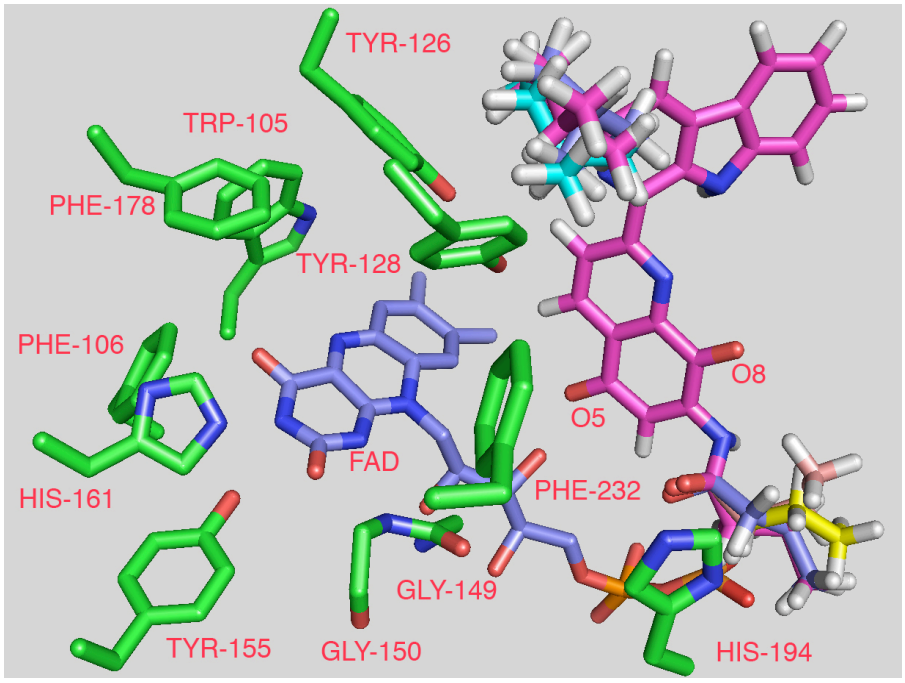

b)

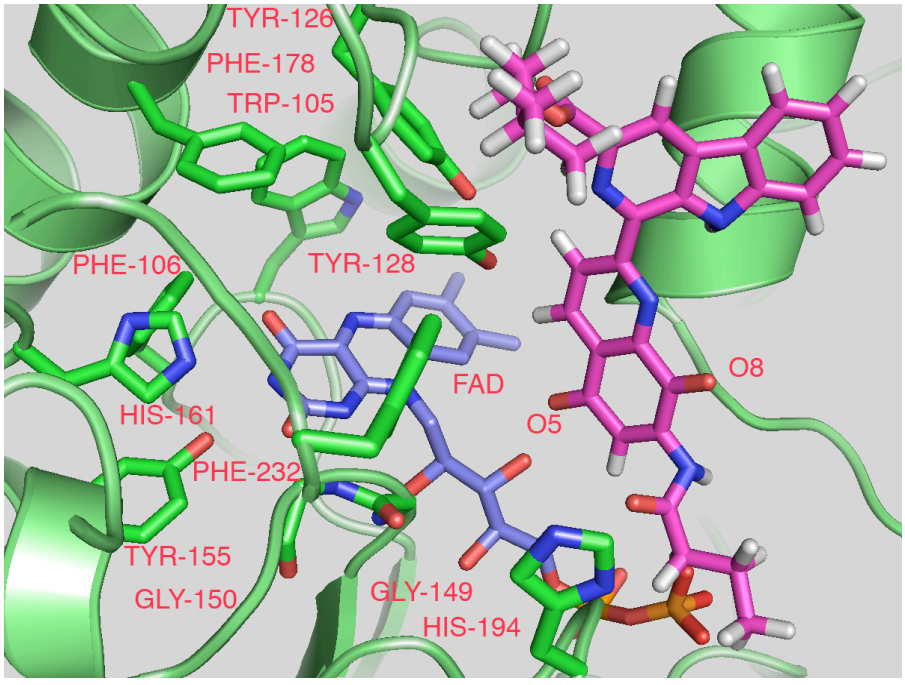

Figure 4.5. Molecular models of the poses of ligand MB-73 docked into the NQO1 active site. **a)** View of the superposition of the docked poses 2, 5, 6, 21 and 25 of MB-73 (magenta, cyan, blue, salmon and yellow) (CSCORE = 4) in the NQO1 active site. **b)** Molecular model of the pose 2 of MB-73 (magenta) (CSCORE = 4) docked into the NQO1 active site. In (a) and (b) residues of the active site (green), FAD (blue) and MB-73 are represented as stick models. In (b) the rest of the structure is represented as a secondary structure cartoon. The atoms are colored: red, oxygen atoms; blue, nitrogen atoms; orange, phosphorus atoms and white, hydrogen atoms.

4.4.3 Metabolism Studies. Metabolism of the lavendamycin analogues by recombinant human NQO1 was examined. Reduction rates by NQO1 were measured using a spectrophotometic assay that employs cytochrome *c* as the terminal electron acceptor[23] and gives initial rates of lavendamycin analogue reduction (Table 4.6). The initial reduction rates (μmol cytochrome *c* reduced/min/mg NQO1) were calculated from the linear portion (0-30 s) of the reaction graphs.

Compound MB-116 with the $NHCOCH_3$ and $CONH(CH_2)_3CH_3$ groups at R^1 and R^3 positions, respectively, displayed the highest metabolism rate by NQO1 among the compounds (Table 4.6). The $NHCOCH_3$ group, a medium size substituent, did not produce steric hindrance with the internal wall of the NQO1 active site resulting in favorable positioning of MB-116 for hydride ion reception from $FADH_2$ and quinone reduction. Our docking studies determined that this group was also capable of hydrogen bonding with FAD and the key residues of the active site. These studies also demonstrated that the $CONH(CH_2)_3CH_3$ group at the R^3 position (pointing towards the outside of the active site) was capable of forming van der Waals interactions with Phe-232 residue of the NQO1 active site. This could be a contributing factor to the substrate specificity of this compound. Compound MB-83 (See Chapter 2), a studied lavendamycin analogue, with the straight chain *n*-octyl ester substituent at the R^3 position ($CO_2C_8H_{17}$-*n*) was determined to be a good substrate for the enzyme similar to MB-116.[13] The docking studies also indicated ligand MB-116 as a good substrate for NQO1.

Table 4.6. Metabolism of lavendamycin analogues by recombinant human NQO1 monitored by spectrophotometric cytochrome *c* assay.

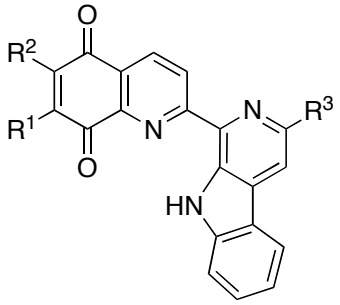

MB	R^1	R^2	R^3	Metabolism by NQO1 (μmol/min/mg) (Cytochrome *c* Reduction)
116	CH_3CONH	H	$CONH(CH_2)_3CH_3$	143 ± 11
137	CH_3CONH	H	$CONHCH(CH_3)C_2H_5$	4.9 ± 2.9
73	*n*-C_3H_7CONH	H	$CO_2C_2H_4CH(CH_3)_2$	3.4 ± 1.7
100	2-Furyl-CONH	H	CO_2CH_3	7.0 ± 1.5
340	NH_2	H	$CO_2(CH_2)_2OH$	60 ± 8

Although MB-137 possessed a similar chemical structure to MB-116 (the best substrate), it was a poor substrate for NQO1 (Table 4.6) that was in accordance with the docking data. Compounds MB-116 and -137 are structural isomers. The $CONH(CH_2)_3CH_3$ group at the R^3 position of MB-116 is a large, non-bulky and straight chain aliphatic group, whereas $CONHCH(CH_3)C_2H_5$ at the R^3 position of MB-137 is a large, bulky and branched structural isomer of the former. According to our docking studies, the branched configuration at R^3 of MB-137 was not capable of forming van der Waals interactions with the Phe-232 residue of the NQO1 active site due to active site constraints and steric effects.

Compound MB-100 exhibited a low metabolism rate by NQO1 (Table 4.6) due to the possible failure of the NHCO-2-furyl group at the R^1 position to intercalate between and form van der Waals interactions with the internal wall residues. Docking studies demonstrated that the lack of R^1-substituent intercalation capability led to the unfavorable positioning of MB-100 and loss of required hydrogen bonding and/or van der Waals interactions with the active site residues. This compound was also ranked as a poor substrate for NQO1 by the docking studies.

Compound MB-340 with a small NH_2 group at R^1 and $CO_2(CH_2)_2OH$ at R^3 displayed a good reduction rate by the enzyme (Table 4.6). According to the docking studies, favorable positioning of MB-340 in the active site was facilitated by lack of steric interactions of the substituents with the residues of the active site and by hydrogen bond formation with FAD and the residues of the NQO1 active site. Our docking studies also indicated high binding affinities for MB-340. A previous study determined that good indolequinone substrates for NQO1 including EO9 possessed a hydroxymethyl

group at the analogous C3 position.[23] Furthermore, RH1, which is a good substrate for NQO1, possesses a CH_2OH group at C3 position.[35,36] We also determined that compound MB-353 (See Chapter 2), decarboxy-2'-(hydroxymethyl)-demethyllavendamycin,[13] that possessed an NH_2 group at R^1 and CH_2OH at R^3 was a good substrate for NQO1.[13]

Compound MB-73 with $NHCOC_3H_7$-*n* and isoamyl ester groups at the R^1 and R^3 positions, respectively, exhibited the lowest metabolism rate by NQO1 and ranked as the poorest substrate (Table 4.6). The recently studied lavendamycin analogue MB-50, 7-*N*-acetyldemethyllavendamycin isoamyl ester,[13] with an acetamide group at R^1 position and isoamyl ester group at the R^3 position displayed a reduction rate 12-fold higher than MB-73 (See Chapter 2). The decreased reduction rate of MB-73 compared to MB-50 can be explained by apparent steric hindrance between the quinolinedione moiety of MB-73 and the NQO1 active site caused by the large $NHCOC_3H_7$-*n* group at R^1 compared to $NHCOCH_3$ in MB-50. This steric interaction could result in exclusion of MB-73 from the active site with subsequent poor hydride ion reception and quinone reduction capability. MB-73 was also ranked as a poor substrate by our docking studies.

Addition of NH_2 or $NHCOCH_3$ groups at R^1 and $CO_2(CH_2)_2OH$ or $CONH(CH_2)_3CH_3$ at R^3 had the greatest positive impact on substrate specificity compared to other substituents at these positions. The best substrates were the 2'-$CONH(CH_2)_3CH_3$-7-$NHCOCH_3$ (MB-116) and 2'-$CO_2(CH_2)_2OH$-7-NH_2 (MB-340) derivatives with reduction rates of 143 ± 11 and 60 ± 8 μmol/min/mg NQO1, respectively (Table 4.6).

4.4.4 *In Vitro* Cytotoxicity. Cytotoxicity studies were also performed on the lavendamycin analogues with cell survival being determined by the colorimetric MTT assay. We previously demonstrated an excellent positive linear correlation between the IC_{50} values (the chemosensitivity results) of the clonogenic and MTT assays for lavendamycin analogues (See Chapter 2).[13] We utilized the BE human colon adenocarcinoma cells stably transfected with human NQO1 cDNA.[36] The BE cells had no measurable NQO1 activity whereas activity in the transfected cells (BE-NQ) was 664 nmol/min/mg total cell protein using dichlorophenolindophenol (DCPIP) as the standard electron acceptor. In this study the cytotoxicity of the lavendamycin analogues (Table 4.7) has been compared in these cell lines.

Table 4.7. Cytotoxicity of lavendamycin analogues towards BE (NQO1-deficient) and BE-NQ (NQO1-rich) human colon adenocarcinoma cell lines.

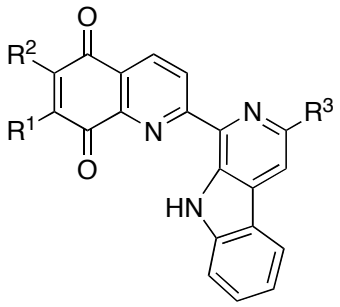

MB	R^1	R^2	R^3	Cytotoxicity IC_{50} (μM)		Selectivity Ratio [IC_{50} (BE) / IC_{50} (BE-NQ)]
				BE-NQ	BE	
116	CH_3CONH	H	$CONH(CH_2)_3CH_3$	1.7 ± 0.1	50.3 ± 1.5	30
137	CH_3CONH	H	$CONHCH(CH_3)C_2H_5$	>50	>50	-
73	*n*-C_3H_7CONH	H	$CO_2C_2H_4CH(CH_3)_2$	>50	>50	-
100	2-Furyl-CONH	H	CO_2CH_3	47 ± 3	49.0 ± 6.5	1
340	NH_2	H	$CO_2(CH_2)_2OH$	0.5 ± 0.0	3.3 ± 0.2	7

Designed analogues such as MB-116 and MB-340 that were good substrates for NQO1 (Table 4.6) were also more toxic to the NQO1-rich BE-NQ cell line than the NQO1-deficient BE cell line (Table 4.7). Compounds MB-116 and MB-340, the best substrates for NQO1 (Table 4.6), had the greatest differential toxicity with a selectivity ratio [IC_{50} (BE) / IC_{50} (BE-NQ)] of 30 and 7, respectively (Table 4.7). Our previous study also determined that good lavendamycin substrates for NQO1 were selectively toxic towards BE-NQ versus BE cells (See Chapter 2).[13] Compounds MB-83, -353, -97, demethyllavendamycin amide,[29] and -22, lavendamycin methyl ester,[37] exhibited high selective toxicity toward BE-NQ cells (selectivity ratios = 10, 11, 9 and 9, respectively) (See Chapter 2).[13] Compound MB-97 was also reported to highly reduce the colony outgrowth of A549 human lung carcinoma cells,[38] and it displayed promising cytotoxic and antitumor activities in the National Cancer Institute's (NCI) 60-cell line panel and *in vivo* hollow fiber tumorigenesis assay.[38]

Lavendamycin analogues, MB-137, -73 and -100 that were poor substrates for NQO1 (Table 4.6) demonstrated no selective toxicity toward BE-NQ cells or had no measurable cytotoxicity (IC_{50} > 50 μM) (Table 4.7). Overall, our results suggested that the best lavendamycin substrates for NQO1 were also the most selectively toxic to the high-NQO1 BE-NQ cell line compared to NQO1-deficient BE cells, consistent with our previous study (See Chapter 2).[13]

It has been reported that lavendamycin analogues possess low animal toxicity especially compared to streptonigrin (SN), a good substrate for NQO1 with high toxicity, and the parent lavendamycin compound.[29,39] The NCI *in vivo* studies have reported that the maximum tolerated dose of three lavendamycin analogues MB-22, -76 and -97 in

mice is 400 mg/kg which is 31 and 1000 times higher than that for lavendamycin and SN, respectively.[29,39] To obtain a preliminary assessment of the safety of lavendamycin analogues, the lavendamycin analogue MB-116 was studied along with SN for toxicity to normal cells using MMT assay. Human aortic endothelial cells (HAEC) that were treated for 2 hours with either SN or MB-116 were used. SN (IC_{50} = 0.47 μM) was 25 times more toxic to the endothelial cells than MB-116 (IC_{50} = 11.8 μM), suggesting that lavendamycins may have a greater safety margin than SN. Further studies in future will be required to obtain a broad range of safety assessment data on lavendamycin analogues to consider these agents as promising chemotherapeutic candidates.

4.5 Conclusions

A number of novel lavendamycin anologues were designed and synthesized. Addition of NH_2 or $NHCOCH_3$ groups at R^1 and $CO_2(CH_2)_2OH$ or $CONH(CH_2)_3CH_3$ at R^3 had the greatest positive impact on substrate specificity compared to other substituents at these positions. The best substrates were the 2'-$CONH(CH_2)_3CH_3$-7-$NHCOCH_3$ (MB-116) and 2'-$CO_2(CH_2)_2OH$-7-NH_2 (MB-340) derivatives and were also the most selectively toxic to the NQO1-rich BE-NQ cell line compared to the NQO1-deficient BE cell line. This study determined that the structure-based design criteria were productive, resulting in the design of two analogues with high substrate specificity and selective toxicity toward the NQO1-rich cells. It also indicated that the *in silico* model of the NQO1 active site correctly distinguished good and poor NQO1 substrates suggesting the model possessed practical predictive power. The docking data were in agreement with

the biological results. Therefore, the *in silico* model of the NQO1 active site could be utilized as a predictive, time- and cost-efficient tool in NQO1-directed lavendamycin antitumor agent development.

4.6 References

(1) Fourie, J.; Oleschuk, C. J.; Guziec, F., Jr.; Guziec, L.; Fiterman, D. J.; Monterrosa, C.; Begleiter, A. The effect of functional groups on reduction and activation of quinone bioreductive agents by DT-diaphorase. *Cancer Chemother. Pharmacol.* **2002**, *49*, 101-110.

(2) Gane, P. J.; Dean, P. M. Recent advances in structure-based rational drug design. *Curr. Opin. Struct. Biol.* **2000**, *10*, 401-404.

(3) Joseph-McCarthy, D. Computational approaches to structure-based ligand design. *Pharmacol. Ther.* **1999**, *84*, 179-191.

(4) Kuntz, I. D. Structure-based strategies for drug design and discovery. *Science* **1992**, *257*, 1078-1082.

(5) Fradera, X.; Mestres, J. Guided docking approaches to structure-based design and screening. *Curr. Top. Med. Chem.* **2004**, *4*, 687-700.

(6) Workman, P.; Walton, M. I. Enzyme-directed bioreductive drug development. *Selective activation of drugs by redox processes* **1990**, 173-191.

(7) Workman, P. Enzyme-directed bioreductive drug development revisited: A commentary on recent progress and future prospects with emphasis on quinone anticancer agents and quinone metabolizing enzymes, particularly DT-diaphorase. *Oncol. Res.* **1994**, *6*, 461-475.

(8) Suleman, A.; Skibo, E. B. A comprehensive study of the active site residues of DT-diaphorase: Rational design of benzimidazolediones as DT-diaphorase substrates. *J. Med. Chem.* **2002**, *45*, 1211-1220.

(9) Erickson, J. A.; Jalaie, M.; Robertson, D. H.; Lewis, R. A.; Vieth, M. Lessons in molecular recognition: the effects of ligand and protein flexibility on molecular docking accuracy. *J. Med. Chem.* **2004**, *47*, 45-55.

(10) Lyne, P. D. Structure-based virtual screening: An overview. *Drug Discov. Today.* **2002**, *7*, 1047-1055.

(11) Kontoyianni, M.; McClellan, L. M.; Sokol, G. S. Evaluation of docking performance: Comparative data on docking algorithms. *J. Med. Chem.* **2004**, *47*, 558-565.

(12) Faig, M.; Bianchet, M. A.; Winski, S.; Hargreaves, R.; Moody, C. J.; Hudnott, A. R.; Ross, D.; Amzel, L. M. Structure-based development of anticancer drugs: Complexes of NAD(P)H:quinone oxidoreductase 1 with chemotherapeutic quinones. *Structure* **2001**, *9*, 659-667.

(13) Hassani, M.; Cai, W.; Holley, D. C.; Lineswala, J. P.; Maharjan, B. R.; Ebrahimian, G. R.; Seradj, H.; Stocksdale, M. G.; Mohammadi, F.; Marvin, C. C.; Gerdes, J. M.; Beall, H. D.; Behforouz, M. Novel lavendamycin analogues as antitumor agents: synthesis, in vitro cytotoxicity, structure-metabolism, and computational molecular modeling studies with NAD(P)H:quinone oxidoreductase 1. *J. Med. Chem.* **2005**, *48*, 7733-7749.

(14) *SYBYL molecular modeling software*; SYBYL 7.0 ed.; Tripos Inc.: St. Louis, MO.

(15) Lemmen, C.; Lengauer, T. Time-efficient flexible superposition of medium-sized molecules. *J. Comput.-Aided Mol. Des.* **1997**, *11*, 357-368.

(16) Rarey, M.; Kramer, B.; Lengauer, T.; Klebe, G. A fast flexible docking method using an incremental construction algorithm. *J. Mol. Biol.* **1996**, *261*, 470-489.

(17) Eldridge, M. D.; Murray, C. W.; Auton, T. R.; Paolini, G. V.; Mee, R. P. Empirical scoring functions: I. The development of a fast empirical scoring function to estimate the binding affinity of ligands in receptor complexes. *J. Comput.-Aided Mol. Des.* **1997***, 11*, 425-445.

(18) Kuntz, I. D.; Blaney, J. M.; Oatley, S. J.; Langridge, R.; Ferrin, T. E. A geometric approach to macromolecule-ligand interactions. *J. Mol. Biol.* **1982***, 161*, 269-288.

(19) Jones, G.; Willett, P.; Glen, R. C.; Leach, A. R.; Taylor, R. Development and validation of a genetic algorithm for flexible docking. *J. Mol. Biol.* **1997***, 267*, 727-748.

(20) Muegge, I.; Martin, Y. C. A general and fast scoring function for protein-ligand interactions: A simplified potential approach. *J. Med. Chem.* **1999***, 42*, 791-804.

(21) DeLano, W. L. *The PyMOL molecular graphics system*; PyMOLX11Hybrid ed.; DeLano Scientific: San Carlos, CA.

(22) Winski, S. L.; Swann, E.; Hargreaves, R. H.; Dehn, D. L.; Butler, J.; Moody, C. J.; Ross, D. Relationship between NAD(P)H:quinone oxidoreductase 1 (NQO1) levels in a series of stably transfected cell lines and susceptibility to antitumor quinones. *Biochem. Pharmacol.* **2001***, 61*, 1509-1516.

(23) Phillips, R. M.; Naylor, M. A.; Jaffar, M.; Doughty, S. W.; Everett, S. A.; Breen, A. G.; Choudry, G. A.; Stratford, I. J. Bioreductive activation of a series of indolequinones by human DT-diaphorase: Structure-activity relationships. *J. Med. Chem.* **1999***, 42*, 4071-4080.

(24) Jaffar, M.; Phillips, R. M.; Williams, K. J.; Mrema, I.; Cole, C.; Wind, N. S.; Ward, T. H.; Stratford, I. J.; Patterson, A. V. 3-substituted-5-aziridinyl-1-

methylindole-4,7-diones as NQO1-directed antitumour agents: Mechanism of activation and cytotoxicity in vitro. *Biochem. Pharmacol.* **2003***, 66*, 1199-1206.

(25) Skelly, J. V.; Sanderson, M. R.; Suter, D. A.; Baumann, U.; Read, M. A.; Gregory, D. S.; Bennett, M.; Hobbs, S. M.; Neidle, S. Crystal structure of human DT-diaphorase: A model for interaction with the cytotoxic prodrug 5-(aziridin-1-yl)-2,4-dinitrobenzamide (CB1954). *J. Med. Chem.* **1999***, 42*, 4325-4330.

(26) Phillips, R. M.; Jaffar, M.; Maitland, D. J.; Loadman, P. M.; Shnyder, S. D.; Steans, G.; Cooper, P. A.; Race, A.; Patterson, A. V.; Stratford, I. J. Pharmacological and biological evaluation of a series of substituted 1,4-naphthoquinone bioreductive drugs. *Biochem. Pharmacol.* **2004***, 68*, 2107-2116.

(27) Boger, D. L.; Yasuda, M.; Mitscher, L. A.; Drake, S. D.; Kitos, P. A.; Thompson, S. C. Streptonigrin and lavendamycin partial structures. Probes for the minimum, potent pharmacophore of streptonigrin, lavendamycin, and synthetic quinoline-5,8-diones. *J. Med. Chem.* **1987***, 30*, 1918-1928.

(28) Kremer, W. B.; Laszlo, J. Comparison of biochemical effects of isopropylidine azastreptonigrin (NSC-62709) with streptonigrin (NSC-45383). *Cancer Chemother. Rep.* **1967***, 51*, 19-24.

(29) Behforouz, M.; Cai, W.; Stocksdale, M. G.; Lucas, J. S.; Jung, J. Y.; Briere, D.; Wang, A.; Katen, K. S.; Behforouz, N. C. Novel lavendamycin analogues as potent HIV-reverse transcriptase inhibitors: Synthesis and evaluation of anti-reverse transcriptase activity of amide and ester analogues of lavendamycin. *J. Med. Chem.* **2003***, 46*, 5773-5780.

(30) Zhou, Z.; Fisher, D.; Spidel, J.; Greenfield, J.; Patson, B.; Fazal, A.; Wigal, C.; Moe, O. A.; Madura, J. D. Kinetic and docking studies of the interaction of quinones with the quinone reductase active site. *Biochemistry* **2003***, 42*, 1985-1994.

(31) Faig, M.; Bianchet, M. A.; Talalay, P.; Chen, S.; Winski, S.; Ross, D.; Amzel, L. M. Structures of recombinant human and mouse NAD(P)H:quinone oxidoreductases: Species comparison and structural changes with substrate binding and release. *Proc. Natl. Acad. Sci. U. S. A.* **2000***, 97*, 3177-3182.

(32) Asher, G.; Dym, O.; Tsvetkov, P.; Adler, J.; Shaul, Y. The crystal structure of NAD(P)H quinone oxidoreductase 1 in complex with its potent inhibitor dicoumarol. *Biochemistry* **2006***, 45*, 6372-6378.

(33) Winski, S. L.; Faig, M.; Bianchet, M. A.; Siegel, D.; Swann, E.; Fung, K.; Duncan, M. W.; Moody, C. J.; Amzel, L. M.; Ross, D. Characterization of a mechanism-based inhibitor of NAD(P)H:quinone oxidoreductase 1 by biochemical, x-ray crystallographic, and mass spectrometric approaches. *Biochemistry* **2001***, 40*, 15135-15142.

(34) Skibo, E. B.; Gordon, S.; Bess, L.; Boruah, R.; Heileman, M. J. Studies of pyrrolo[1,2-alpha]benzimidazolequinone DT-diaphorase substrate activity, topoisomerase II inhibition activity, and DNA reductive alkylation. *J. Med. Chem.* **1997***, 40*, 1327-1339.

(35) Danson, S.; Ward, T. H.; Butler, J.; Ranson, M. DT-diaphorase: A target for new anticancer drugs. *Cancer Treat. Rev.* **2004***, 30*, 437-449.

(36) Winski, S. L.; Hargreaves, R. H.; Butler, J.; Ross, D. A new screening system for NAD(P)H:quinone oxidoreductase (NQO1)-directed antitumor quinones: Identification of a new aziridinylbenzoquinone, RH1, as a NQO1-directed antitumor agent. *Clin. Cancer Res.* **1998***, 4*, 3083-3088.

(37) Behforouz, M.; Gu, Z.; Cai, W.; Horn, M. A.; Ahmadian, M. A highly concise synthesis of lavendamycin methyl ester. *J. Org. Chem.* **1993***, 58*, 7089-7091.

(38) Fang, Y.; Linardic, C. M.; Richardson, D. A.; Cai, W.; Behforouz, M.; Abraham, R. T. Characterization of the cytotoxic activities of novel analogues of the antitumor agent, lavendamycin. *Mol. Cancer Ther.* **2003***, 2*, 517-526.

(39) Behforouz, M.; Cai, W.; Mohammadi, F.; Stocksdale, M. G.; Gu, Z.; Ahmadian, M.; Baty, D. E.; Etling, M. R.; Al-Anzi, C. H.; Swiftney, T. M.; Tanzer, L. R.; Merriman, R. L.; Behforouz, N. C. Synthesis and evaluation of antitumor activity of novel N-acyllavendamycin analogues and quinoline-5,8-diones. *Bioorg. Med. Chem.* **2007***, 15*, 495-510.

Chapter 5

Mechanisms of Lavendamycin Antitumor Agent Toxicity: NAD(P)H:Quinone Oxidoreductase 1 (NQO1)-mediated Induction of Oxidative Stress and Apoptosis

5.1 Abstract

Lavendamycin antitumor agents that are good substrates for NQO1 are selectively toxic to tumor cells with elevated NQO1 activity (See Chapter 2). The purpose of this study was to investigate the mechanisms of NQO1-mediated selective cytotoxicity of good lavendamycin substrates towards human colon adenocarcinoma NQO1-rich BE-NQ cells compared to NQO1-deficient BE cells. Lavendamycin analogues possess structural similarity to streptonigrin (SN), a good redox-cycling substrate for NQO1 that produces large quantities of reactive oxygen species (ROS) after reduction by NQO1. Therefore, we examined whether good lavendamycin substrates for NQO1 could induce NQO1-mediated oxidative stress and subsequent apoptosis in BE-NQ cells. Biomarkers of oxidative stress including formation of 8-hydroxy-2'-deoxyguanosine (8-oxo-2dG), an indicator of oxidative DNA damage, and depletion of the reduced form of glutathione (GSH) in the cells were investigated. BE and BE-NQ cells were treated with MB-353 (NQO1 good substrate, reduction rate = 263 ± 30 μmol/min/mg NQO1) and MB-323 (NQO1 poor substrate, reduction rate = 0.1 ± 0.1 μmol/min/mg NQO1). An HPLC-based analysis was utilized to determine levels of 8-oxo-2dG and 2′-deoxyguanosine (2-dG) in the cells, and the molar ratio, 8-oxo-2dG (fmol)/2-dG (nmol). Among MB-353 treated cells, a significant increase in the molar ratio of 8-oxo-2dG to 2-dG was observed only in

BE-NQ cells demonstrating the importance of NQO1 in selective induction of oxidative DNA damage in BE-NQ cells by MB-353. No significant increase in the corresponding molar ratio was observed in either cell line treated with MB-323 implying that NQO1-mediated induction of oxidative DNA damage in BE-NQ cells was specific to MB-353. Since we observed the production of oxidative DNA damage in BE-NQ cells by MB-353, depletion of GSH as a biomarker of oxidative stress was also examined using a colorimetric assay. MB-353 significantly decreased the levels of GSH in BE-NQ cells, whereas no reduction in GSH levels was observed in BE cells suggesting an NQO1-mediated selective depletion of GSH in BE-NQ cells by MB-353. No difference was observed in the GSH levels in either cell line treated with MB-323 indicating that GSH depletion in BE-NQ cells was specific to the good lavendamycin substrate, MB-353. In addition, we hypothesized that the observed MB-353-induced oxidative stress in BE-NQ cells could result in induction of apoptosis in these cells. Therefore, the role of NQO1 in lavendamycin-induced apoptosis was examined using a colorimetric assay. MB-353 selectively induced apoptosis only in the BE-NQ cell line, while apoptosis induction was not observed in either cell line treated with MB-323. Overall, our results demonstrated that only the good lavendamycin substrate, MB-353, caused oxidative stress leading to oxidative DNA damage and apoptosis in NQO1-rich BE-NQ cells at nM concentrations via NQO1-mediated activation.

5.2 Introduction

Oxidative stress is defined as a condition in which overwhelming production of reactive oxygen species (ROS) imposes an imbalance between ROS and antioxidant

levels in excess of the former.[1,2] Upon this challenge, inadequate levels of antioxidant defense elements cannot efficiently neutralize ROS resulting in persistence of oxidative stress and subsequent damage to cellular macromolecules.[1,2] One crucial mechanism of action for many anticancer agents is the production of ROS.[3]

Redox-cycling quinones undergo enzymatic reduction and autoxidation, and subsequently generate ROS.[4] Metabolism of redox-cycling quinones alters the intracellular oxidant-antioxidant balance.[4] Watanabe et al. have demonstrated that NQO1-mediated autoxidation of the hydroquinone forms of menadione and 2,3-dimethoxy-1,4-naphthoquinone (DMNQ) results in the generation of hydrogen peroxide (H_2O_2) in lung epithelial A549-S cells treated with these agents.[5] The menadione- and DMNQ-induced production of H_2O_2 can be inhibited up to 90% and 100%, respectively, by the NQO1 inhibitor, dicoumarol.[5] In this study catalase prevented H_2O_2 accumulation and protected A549-S cells from menadione- and DMNQ-induced cell death.[5] Their findings suggest that the observed H_2O_2 generation and cytotoxicity in menadione- and DMNQ-treated A549-S cells were mainly due to NQO1-mediated autoxidation of the corresponding hydroquinones.[5] ROS-mediated cytotoxicity of phenanthrenequinone, 2-amino-1,4-naphthoquinone and naphthazarin towards NQO1-enriched L5178Y/HBM10 lymphoblasts versus parental L5178Y cells has also been reported.[6] Cytotoxic effects of these compounds toward L5178Y/HBM10 mouse lymphoma cells were reduced when treated by dicoumarol and catalase indicating NQO1-mediated redox cycling-related cytotoxicity of these compounds.[6] Another group determined NQO1-mediated, autoxidation of variously substituted naphthoquinones in cell-free assays.[7] In addition, Beall et al. demonstrated NQO1-mediated redox cycling, selective cytotoxicity and

induction of DNA strand breaks in NQO1-rich human colon carcinoma HT-29 cells versus NQO1-deficient BE cells by streptonigrin (SN).[8]

Direct assessment of the levels of ROS to detect the presence of oxidative stress is an impractical and unreliable approach due to the fact that ROS are short-lived and highly reactive species.[1,2] One alternative approach frequently used in some laboratories to determine the presence of oxidative stress is to take advantage of its biological markers.[1,2] Measurement of biological markers of oxidative DNA damage such as 8-hydroxy-2'-deoxyguanosine (8-oxo-2dG) and the cellular glutathione (GSH) levels have been routinely used as indices of oxidative stress induction.[1,2]

One method that can be utilized as an index of oxidative stress is the measurement of 8-oxo-2dG, a product of oxidative DNA damage.[1] 8-Oxo-2dG is the most frequently detected and studied oxidative DNA lesion.[2,9] Due to the mutagenic activity, 8-oxo-2dG is capable of imposing deleterious effects on cells including apoptosis induction.[9,10] Lin et al. investigated the generation of 8-oxo-2dG in calf thymus DNA after 2 hours of exposure to 1 and 10 μM tetrachloro-1,4-benzoquinone in the presence of NADPH and Cu(II).[11] They observed significant production of 8-oxo-2dG in calf thymus DNA treated with the compound versus untreated calf thymus DNA suggesting that tetrachloro-1,4-benzoquinone undergoes redox cycling and produces ROS that are capable of oxidative DNA lesion induction.[11]

Assessment of cellular levels of GSH has been frequently used as a marker of oxidative stress.[1] GSH is the most important cellular antioxidant defense nucleophile and is capable of the detoxification of ROS.[12] Failure to maintain the levels of intracellular GSH upon an oxidative challenge can result in severe consequences for cells including

loss of function and integrity.[12,13] One key aspect of quinone-induced toxicity is the oxidation of critical intracellular thiols due to redox cycling and induction of oxidative stress.[14,15] GSH depletion has been considered as a marker of oxidative damage induced by redox-cycling β-lapachone.[16] GSH oxidation and depletion during NQO1-mediated redox cycling of 2-methylmethoxy-1,4-naphthoquinone[17] and diaziquone (AZQ)[18] in cell-free assays have been reported.

The ability of cells to maintain a proper oxidant/antioxidant balance is a crucial factor to determine the result of an apoptosis-inducing signal.[4] Metabolism of redox-cycling quinones impacts the intracellular redox balance.[4] Due to the fact that oxidative stress is a known trigger of apoptosis, and cytotoxicity of quinone compounds has been related to the production of free radicals and DNA damage, these compounds should be potent apoptosis inducers.[4]

The ability of lavendamycin substrates to induce NQO1-mediated oxidative stress, oxidative DNA damage and subsequent apoptosis has not been previously investigated. It is of great importance to examine cytotoxic mechanisms of lavendamycin analogues to be able to effectively utilize them in combination with other antitumor agents in cancer therapy. This will facilitate selection of a proper set of antitumor agents in combination with lavendamycins in chemotherapy and can result in the desired synergistic antitumor effects of the agents with different mechanisms of action and toxicities. In addition, combination cancer therapy with antitumor agents with known, different mechanisms of cytotoxicity could act on various regions of the tumor microenvironment. This study was designed to investigate the selective induction of oxidative stress and apoptosis in NQO1-rich cells by good lavendamycin substrates for

NQO1 versus poor substrates. To determine the induction of oxidative stress in NQO1-rich and NQO1-deficient cells by lavendamycin analogues, we examined the generation of 8-oxo-2dG, an indicator of oxidative DNA damage, and depletion of GSH as relevant biomarkers of oxidative stress. This is the first study to demonstrate that lavendamycin antitumor agents cause oxidative stress leading to oxidative DNA damage and apoptosis in NQO1-rich cancer cells at nM concentrations via NQO1-mediated activation.

5.3 Materials and Methods

5.3.1 8-Oxo-2dG Assay. Oxidative DNA damage was determined by formation of 8-oxo-2dG according to the protocol developed by Bolin et al.[9] Cultured cells (BE and BE-NQ cells) were harvested by trypsinization. Cells were then transferred into microcentrifuge tubes (10^7 cells per tube). Cells were treated with a concentration of 500 nM of compound MB-353 (good substrate) and MB-323 (poor substrate). Treated and untreated (negative control) cells were incubated at 37 °C under a humidified atmosphere containing 5% CO_2 for 2 hours on a rotator. Next, cells were centrifuged at 1500 rpm for 5 min, supernatant was discarded and the cell pellet was washed twice with 1mL culture medium and once with 1mL PBS. At this step 300 µL of extraction buffer (Tris-base, EDTA, DTT, Spermine, Spermidine, protease inhibitors, glycerol and ddH_2O) was added to the cell pellet and cells were sonicated by exposure to five 4-s ultrasound pulses (sonic disruption on ice for 20 s in 4-s bursts). 30 µL KCl (2.5 M) was then added and rocked for 30 min in cold room. Next, samples were centrifuged at 14000 x g for 30 min. The cell pellet was used for the extraction of DNA and subsequent analysis of oxidative DNA damage. Briefly, the cell pellet was washed with DNA extraction buffer and treated with

DNAase-free RNAase followed by digestion with proteinase K. The protein fraction was separated from DNA by three consecutive organic extractions. The DNA was then precipitated by adding two volumes of ethanol (with respect to the aqueous volume) and incubated overnight at -20 °C. The DNA was prepared for HPLC analysis by resolving it into deoxynucleoside components. The amount of 8-oxo-2dG and 2′-deoxyguanosine (2-dG) was calculated by comparing the peak area of 8-oxo-2dG and 2-dG obtained from the enzymatic hydrolysate of the DNA sample to a calibration curve for both compounds. Levels of 8-oxo-2dG in the samples were expressed relative to the content of 2-dG, e.g., the molar ratio of 8-oxo-2dG /2-dG (fmol 8-oxo-2dG/nmol of 2-dG). HPLC system: The mobile phase consisted of 100 mM sodium acetate, pH 5.2, with 5% methanol. Flow rate was kept at 1 mL/min using a Model 582 Solvent Delivery Module (ESA, Chelmsford, MA). DNA was analyzed using a reverse phase YMCbasic HPLC column (4.6 x 150 mm) with a 3-micron particle size (YMC Inc., Wilmington, NC, USA). 8-Oxo-2dG and 2-dG were detected by a Model 5600A CoulArray Detector (ESA, Chelmsford, MA) with three model 6210 four channel electrochemical cells. Potentials were set at 175, 200 and 250 V for 8-oxo-2dG and at 785, 850 and 890 V for 2-dG. Data were recorded, stored and analyzed on a PC Pentium computer using CoulArray for Windows 32Software (ESA, Chelmsford, MA). Data were expressed as femtomoles of 8-oxo-2dG per nanomoles of 2-dG.

5.3.2 Reduced Glutathione Assay. The reduced form of glutathione was determined by a non-recycling system in sample solutions using the ApoGSH^{TM} Glutathione Colorimetric Detection kit (BioVision, Inc., CA, USA). Cultured cells (BE and BE-NQ cells) were harvested by trypsinization and diluted with culture medium to

obtain a cell concentration of 0.5-1 x 10^6 cells/mL. Cells were then plated in 6-well plates at a density of 0.5-1 x 10^6 cells/well and allowed to attach overnight. 500 µL of culture medium was removed and replaced with 500 µL of medium containing MB-353 (good substrate) and MB-323 (poor substrate) at a concentration of 500 nM. Treated and untreated (negative control) cells were incubated at 37 °C under a humidified atmosphere containing 5% CO_2 for 2 hours. Next, cells were harvested by trypsinization, centrifuged at 700 x g for 5 min at 4 °C and supernatant was discarded. The cell pellet was resuspended in 1 mL culture medium. At this step, cells were incubated for 0, 6, 12 or 24 hours at 37 °C. Cells were then centrifuged at 700 x g for 5 min. The cell pellet was resuspended in 500 µL ice-cold glutathione buffer, centrifuged at 700 x g for 5 min at 4 °C and supernatant was discarded. Cells were lysed in 80 µL ice-cold glutathione buffer and incubated on ice for 10 min. 20 µL of 5% sulfosalicylic acid (SSA) was added, vortexed and centrifuged at 8000 x g for 10 minutes. Then, supernatant was carefully transferred to fresh microcentrifuge tubes. Reduced form of glutathione was determined from the supernatant using 5,5'-dithionitrobenzoic acid (DTNB) in the presence of NADPH without recycling system according to the manufacturer's instructions.

5.3.3 Detection of Apoptosis. Apoptosis was detected by the enrichment of mono and oligonucleosomes in the cytoplasm of the apoptotic cells using the cell death detection ELISA kit (Roche Diagnostics GmbH, Roche Applied Science, Germany). Cultured cells (BE and BE-NQ cells) were harvested by trypsinization and diluted with culture medium to obtain a cell concentration of 1 x 10^5 cells/mL. Cells were then transferred into microcentrifuge tubes (500 µL/tube = 5 x 10^4 cells/tube). 500 µL of culture medium containing compound MB-323 (poor substrate) and MB-353 (good

substrate) at a concentration of 500 nM were added to the tubes. Treated cells were incubated at 37 °C under a humidified atmosphere containing 5% CO_2 for 2 hours. Next, cells were centrifuged at 200 x g for 5 min, supernatant was discarded and the cell pellet was resuspended in 1 mL culture medium. At this step, cells were incubated for 0, 12 or 24 hours at 37 °C. Cells were then centrifuged at 1500 x g for 5 min. The cell pellet was resuspended with 500 µL incubation buffer per tube (1×10^5 cells/mL). The samples were incubated for 30 min at 15 to 25 °C to allow the cells to lyse. The lysate was centrifuged at 20000 x g for 10 min. 400 µL of the supernatant (cytoplasmic fraction) was carefully removed. The resulting supernatant was prediluted 1:10 with incubation buffer. The enrichment of mono and oligonucleosomes in the cytoplasmic fraction of the apoptotic cells was detected by immunoassay according to the manufacturer's instructions.

5.4 Statistics

For the 8-oxo-2dG assay, differences between lavendamycin analogue-treated and untreated cells (negative control) were assessed using single-factor analysis of variance (one-way ANOVA) and post hoc Tukey's multiple comparison tests. All results were reported as mean ± SEM and $P \leq 0.05$ was considered significant.

For the reduced glutathione assay, since results were reported as percentage of negative control (negative control = 100%), differences between lavendamycin analogue-treated cells at different post-exposure incubation periods and untreated cells (negative control) were assessed using a one-sample *t-test* adjusted for the number of group means

tested and directionality of the hypothesis (Bonferroni correction). Results were reported as mean ± SEM and $P \leq 0.05$ (adjusted) was considered significant. To evaluate differences between lavendamycin analogue-treated cells at different post-exposure incubation periods, a one-way ANOVA and post hoc Tukey's multiple comparison test were used. All results were reported as mean ± SEM and $P \leq 0.05$ was considered significant.

For the apoptosis assay, since the enrichment factor value of the negative control was considered 1, differences between lavendamycin analogue-treated cells at different post-exposure incubation periods and untreated cells (negative control) were assessed using a one-sample *t-test* adjusted for the number of group means tested and directionality of the hypothesis (Bonferroni correction). Results were reported as mean ± SEM and $P \leq 0.05$ (adjusted) was considered significant. To evaluate differences between lavendamycin analogue-treated cells at different post-exposure incubation periods, a one-way ANOVA and post hoc Tukey's multiple comparison test were used. All results were reported as mean ± SEM and $P \leq 0.05$ was considered significant.

5.5 Results and Discussion

Many quinone-based antitumor agents including SN,[8,19] mitomycin C (MMC),[20] β-lapachone,[21] AZQ,[22-24] EO9[25-27] and RH1[28-30] are bioactivated to ctotoxic species by NQO1. The hydroquinone produced after the two-electron reduction of these agents is the biologically active form that can cause DNA alkylation and/or oxidative stress.[4,21,31] Production of ROS, induction of oxidative stress and DNA damage are important events

related to quinone reactions and DNA represents the primary biomolecular target for quinone-based anticancer agents.[4,32]

5.5.1 Detection of 8-Oxo-2dG Production. Cellular generation of ROS by redox-cycling quinones can overwhelm cellular antioxidant defense systems, cause severe oxidative stress and result in the formation of biological markers for oxidative DNA damage such as 8-oxo-2dG.[32-34] The investigation of oxidative stress induction generally is performed via the measurement of indicators that reflect ROS-induced damage.[2] We observed generation of the biological marker of oxidative DNA damage, 8-oxo-2dG, and a significant increase in the molar ratio of 8-oxo-2dG to 2-dG in NQO1-rich BE-NQ cells treated by 500 nM MB-353 (good substrate) for 2 hours versus untreated BE-NQ negative control (Figure 5.1). 8-Oxo-2dG analysis data from cellular DNA are usually expressed as the ratio of 8-oxo-2dG to the unmodified 2-dG base.[2]

No significant increase in the corresponding molar ratio was observed in NQO1-deficient BE cell line treated with MB-353 compared to untreated BE cells (Figure 5.2). This suggests that MB-353 as a good substrate for NQO1 can undergo NQO1-mediated activation in NQO1-rich BE-NQ cells with concomitant production of ROS that can cause mutagenic oxidative DNA lesions such as 8-oxo-2dG. The cytotoxic mechanisms of quinones can be attributed to two primary events including redox cycling and electrophilic alkylation of cellular nucleophiles.[4,31] Further studies will be required to investigate possible DNA strand break formation in BE-NQ cells by MB-353 and the ability of this compound to alkylate DNA.

Lack of enzymatic activity of NQO1 in BE cells can be considered as the underlying reason that MB-353 is not activated by NQO1 and cannot induce oxidative

stress in these cells resulting in subsequent lack of oxidative DNA damage. These findings suggest an NQO1-mediated selective induction of oxidative DNA damage in BE-NQ cells by the good substrate MB-353 possibly due to the redox cycling of this compound.

Figure 5.1. Effect of MB-353 and MB-323 on the molar ratio of 8-oxo-2dG to 2-dG in BE-NQ cells after 2-h treatment with the compounds at a concentration of 500 nM.

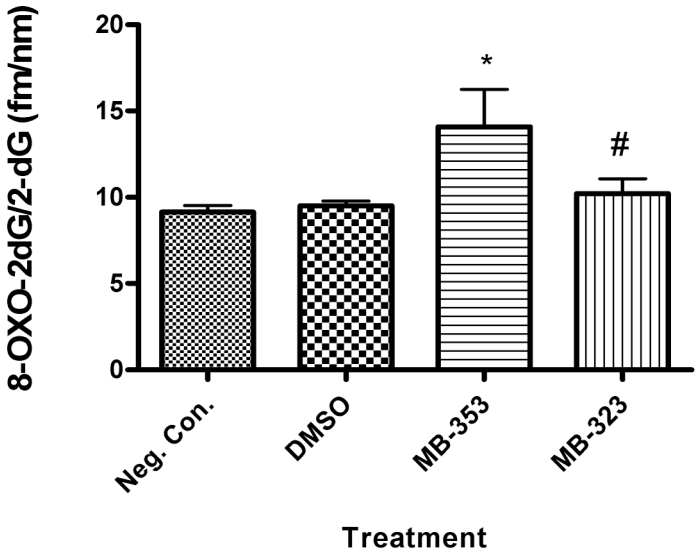

Figure 5.1. Effect of MB-353 and MB-323 on the molar ratio of 8-oxo-2dG to 2-dG in BE-NQ cells after 2-h treatment with the compounds at a concentration of 500 nM. An HPLC-based analysis was utilized to determine levels of 8-oxo-2dG and 2-dG as described under Materials and Methods. *Significantly different from negative control (untreated cells) ($P \leq 0.05$). #Significantly different from MB-323 ($P \leq 0.05$). Results are reported as means ± SEM for n = 6 experiments.

Figure 5.2. Effect of MB-353 and MB-323 on the molar ratio of 8-oxo-2dG to 2-dG in BE cells after 2-h treatment with the compounds at a concentration of 500 nM.

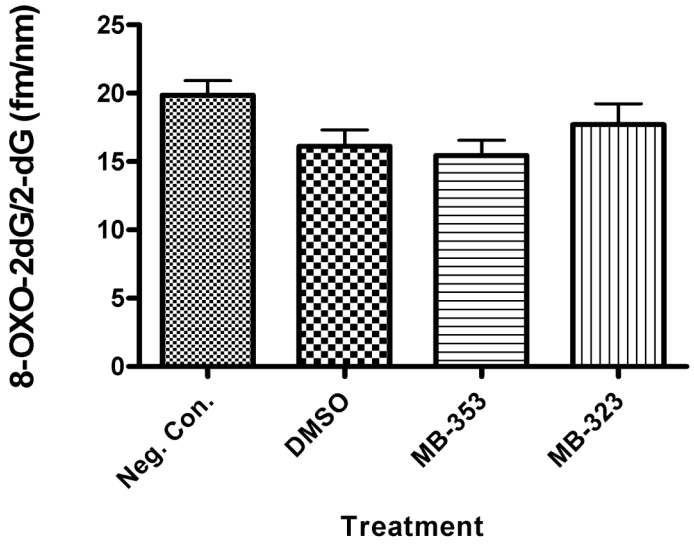

Figure 5.2. Effect of MB-353 and MB-323 on the molar ratio of 8-oxo-2dG to 2-dG in BE cells after 2-h treatment with the compounds at a concentration of 500 nM. An HPLC-based analysis was utilized to determine levels of 8-oxo-2dG and 2-dG as described under Materials and Methods. Results are reported as means ± SEM for n = 6 experiments.

Generation of 8-oxo-2dG by quinone compounds has been reported. Unpublished data of Gutierrez et al. determined production of 8-oxo-2dG lesions due to redox cycling of the benzoquinone AZQ.[35] Another study demonstrated significant induction of 8-oxo-2dG generation in sea urchin embryos exposed to the concentration of MMC as low as 1 μM.[36] This study also determined a direct association between MMC-induced toxicity in the embryos and the related 8-oxo-2dG levels. It has been reported that DNA damage can induce apoptosis, which is of primary importance to DNA damage-based chemotherapeutic strategies.[37] 8-Oxo-2dG has been also considered as a biomarker of apoptosis.[37,38] Although, generation of 8-oxo-2dG is an important biomarker for estimating oxidative DNA damage,[9,10] to date it has never been examined in cancer cells following exposure to lavendamycin antitumor agents.

No significant increase was observed in the molar ratio of 8-oxo-2dG to 2-dG in either BE or BE-NQ cells treated by MB-323 (poor substrate) for 2 hours, at the same concentration as MB-353, versus negative controls (Figures 5.1 and 5.2). This finding suggests that MB-323 cannot be bioactivated by NQO1 to cytotoxic species capable of induction of oxidative stress as is indicated by the lack of oxidative DNA damage in NQO1-rich BE-NQ cells treated by this compound. This is consistent with our metabolism data for MB-323 that determined this compound as a poor substrate for NQO1 (See Chapter 2).

Since we observed the production of oxidative DNA damage in BE-NQ cells by MB-353, depletion of GSH as a biomarker of oxidative stress was also investigated.

5.5.2 Glutathione Depletion. ROS can easily oxidize thiols and deplete intracellular reduced form of glutathione due to oxidative stress.[4] GSH oxidation by ROS

during redox cycling of quinones is considered a key element of quinone cytotoxicity.[15] Our data suggested that reductive bioactivation of MB-353 by NQO1 caused depletion of GSH in an NQO1-mediated manner in NQO1-rich BE-NQ cells possibly due to redox cycling of MB-353 (Figure 5.3). Significant reductions in the levels of GSH in these cells were observed immediately after 2 hours of treatment (zero hour post-exposure time point) with 500 nM MB-353 implying that GSH depletion is an early event in the induced oxidative stress process. The levels of GSH in the cells remained significantly low compared to untreated cells (negative controls) at 6, 12 and up to 24 hours post-exposure periods (Figure 5.3). The greatest decrease in the GSH levels occurred at the 12 hour time point suggesting that MB-353 acted as a powerful redox-cycling agent that exhausted the intracellular GSH pool delaying the GSH replenishment process. One equivalent of a redox-cycling quinone is capable of producing multiple equivalents of superoxide anion ($O_2^{-\cdot}$), therefore it can exert its toxicity by exhausting the antioxidant defense system.[39] A trend toward the recovery of the GSH levels in BE-NQ cells was observed at the 24 hour post-exposure time point, although the level of GSH depletion was still significant at this time point compared to the negative control (Figure 5.3). No significant differences between the MB-353-treated BE-NQ cells at different post-exposure incubation periods were observed (Figure 5.3). If the cells are not exposed to the compound in repetitive intervals, the cellular GSH content can recover due to possible reduction of oxidized form of GSH (GSSG) by glutathione reductase, uptake of intact glutathione or *de novo* synthesis of GSH by γ-glutamylcysteine and GSH synthetase.

No GSH depletion was detected in BE cells treated by MB-353 at any of the post-exposure time points implying that the reduction in the levels of GSH is an NQO1-related

selective event for BE-NQ cells compared to BE cells when treated by MB-353 (Figure 5.4). Although the reduction in the levels of GSH in BE cells after MB-353 treatment was not significant, a trend similar to that for BE-NQ cells was observed exhibiting the highest reduction in GSH levels at the 12 hour time point.

Figure 5.3. Effect of MB-353 on the levels of reduced form of glutathione in BE-NQ cells after 2-h treatment with the compound at a concentration of 500 nM at 0, 6, 12 and 24 h post-exposure incubation periods.

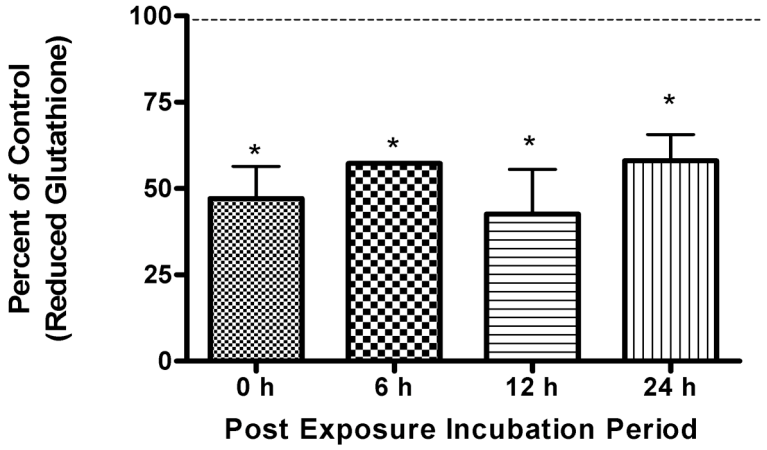

Figure 5.3. Effect of MB-353 on the levels of reduced form of glutathione in BE-NQ cells after 2-h treatment with the compound at a concentration of 500 nM at 0, 6, 12 and 24 h post-exposure incubation periods. Reduced form of glutathione was determined by a non-recycling system in sample solutions using the glutathione colorimetric detection kit as described under Materials and Methods. Reduced form of glutathione is expressed as percentage of negative control (untreated cells). Dashed line represents negative control. *Significantly different from negative control ($P \leq 0.05$). Results are reported as means ± SEM for n = 3 experiments.

Figure 5.4. Effect of MB-353 on the levels of reduced form of glutathione in BE cells after 2-h treatment with the compound at a concentration of 500 nM at 0, 6, 12 and 24 h post-exposure incubation periods.

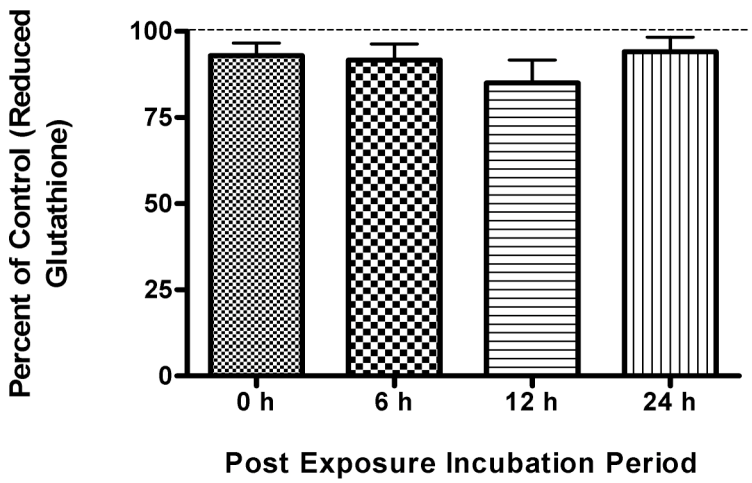

Figure 5.4. Effect of MB-353 on the levels of reduced form of glutathione in BE cells after 2-h treatment with the compound at a concentration of 500 nM at 0, 6, 12 and 24 h post-exposure incubation periods. Reduced form of glutathione was determined by a non-recycling system in sample solutions using the glutathione colorimetric detection kit as described under Materials and Methods. Reduced form of glutathione is expressed as percentage of negative control (untreated cells). Dashed line represents negative control. Results are reported as means ± SEM for n = 3 experiments.

Tissue GSH levels decrease in response to chemical compound-induced oxidative stress.[14] The metabolism of redox-cycling quinones in cells and subsequent induction of oxidative stress cause oxidation of cellular thiol groups that is considered as one mechanism of quinone-induced toxicity.[14] One study determined significant GSH depletion in primary cultured rat hepatocytes after exposure to 1,4-naphthoquinone.[14] This study demonstrated that aloe extract can protect the hepatocytes against 1,4-naphthoquinone cytotoxicity via maintenance of cellular thiols.[14] GSH oxidation during NQO1-catalysed redox cycling of AZQ has also been reported.[18]

Another possible mechanism of GSH depletion after exposure to quinones is due to alkylation of thiols by these compounds.[15,33] The fact that we did not observe significant GSH depletion in BE cells treated with MB-353 compared to the corresponding negative control suggested the importance of GSH oxidation rather than GSH alkylation as the primary mechanism of toxicity of MB-353. Although our results indicate that MB-353 does not react with GSH significantly, the possibility of some degree of the alkylation reaction cannot be completely ruled out with our current data. There is the possibility of low levels of GSH alkylation by MB-353 that can impact the redox state of the cells. Buffinton et al. determined that menadione-glutathionyl conjugates can act as NQO1 substrates and undergo redox-cycling reactions.[7] Therefore, the potential generated MB-353-glutathionyl conjugates may act as substrates for NQO1, be bioactivated by NQO1 and undergo redox cycling with concomitant production of ROS contributing to the overall induction of oxidative stress in NQO1-rich cells.

To determine whether GSH depletion in the cells was specific to the good substrate MB-353, we measured the levels of GSH in BE and BE-NQ cells after

treatment with MB-323. No difference was observed in GSH levels in either cell line treated with MB-323 (Figures 5.5 and 5.6) suggesting that the observed GSH depletion in BE-NQ cells was specific to MB-353. The absence of significant depletion of GSH in BE and BE-NQ cells treated with MB-323 in comparison with negative controls suggests the lack of GSH alkylation by MB-323 and lack of bioactivation of MB-323 by NQO1, respectively.

The selective GSH depletion as well as production of 8-oxo-2dG in BE-NQ cells by MB-353 can result in apoptosis induction in these cells. It has been reported that several classes of polycyclic aromatic hydrocarbon (PAH) *o*-quinones can cause cell death by altering the cellular redox state and causing GSH depletion.[33] The effect of lavendamycin agents on the redox state of cancer cells and the possible involvement of redox state alteration in the cytotoxicity of these agents have not been previously examined.

Additional experiments using ROS scavengers and antioxidants will be required to better determine redox-cycling ability of the lavendamycin analogue MB-353 and the underlying mechanism of GSH depletion in BE-NQ cells.

Figure 5.5. Effect of MB-323 on the levels of reduced form of glutathione in BE-NQ cells after 2-h treatment with the compound at a concentration of 500 nM at 0, 6, 12 and 24 h post-exposure incubation periods.

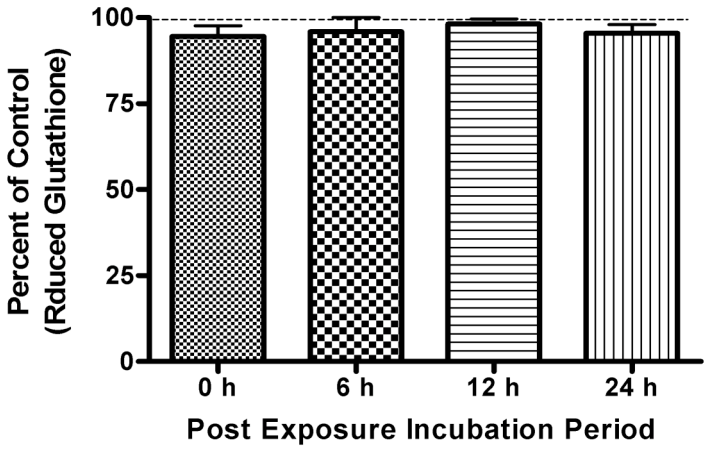

Figure 5.5. Effect of MB-323 on the levels of reduced form of glutathione in BE-NQ cells after 2-h treatment with the compound at a concentration of 500 nM at 0, 6, 12 and 24 h post-exposure incubation periods. Reduced form of glutathione was determined by a non-recycling system in sample solutions using the glutathione colorimetric detection kit as described under Materials and Methods. Reduced form of glutathione is expressed as percentage of negative control (untreated cells). Dashed line represents negative control. Results are reported as means ± SEM for n = 3 experiments.

Figure 5.6. Effect of MB-323 on the levels of reduced form of glutathione in BE cells after 2-h treatment with the compound at a concentration of 500 nM at 0, 6, 12 and 24 h post-exposure incubation periods.

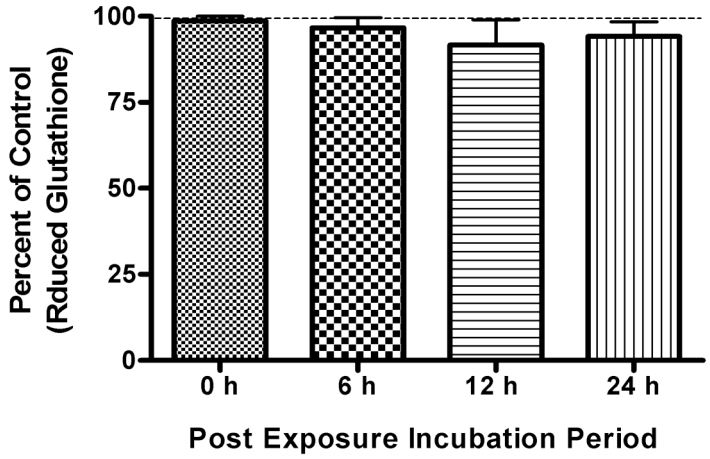

Figure 5.6. Effect of MB-323 on the levels of reduced form of glutathione in BE cells after 2-h treatment with the compound at a concentration of 500 nM at 0, 6, 12 and 24 h post-exposure incubation periods. Reduced form of glutathione was determined by a non-recycling system in sample solutions using the glutathione colorimetric detection kit as described under Materials and Methods. Reduced form of glutathione is expressed as percentage of negative control (untreated cells). Dashed line represents negative control. Results are reported as means ± SEM for n = 3 experiments.

5.5.3 Apoptosis Induction. Oxidative stress has been considered an important mediator of apoptosis in cells.[4] Internucleosomal DNA fragmentation has long been used as a biochemical index of apoptosis.[37] We measured the enrichment of mono and oligonucleosomes in the cytoplasm of the apoptotic cells to detect apoptosis. BE and BE-NQ cells incubated with a hypertonic buffer for 2 hours were used as the corresponding positive controls. Significant induction of apoptosis in positive controls of BE and BE-NQ cell lines was observed (Figures 5.7 and 5.8). Our data demonstrated that a 2-hour treatment with MB-353 at a concentration of 500 nM caused significant induction of apoptosis in BE-NQ cells at 12 and 24 hours post-exposure time points versus the untreated negative control (Figure 5.7). The greatest induction of apoptosis occurred at the 12-hour time point (Figure 5.7), which is in accordance with the observed highest depletion of GSH in these cells at the same time point by MB-353 (Figure 5.3). A trend toward reduction in apoptosis induction was observed at the 24-hour time point although it was still significantly higher than the negative control (Figure 5.7). This trend toward reduced apoptosis induction at the 24-hour time point in the cells can be in part due to the observed recovery of GSH in the cells at this time point and possible activation of other repair mechanisms. There was no apoptosis induction immediately after the 2-hour treatment by MB-353 in BE-NQ cells (Figure 5.7). These findings suggest that induction of apoptosis in BE-NQ cells by MB-353 compared to the corresponding production of 8-oxo-2dG and GSH depletion in these cells (which occur immediately after 2 hours of the treatment) is a late event that could be in turn the result of the observed oxidative DNA damage and GSH depletion.

No significant induction of apoptosis was detected in BE cells treated by MB-353 at any of the post-exposure time points suggesting that bioactivation of MB-353 by NQO1 results in the induction of apoptosis in BE-NQ cells versus BE cells (Figure 5.8). Lack of apoptosis induction in the MB-353-treated BE cells is consistent with the lack of GSH depletion and oxidative DNA damage in these cells after treatment with MB-353. This suggests that there is a direct association between the presence of the observed oxidative stress biomarkers and the induction of apoptosis in the MB-353-treated BE-NQ cells.

Figure 5.7. Detection of apoptosis in BE-NQ cells after 2-h treatment with MB-353 at a concentration of 500 nM at 0, 12 and 24 h post-exposure incubation periods.

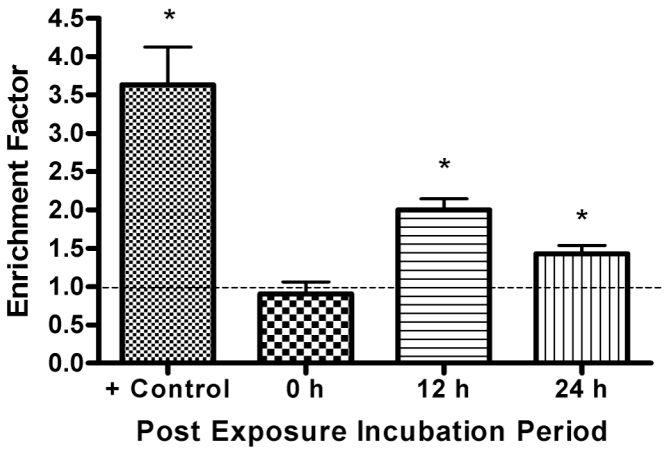

Figure 5.7. Detection of apoptosis in BE-NQ cells after 2-h treatment with MB-353 at a concentration of 500 nM at 0, 12 and 24 h post-exposure incubation periods. The enrichment of mono and oligonucleosomes in the cytoplasm of the apoptotic cells was detected using the cell death detection ELISA kit as described under Materials and Methods. The enrichment factor value of the negative control (untreated cells) is considered 1. Dashed line represents negative control. *Significantly different from negative control ($P \leq 0.05$). Results are reported as means ± SEM for n = 3 experiments.

Figure 5.8. Detection of apoptosis in BE cells after 2-h treatment with MB-353 at a concentration of 500 nM at 0, 12 and 24 h post-exposure incubation periods.

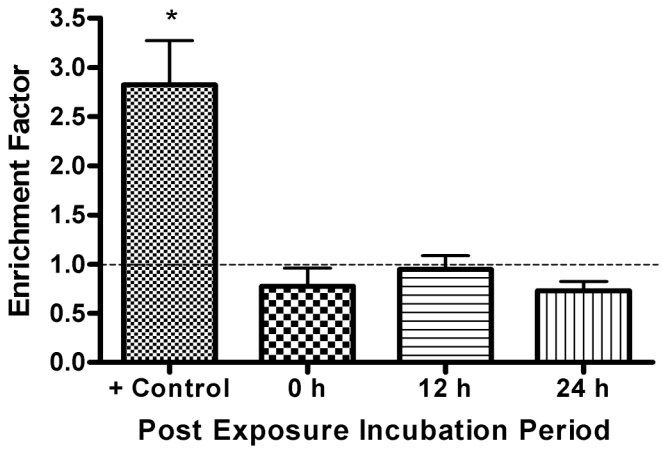

Figure 5.8. Detection of apoptosis in BE cells after 2-h treatment with MB-353 at a concentration of 500 nM at 0, 12 and 24 h post-exposure incubation periods. The enrichment of mono and oligonucleosomes in the cytoplasm of the apoptotic cells was detected using the cell death detection ELISA kit as described under Materials and Methods. The enrichment factor value of the negative control (untreated cells) is considered 1. Dashed line represents negative control. *Significantly different from negative control ($P \leq 0.05$). Results are reported as means ± SEM for n = 3 experiments.

Since two key elements of cytotoxicity of quinones are the production of ROS and DNA damage, these compounds should be potent inducers of apoptosis.[4] The benzoquinone RH1 has been demonstrated to preferentially cause apoptosis in NQO1-rich human breast cancer NQ16 cells compared to parental NQO1-deficient MDA468 cells at lower concentrations.[30] Sun et al. demonstrated that SN and MMC induced significant apoptosis in human colon adenocarcinoma NQO1-rich HT29 cells compared to NQO1-deficient BE cells implying that bioactivation of these compounds by NQO1 led to apoptosis induction in HT29 cells.[19] It has also been shown that NQO1 plays a key role in apoptosis induction in NQO1-expressing human prostate cancer cells by the naturally occurring *o*-naphthoquinone β-lapachone.[40] ROS have been implicated in both death receptor-mediated (extrinsic pathway) and mitochondria-mediated (intrinsic pathway) apoptosis.[41] Further research is required to investigate which apoptotic pathway is involved in ROS-induced lavendamycin-related cytotoxicity.

MB-323 did not cause apoptosis in BE and BE-NQ cells in comparison with negative controls at the same concentration as MB-353 (Figures 5.9 and 5.10). Lack of apoptosis in the BE-NQ cells after exposure to MB-323 is consistent with lack of detection of biomarkers of oxidative stress in these cells, which suggests that this compound cannot be bioactivated by NQO1. No observation of an apoptosis event in BE cells after MB-323 treatment implies that this compound at this concentration cannot cause enough, direct alkylation of DNA or thiol groups that can result in apoptosis.

Figure 5.9. Detection of apoptosis in BE-NQ cells after 2-h treatment with MB-323 at a concentration of 500 nM at 0, 12 and 24 h post-exposure incubation periods.

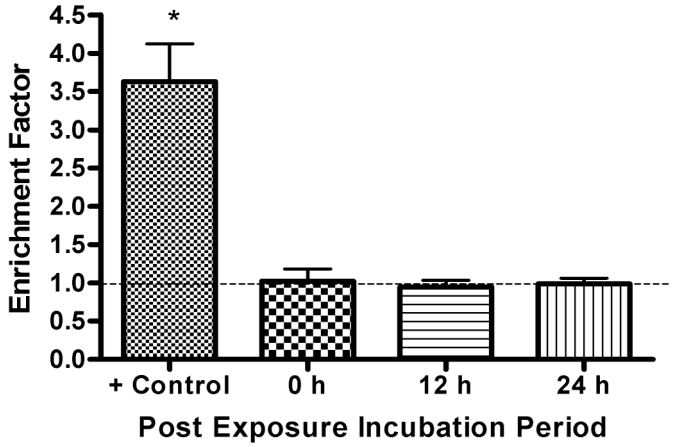

Figure 5.9. Detection of apoptosis in BE-NQ cells after 2-h treatment with MB-323 at a concentration of 500 nM at 0, 12 and 24 h post-exposure incubation periods. The enrichment of mono and oligonucleosomes in the cytoplasm of the apoptotic cells was detected using the cell death detection ELISA kit as described under Materials and Methods. The enrichment factor value of the negative control (untreated cells) is considered 1. Dashed line represents negative control. *Significantly different from negative control ($P \leq 0.05$). Results are reported as means ± SEM for n = 3 experiments.

Figure 5.10. Detection of apoptosis in BE cells after 2-h treatment with MB-323 at a concentration of 500 nM at 0, 12 and 24 h post-exposure incubation periods.

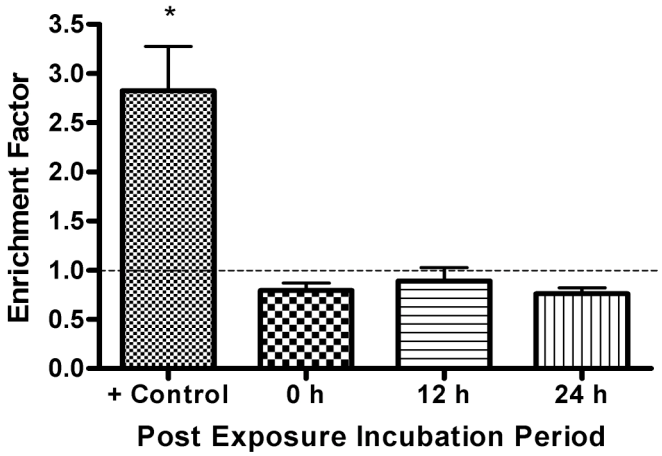

Figure 5.10. Detection of apoptosis in BE cells after 2-h treatment with MB-323 at a concentration of 500 nM at 0, 12 and 24 h post-exposure incubation periods. The enrichment of mono and oligonucleosomes in the cytoplasm of the apoptotic cells was detected using the cell death detection ELISA kit as described under Materials and Methods. The enrichment factor value of the negative control (untreated cells) is considered 1. Dashed line represents negative control. *Significantly different from negative control ($P \leq 0.05$). Results are reported as means ± SEM for n = 3 experiments.

5.6 Conclusions

The good lavendamycin substrate for NQO1, MB-353, significantly increased the molar ratio of 8-oxo-2dG to 2-dG in NQO1-rich BE-NQ cells compared to NQO1-deficient BE cells. However, no significant increase in the corresponding molar ratio was observed in BE and BE-NQ cells treated with the poor substrate for NQO1, MB-323. The acquired data indicate the importance of the role for NQO1 in the bioactivation of MB-353 and selective induction of oxidative DNA damage in NQO1-rich cells by this compound. Similarly, MB-353 significantly decreased the levels of GSH only in BE-NQ cells, while no GSH depletion was observed in either cell line treated with MB-323. This suggests NQO1-mediated selective depletion of GSH in BE-NQ cells by MB-353 and that this event is specific to this compound versus MB-323. Therefore, selective induction of oxidative stress in NOQ1-rich cells was due to NQO1-mediated activation of MB-353. In addition, this bioactivation of MB-353 by NQO1 resulted in apoptosis induction in BE-NQ cells versus BE cells, whereas MB-323 did not induce apoptosis in either cell line. These data are consistent with high and low substrate specificity of MB-353 and MB-323 for NQO1, respectively. Overall, our results demonstrated that only the good lavendamycin substrate, MB-353, caused oxidative stress resulting in oxidative DNA damage and subsequent apoptosis in NQO1-rich BE-NQ cells at nM concentrations via NQO1-mediated activation. Future studies are required to further determine other possible underlying mechanisms of toxicity of lavendamycin analogues including DNA alkylation and strand break formation. These findings enhance our understanding of the mechanisms of action of lavendamycin antitumor agents. They can also contribute to the

development of these compounds as potential anticancer drugs to impact cancer therapy. A good knowledge of cytotoxic mechanisms of lavendamycin antitumor agents will place them in a proper combination cancer therapy. Therefore, antitumor agents with known, various mechanisms of action could act upon different regions of the tumor microenvironment resulting in an effective antitumor therapy.

5.7 References

(1) Opara, E. C. Oxidative stress. *Dis. Mon.* **2006**, *52*, 183-198.

(2) Peoples, M. C.; Karnes, H. T. Recent developments in analytical methodology for 8-hydroxy-2'-deoxyguanosine and related compounds. *J. Chromatogr. B Analyt. Technol. Biomed. Life Sci.* **2005**, *827*, 5-15.

(3) Engel, R. H.; Evens, A. M. Oxidative stress and apoptosis: a new treatment paradigm in cancer. *Front. Biosci.* **2006**, *11*, 300-312.

(4) Ollinger, K.; Kagedal, K. Induction of apoptosis by redox-cycling quinones. *Subcell. Biochem.* **2002**, *36*, 151-170.

(5) Watanabe, N.; Forman, H. J. Autoxidation of extracellular hydroquinones is a causative event for the cytotoxicity of menadione and DMNQ in A549-S cells. *Arch. Biochem. Biophys.* **2003**, *411*, 145-157.

(6) Halinska, A.; Belej, T.; O'Brien, P. J. Cytotoxic mechanisms of anti-tumour quinones in parental and resistant lymphoblasts. *Br. J. Cancer Suppl.* **1996**, *27*, S23-27.

(7) Buffinton, G. D.; Ollinger, K.; Brunmark, A.; Cadenas, E. DT-diaphorase-catalysed reduction of 1,4-naphthoquinone derivatives and glutathionyl-quinone conjugates. *Biochem. J.* **1989**, *257*, 561-571.

(8) Beall, H. D.; Liu, Y.; Siegel, D.; Bolton, E. M.; Gibson, N. W.; Ross, D. Role of NAD(P)H:quinone oxidoreductase (DT-diaphorase) in cytotoxicity and induction of DNA damage by streptonigrin. *Biochem. Pharmacol.* **1996**, *51*, 645-652.

(9) Bolin, C.; Stedeford, T.; Cardozo-Pelaez, F. Single extraction protocol for the analysis of 8-hydroxy-2'-deoxyguanosine (oxo8dG) and the associated activity of 8-oxoguanine DNA glycosylase. *J. Neurosci. Methods* **2004**, *136*, 69-76.

(10) Shigenaga, M. K.; Ames, B. N. Assays for 8-hydroxy-2'-deoxyguanosine: A biomarker of in vivo oxidative DNA damage. *Free Radic. Biol. Med.* **1991**, *10*, 211-216.

(11) Lin, P. H.; Nakamura, J.; Yamaguchi, S.; Upton, P. B.; La, D. K.; Swenberg, J. A. Oxidative damage and direct adducts in calf thymus DNA induced by the pentachlorophenol metabolites, tetrachlorohydroquinone and tetrachloro-1,4-benzoquinone. *Carcinogenesis.* **2001**, *22*, 627-634.

(12) Shi, M. M.; Kugelman, A.; Iwamoto, T.; Tian, L.; Forman, H. J. Quinone-induced oxidative stress elevates glutathione and induces gamma-glutamylcysteine synthetase activity in rat lung epithelial L2 cells. *J. Biol. Chem.* **1994**, *269*, 26512-26517.

(13) Coleman, M. D.; Rustioni, C. V. Resistance to glutathione depletion in diabetic and non-diabetic human erythrocytes in-vitro. *J. Pharm. Pharmacol.* **1999**, *51*, 21-25.

(14) Norikura, T.; Kennedy, D. O.; Nyarko, A. K.; Kojima, A.; Matsui-Yuasa, I. Protective effect of aloe extract against the cytotoxicity of 1,4-naphthoquinone in isolated rat hepatocytes involves modulations in cellular thiol levels. *Pharmacol. Toxicol.* **2002**, *90*, 278-284.

(15) Cadenas, E. Antioxidant and prooxidant functions of DT-diaphorase in quinone metabolism. *Biochem. Pharmacol.* **1995**, *49*, 127-140.

(16) Molina Portela, M. P.; Fernandez Villamil, S. H.; Perissinotti, L. J.; Stoppani, A. O. M. Redox cycling of o-naphthoquinones in trypanosomatids. Superoxide and hydrogen peroxide production. *Biochem. Pharmacol.* **1996***, 52*, 1875-1882.

(17) Giulivi, C.; Cadenas, E. One- and two-electron reduction of 2-methyl-1,4-naphthoquinone bioreductive alkylating agents: Kinetic studies, free-radical production, thiol oxidation and DNA-strand-break formation. *Biochem. J.* **1994***, 301 (Pt 1)*, 21-30.

(18) Ordonez, I. D.; Cadenas, E. Thiol oxidation coupled to DT-diaphorase-catalysed reduction of diaziquone. Reductive and oxidative pathways of diaziquone semiquinone modulated by glutathione and superoxide dismutase. *Biochem. J.* **1992***, 286 (Pt 2)*, 481-490.

(19) Sun, X.; Ross, D. Quinone-induced apoptosis in human colon adenocarcinoma cells via DT-diaphorase mediated bioactivation. *Chem. Biol. Interact.* **1996***, 100*, 267-276.

(20) Siegel, D.; Gibson, N. W.; Preusch, P. C.; Ross, D. Metabolism of mitomycin C by DT-diaphorase: Role in mitomycin C-induced DNA damage and cytotoxicity in human colon carcinoma cells. *Cancer Res.* **1990***, 50*, 7483-7489.

(21) Pink, J. J.; Planchon, S. M.; Tagliarino, C.; Varnes, M. E.; Siegel, D.; Boothman, D. A. NAD(P)H:Quinone oxidoreductase activity is the principal determinant of beta-lapachone cytotoxicity. *J. Biol. Chem.* **2000***, 275*, 5416-5424.

(22) Ngo, E. O.; Nutter, L. M.; Sura, T.; Gutierrez, P. L. Induction of p53 by the concerted actions of aziridine and quinone moieties of diaziquone. *Chem. Res. Toxicol.* **1998***, 11*, 360-368.

(23) Siegel, D.; Gibson, N. W.; Preusch, P. C.; Ross, D. Metabolism of diaziquone by NAD(P)H:(quinone acceptor) oxidoreductase (DT-diaphorase): Role in diaziquone-induced DNA damage and cytotoxicity in human colon carcinoma cells. *Cancer Res.* **1990**, *50*, 7293-7300.

(24) Fisher, G. R.; Gutierrez, P. L. Free radical formation and DNA strand breakage during metabolism of diaziquone by NAD(P)H quinone-acceptor oxidoreductase (DT-diaphorase) and NADPH cytochrome c reductase. *Free Radic. Biol. Med.* **1991**, *11*, 597-607.

(25) Beall, H. D.; Winski, S.; Swann, E.; Hudnott, A. R.; Cotterill, A. S.; O'Sullivan, N.; Green, S. J.; Bien, R.; Siegel, D.; Ross, D.; Moody, C. J. Indolequinone antitumor agents: Correlation between quinone structure, rate of metabolism by recombinant human NAD(P)H:quinone oxidoreductase, and in vitro cytotoxicity. *J. Med. Chem.* **1998**, *41*, 4755-4766.

(26) Swann, E.; Barraja, P.; Oberlander, A. M.; Gardipee, W. T.; Hudnott, A. R.; Beall, H. D.; Moody, C. J. Indolequinone antitumor agents: Correlation between quinone structure and rate of metabolism by recombinant human NAD(P)H:quinone oxidoreductase. Part 2. *J. Med. Chem.* **2001**, *44*, 3311-3319.

(27) Walton, M. I.; Smith, P. J.; Workman, P. The role of NAD(P)H: quinone reductase (EC 1.6.99.2, DT-diaphorase) in the reductive bioactivation of the novel indoloquinone antitumor agent EO9. *Cancer Commun.* **1991**, *3*, 199-206.

(28) Nemeikaite-Ceniene, A.; Dringeliene, A.; Sarlauskas, J.; Cenas, N. Role of NAD(P)H:quinone oxidoreductase (NQO1) in apoptosis induction by

aziridinylbenzoquinones RH1 and MeDZQ. *Acta Biochim. Pol.* **2005***, 52*, 937-941.

(29) Dehn, D. L.; Winski, S. L.; Ross, D. Development of a new isogenic cell-xenograft system for evaluation of NAD(P)H:quinone oxidoreductase-directed antitumor quinones: evaluation of the activity of RH1. *Clin. Cancer Res.* **2004***, 10*, 3147-3155.

(30) Dehn, D. L.; Inayat-Hussain, S. H.; Ross, D. RH1 induces cellular damage in an NAD(P)H:quinone oxidoreductase 1-dependent manner: Relationship between DNA cross-linking, cell cycle perturbations, and apoptosis. *J. Pharmacol. Exp. Ther.* **2005***, 313*, 771-779.

(31) Beall, H. D.; Winski, S. I. Mechanisms of action of quinone-containing alkylating agents. I: NQO1-directed drug development. *Front. Biosci.* **2000***, 5*, 639-648.

(32) Asche, C. Antitumour quinones. *Mini-Rev. Med. Chem.* **2005***, 5*, 449-467.

(33) Bolton, J. L.; Trush, M. A.; Penning, T. M.; Dryhurst, G.; Monks, T. J. Role of quinones in toxicology. *Chem. Res. Toxicol.* **2000***, 13*, 135-160.

(34) Gutierrez, P. L. The role of NAD(P)H oxidoreductase (DT-Diaphorase) in the bioactivation of quinone-containing antitumor agents: A review. *Free Radic. Biol. Med.* **2000***, 29*, 263-275.

(35) Li, B.; Blough, N. V.; Gutierrez, P. L. Trace detection of hydroxyl radicals during the redox cycling of low concentrations of diaziquone: a new approach. *Free Radic. Biol. Med.* **2000***, 29*, 548-556.

(36) Pagano, G.; Degan, P.; De Biase, A.; Iaccarino, M.; Warnau, M. Diepoxybutane and mitomycin C toxicity is associated with the induction of oxidative DNA damage in sea urchin embryos. *Hum. Exp. Toxicol.* **2001***, 20*, 651-655.

(37) Norbury, C. J.; Zhivotovsky, B. DNA damage-induced apoptosis. *Oncogene* **2004***, 23*, 2797-2808.

(38) Abu-Qare, A. W.; Abou-Donia, M. B. Biomarkers of apoptosis: release of cytochrome c, activation of caspase-3, induction of 8-hydroxy-2'-deoxyguanosine, increased 3-nitrotyrosine, and alteration of p53 gene. *J. Toxicol. Environ. Health B Crit. Rev.* **2001***, 4*, 313-332.

(39) Rodriguez, C. E.; Shinyashiki, M.; Froines, J.; Yu, R. C.; Fukuto, J. M.; Cho, A. K. An examination of quinone toxicity using the yeast Saccharomyces cerevisiae model system. *Toxicology.* **2004***, 201*, 185-196.

(40) Planchon, S. M.; Pink, J. J.; Tagliarino, C.; Bornmann, W. G.; Varnes, M. E.; Boothman, D. A. beta-Lapachone-induced apoptosis in human prostate cancer cells: Involvement of NQO1/xip3. *Exp. Cell Res.* **2001***, 267*, 95-106.

(41) Simon, H. U.; Haj-Yehia, A.; Levi-Schaffer, F. Role of reactive oxygen species (ROS) in apoptosis induction. *Apoptosis.* **2000***, 5*, 415-418.